MEASURING BRAIN ENDOTHELIAL CELL BIOENERGETICS VIA EXTRACELLULAR FLUX ANALYSIS

A THESIS

SUBMITTED TO THE FACULTY OF THE

UNIVERSITY OF MINNESOTA

BY

CADE JOHN MCDONALD

IN PARTIAL FULFILLMENT OF THE REQUIREMENTS

FOR THE DEGREE OF

MASTER OF SCIENCE

LESTER R. DREWES

JULY 2019

Table of Contents

List of Tables……...ii

List of Figures……iii

Abbreviations……..…vi

Introduction……..1

Chapter 1 : Background…….……..4

Chapter 2 : Materials and Methods……13

Chapter 3 : hCMEC/D3 Cells as a Model for Bioenergetic Studies..……23

Chapter 4 : OCR and ECAR..……25

Chapter 5 : ATP Production Rates…….……30

Chapter 6 : Metabolite Effect on Bioenergetics…….……34

Chapter 7 : Inhibitor Effect on Bioenergetics……56

Chapter 8 : Discussion…...……81

References……..88

List of Tables

Table 1: HCMEC/D3 CELL METABOLITE ENERGETIC VALUES ……...45

Table 2: HCMEC/D3 INHIBITOR ENERGETIC VALUES ……..……70

List of Figures

Figure 1 : EXTRACELLULAR FLUX ANALYSIS CONFIGURATION AND ECAR/OCR CONTRIBUTIONS ……...…..16

Figure 2 : MITO STRESS TEST PROTOCOL ……..……..18

Figure 3 : GLYCOLYTIC RATE ASSAY PROTOCOL ……...……..20

Figure 4 : ATP RATE ASSAY PROTOCOL …….……..21

Figure 5 : HCMEC/D3 CELL PHOTOMICROGRAPH ……..25

Figure 6 : HCMEC/D3 CELL OCR TRACE …….……..26

Figure 7 : HCMEC/D3 CELL OCR VALUES ……...…..27

Figure 8 : HCMEC/D3 PER VALUES ……...……..28

Figure 9 : HCMEC/D3 VS. HMVEC OCR VALUES ……...……..29

Figure 10: HCMEC/D3 VS. HMVEC PER VALUES …….30

Figure 11 : HCMEC/D3 CELL ATP PRODUCTION RATES ……33

Figure 12 : CELLULAR METABOLITE PATHWAYS …….……35

Figure 13 : HCMEC/D3 CELL METABOLITE OCR TRACE (A) ……43

Figure 14 : HCMEC/D3 CELL METABOLITE OCR TRACE (B) …….…44

Figure 15 : HCMEC/D3 METABOLITE BASAL OCR ……..…46

Figure 16 : HCMEC/D3 METABOLITE ATP COUPLED OCR ……47

Figure 17 : HCMEC/D3 METABOLITE COUPLING EFFICIENCY ……48

Figure 18 : HCMEC/D3 METABOLITE MAXIMAL RESPIRATION …..……49

Figure 19 : HCMEC/D3 METABOLITE SPARE RESPIRATORY CAPACITY ..……50

Figure 20 : HCMEC/D3 METABOLITE PROTON LEAK …….……51

Figure 21 : HCMEC/D3 METABOLITE NON-MITOCHONDRIAL OCR ...……52

Figure 22 : HCMEC/D3 METABOLITE COMPENSATORY PER……53

Figure 23 : HCMEC/D3 METABOLITE MITOCHONDRIAL ATP PRODUCTION RATES ……..……54

Figure 24 : HCMEC/D3 METABOLITE GLYCOLYTIC ATP PRODUCTION RATES ..……55

Figure 25 : HCMEC/D3 METABOLITE TOTAL ATP PRODUCTION RATES ..……56

Figure 26 : INHIBITOR TARGETS ……..……58

Figure 27 : HCMEC/D3 CELL INHIBITOR OCR TRACE (A) ……..……68

Figure 28 : HCMEC/D3 INHIBITOR OCR TRACE (B) ……..……69

Figure 29 : HCMEC/D3 INHIBITOR BASAL OCR ……...……71

Figure 30 : HCMEC/D3 INHIBITOR ATP COUPLED OCR ..……72

Figure 31 : HCMEC/D3 INHIBITOR COUPLING EFFICIENCY ..……73

Figure 32 : HCMEC/D3 INHIBITOR MAXIMAL RESPIRATION ...……74

Figure 33 : HCMEC/D3 INHIBITOR SPARE RESPIRATORY CAPACITY ...……75

Figure 34 : HCMEC/D3 INHIBITOR PROTON LEAK ……...……76

Figure 35 : HCMEC/D3 INHIBITOR NON-MITOCHONDRIAL OCR ……77

Figure 36 : HCMEC/D3 INHIBITOR COMPENSATORY PER ……78

Figure 37 : HCMEC/D3 INHIBITOR MITOCHONDRIAL ATP PRODUCTION RATES ……..79

Figure 38 : HCMEC/D3 INHIBITOR GLYCOLYTIC ATP PRODUCTION RATES ..……80

Figure 39 : HCMEC/D3 INHIBITOR TOTAL ATP PRODUCTION RATES ……..……81

Abbreviations

OCR: Oxygen consumption rate

ECAR: Extracellular acidification rate

PER: Proton efflux rate

GLUT1: Glucose transporter 1

MPC: Mitochondrial pyruvate carrier

MCT: Monocarboxylate transporter

GLS: Glutaminase

OXPHOS: Oxidative phosphorylation

NVU: Neurovascular unit

CNS: Central nervous system

AZD3965: Monocarboxylate transporter 1 small molecule inhibitor

BAY876: Glucose transporter 1 small molecule inhibitor

UK5099: Mitochondrial pyruvate carrier small molecule inhibitor

MD1: Experimental monocarboxylate transporter 1 and 4 dual small molecule inhibitor

BPTES: Glutaminase small molecule inhibitor

Introduction

Abstract:

The neurovascular unit (NVU) is an important structural component in the central nervous system (CNS). The NVU consists of multiple cell types that include endothelial cells, pericytes, astrocytes, and others, working collectively as a restrictive interface between blood and neural tissue within the CNS. The NVU functions to transport nutrients, ions, and other substances to and from the blood to maintain homeostasis within the neural cell microenvironment. The NVU is responsible for the regulation of nutrient and ion transport from the blood as neurons require a fastidious supply of nutrients and ions in order to function properly. It is also important to regulate the neural cell microenvironment as many molecules and substrates in blood serum can be detrimental to neural function. This neural dysfunction may, in turn, lead to CNS complications. A dysfunctional NVU is associated with many disease states, including Alzheimer's, ALS, strokes, multiple sclerosis, epilepsy, and glioblastomas. These disease states are linked to, but not limited to, deregulation of nutrient transport, NVU inflammation and leakage of blood constituents into the neural environment, downregulation of the basal lamina, reduced efficacy and downregulation of ATP-binding cassette (ABC) transporters, and downregulation of tight junction proteins. Therefore, it is important that the NVU possesses mechanisms for which it can restrict passage of detrimental substances into the CNS. The endothelial cell is a principal barrier-forming cell of the NVU because of its direct contact with the blood, its intercellular tight junctions, biotransforming enzymes, and asymmetric distribution of active and carrier-mediated transporters. These properties are important in the separation

of blood from neural tissue and regulation of nutrients and ions within the neural environment. Maintaining and regulating these properties requires an abundant supply of energy, in the form of adenosine triphosphate (ATP). Therefore, endothelial cell energy metabolism is a critically important area of study. Cellular energy metabolism is considered the process of exploiting various metabolic substrates to produce ATP. Cells typically utilize glycolysis and oxidative phosphorylation (OXPHOS) as energy producing pathways to maintain cellular ATP demand. OXPHOS is considered the major contributor in ATP production as it produces ~ 33 molecules of ATP per glucose molecule, whereas glycolysis produces only two molecules of ATP per glucose molecule. Glycolysis is often overlooked due to this imbalance of ATP production. However, it is becoming more evident that glycolysis may be a primary energy producing pathway due to its rapid turnover rate and production of molecules that are able to be utilized as building blocks for cellular compartments. Cellular bioenergetics using extracellular flux analysis has been extensively used to study many different cell types such as tumor, immune, and stem cells, but little is known about the energy producing pathways of brain endothelial cells. Here, we characterize the bioenergetics of human brain microvascular endothelial cells by using human brain microvascular endothelial hCMEC/D3 cells as a model. hCMEC/D3 cell bioenergetic properties were characterized by investigating metabolite preference and the effects of various metabolic inhibitors on extracellular acidification and OXPHOS rates. Glycolysis and OXPHOS can be quantitatively measured by using extracellular flux analysis. Using sensitive probes, extracellular flux analysis can measure extracellular acidification and oxygen consumption to quantify glycolytic and OXPHOS rates, respectively. In this study, we show that these cells utilize

glycolysis as a primary metabolic pathway and glucose as the preferred metabolite. Although glucose is the primary metabolite hCMEC/D3 cells utilize, they are able to maintain ATP production by utilizing pyruvate and glutamine as well via OXPHOS. Using monocarboxylate transporter 1 (MCT1), mitochondrial pyruvate carrier (MPC), glutaminase (GLS), and glucose transporter 1 (GLUT1) inhibitors, we were able to explore the metabolic flexibility of hCMEC/D3 cells. Nutrient transport inhibition significantly altered glycolytic and oxidative properties of hCMEC/D3 cells. These findings reveal a basic understanding of brain endothelial cell energy production and metabolism. This data may also contribute to our understanding of altered brain endothelial cell function in disease or under conditions of active angiogenesis during development or tumorigenesis. Further understanding of altered brain endothelial cell energy metabolism in a diseased state can allow for the development of therapeutics that target these altered pathways.

Chapter 1: Background

Endothelial cells, astrocytes, pericytes, and neurons cooperate together to create a unique barrier between neural tissue of the central nervous system (CNS) and constituents of the blood [1–13]. These cell types, that form an intricate interface between the CNS and its vasculature, are collectively named the neurovascular unit (NVU) [3,6,7,10–12,14–16]. The NVU is also commonly termed the blood-brain barrier. Animals with a developed CNS possess an NVU [2]. Through decreased paracellular transport and active efflux, the NVU provides a stable environment for neural function by effectively separating blood and neural tissue. The NVU is also important in maintaining neural tissue environment by utilizing nutrient and ion transporters to sustain adequate levels of molecules, nutrients, and ions within the CNS tissue.

Brain endothelial cells are a key component of NVU integrity and function due to their direct contact with blood, restricted paracellular transport, biotransforming enzymes, expression of ATP binding cassette (ABC) efflux transporters, and asymmetric distribution of ion and nutrient transporters. These properties are important as normal neural function requires a very particular, and consistent, composition of nutrients and ions within the neural environment [2]. It has been observed that ion and nutrient composition, such as amino acid, potassium, and calcium levels, remain consistent in the CNS tissue even when blood serum concentrations fluctuate [17]. Some blood constituents can be detrimental to neural function, such as the amino acid glutamate [3], therefore it is important to restrain some substances from getting into the CNS tissue. Proteins, hormones, and ions within blood serum can disrupt normal neural function by acting as neurotransmitters, affecting transcription and intercellular signaling, and

activating voltage gated ion channels, respectively. Brain endothelial cells are an important component in regulating harmful blood constituents from neural tissue due to restricted permeability of many small molecules and water-soluble substances via tight junctions [18–21]. Lipophilic and xenobiotic substances are restricted from crossing into the CNS through the use of active efflux transporters [2,22–24].

Tight Junctions

Claudins, VE-cadherin, junction adherence molecules, and occludins interact with cytosolic catenins, zonula occludens, and the cellular actin cytoskeleton to create a highly restrictive junction between endothelial cells [20,21]. This restrictive junction is termed the "tight junction". Tight junctions between endothelial cells considerably decrease paracellular transport of hydrophilic and small molecules from the blood into the CNS [15,18–21]. Claudin-1, -3, -5, and -12 are tight junction proteins that are expressed in brain endothelial cells and are essential in restricting paracellular transport of various small molecules [11,18,20,25,26]. Claudin-5 is said to be the predominant junction-forming protein and is important in the regulation of small molecule transport between cells [19,27]. Compared to endothelial cells within other tissues, brain endothelial cells have shown to express 600-fold higher amount of claudin-5 than claudin-3 [26]. Claudin-3 and -5 are essential for maintaining tight junction integrity as experiments show the genetic loss of either protein, in mice models, leads to a compromised and leaky NVU and death [19]. It has also been revealed that disruption of tight junctions, via edema formation in the brain, was associated with a decrease in intracellular ATP generation in mice brain microvascular endothelial cells [28]. ATP repletion has also found to have a regenerative effect as it allows zonula occludens to associate more with tight junction

proteins, rather than the cellular cytoskeleton, in MDCK epithelial cells [29]. Due to the restricted paracellular permeability of brain endothelial cells, many molecules, nutrients, and ions in blood need to be transported into the CNS environment by alternative transport mechanisms, such as transcellular transport.

Endothelial Cell Transport

Transcellular transport mechanisms include diffusion, ion channels, receptor mediated and adsorptive transcytosis, and use of either passive or active membrane transporters. Membrane transport proteins such as the glucose transporter, GLUT1, and transporters of the solute carrier (SLC) family are essential in providing the CNS with the needed nutrients and amino acids from the blood in order to function properly [2,30]. The CNS is known to consume a large supply of glucose, the main energy source for the brain, to support its high energy needs [31]. Of the solute carriers, GLUT1 is one of the highest expressed nutrient transporter in brain endothelial cells [32,33]. Another important SLC transporter expressed in brain endothelial cells is MCT1. MCT1 allows transportation of lactate, pyruvate, and ketone bodies as alternative fuels when glucose is limited [34]. Transport of nutrients and ions is also achieved by the asymmetrical distribution of these transporters in brain endothelial cells between the lumen of the vasculature and the CNS tissue [2,35]. GLUT1 and MCT1 are expressed on both luminal and abluminal aspects of the brain endothelial cell membrane [2,33]. Many amino acid carriers are located on the abluminal side of endothelial cells, allowing for high regulation of the neural environment [36]. Amino acid regulation is important as the CNS environment contains a very limited amount of amino acids compared to blood serum [2]. Expression of SLCs and ion transporters on luminal, abluminal, or both sides of brain endothelial cells allows

for the transport of nutrients, nucleotides, amino acids, ions, and other molecules into or out of the CNS tissue to support neuronal function. Ion transporters, such as Na^+/K^+ ATPase require ATP for active transport of ions into and out of the neural environment [28,36]. Nutrient transport also allows endothelial cells to utilize these nutrients to generate ATP to perform cellular functions and maintain NVU integrity. ATP generation from nutrient metabolism can be used to maintain tight junction integrity, for active efflux of harmful molecules, and for maintaining adequate ion concentrations in the CNS environment via Ca^{2+}- and Na^+/K^+-ATPases [28,29].

Active efflux

Active efflux of lipophilic, neurotoxic, and xenobiotic molecules further complements the restrictive properties of brain endothelial cells. Efflux transporters are considered a family of ATP-binding cassette (ABC) transporters. The primary ABC transporters of the NVU are Multidrug Resistance-associated Proteins (MRPs), P-glycoproteins (Pgp), and Breast Cancer Resistance Proteins (BRCP) [2,22]. These efflux transporters have made it difficult to develop small molecule drugs to treat CNS diseases as they are rapidly exported back out into the blood. As these transporters function via ATP hydrolysis, cellular ATP generation is important to allow consistent efflux of harmful molecules from the CNS.

Cells require energy, in the form of ATP, in order to perform many different functions such as cell division, signaling cascades, enzyme activation, transcytosis, tight junction maintenance, active efflux, and active transport of nutrients and ions. Cells are able to utilize various metabolites, such as glucose, glutamine, pyruvate, fatty acids, ketone

bodies, and amino acids to generate ATP through several metabolic pathways. Two primary energy producing pathways cells exploit are glycolysis and OXPHOS.

Glycolysis

Glycolysis involves the conversion of one glucose molecule into two molecules of pyruvate, which then may be converted to lactate [37,38]. The first and third steps of glycolysis consume two molecules of ATP to convert glucose into glucose-6-phosphate and fructose-6-phosphate into fructose-1,6-bisphosphate, respectively [39]. Fructose-1,6-bisphosphate is then converted into two glyceraldehyde-3-phosphate molecules, which are subsequently converted into two pyruvate molecules via multiple enzymatic steps [38,39]. From this process, four ATP molecules are produced, yielding a total of two molecules of ATP produced from one molecule of glucose [39]. Pyruvate can be converted into lactate, by lactate dehydrogenase, and exported into the extracellular environment, along with a hydrogen ion, through monocarboxylate transporters (MCTs) [8,40–42]. The process of which glucose is subsequently converted into lactate is considered glycolysis.

OXPHOS

Pyruvate produced from glycolysis, though, is primarily thought to be transported into the mitochondria, via mitochondrial pyruvate carrier (MPC), and converted into acetyl-CoA, which enters the tricarboxylic acid (TCA) cycle [43]. The TCA cycle converts acetyl-CoA into oxaloacetate, using multiple enzymatic reactions, and produces three NADH molecules and one FADH2 molecule. Other molecules, such as glutamine, can also fuel the TCA cycle through multiple enzymatic steps where glutamine is converted into glutamate, via glutaminase (GLS), which is then converted into alpha-ketoglutarate,

a TCA cycle intermediate [44,45,107,111]. NADH and FADH2 participate in the electron transport chain (ETC) to carry and donate electrons and create a proton gradient between the intermembrane space and the mitochondrial matrix [46]. The electrical-chemical gradient, from the transport of protons, is then exploited by ATP synthase to produce ~33.45 molecules of ATP (per glucose molecule) [47]. The electrons participating in the ETC then use oxygen as a final electron acceptor and H2O is produced.

Cells are able to utilize various metabolites to generate ATP through either glycolysis or OXPHOS, such as glucose, pyruvate, glutamine, lactate, and fatty acids [48–53]. Numerous metabolic pathways have gained attention as targets for various diseases, especially for different cancer types. Such pathways include glycolysis, lactate export and/or import, glutamine metabolism, and mitochondrial transport of pyruvate. Targeting glucose metabolism by inhibiting GLUT1, a primary glucose transporter, has shown to decrease cell proliferation in various cancer types [54,55], as many tumors and cancerous cells consume large amounts of glucose to proliferate rapidly [56,57]. Depending on the metabolic state of the cells, targeting lactate and pyruvate metabolism by inhibiting MCTs and MPCs have also shown to be promising treatments for various cancer types [41,51,58–60]. Metabolic pathways have also gained attention in immune and stem cell activation. It is shown that both immune cells and stem cells exhibit a change in cellular metabolism when in transition to an activated or quiescent state [61–64]. There have been extensive studies investigating the effectiveness of inhibiting bioenergetic pathways for treating various cancers and observing a change in the metabolic phenotype of immune and stem cells. However, characterizing the metabolic phenotype and studying the effects of inhibiting various pathways have not been studied for brain endothelial cell

metabolism. Studying the metabolic phenotype and the effect of disrupting glucose, pyruvate, or glutamine metabolism in brain endothelial cells may give insights to brain endothelial cell energetic characteristics and possible disease treatments involving the NVU dysfunction.

It has been estimated that the NVU is impermeable to more than 98% of small-molecule drugs, making treatment for many neurological diseases difficult [23]. Such neurological conditions, including Alzheimer's disease, stroke/ischemia, and glioblastomas involve tight junction break-down and a change in brain endothelial cell function and integrity [4,6,14,16,65,66]. Studies have shown that GLUT1 deficiencies in brain endothelium lead to cognitive impairments and increased permeability of the NVU [67,68]. Alzheimer's disease has also shown to exhibit a decreased expression of GLUT1 in brain endothelium [2]. Strokes and ischemia involve the release of pro-inflammatory cytokines, VEGF, and nitric oxide, which leads to tight junction disruption, angiogenesis, and increased NVU permeability [4].

Changes in brain endothelial cell function and integrity can be accompanied by changes in cellular energy demand and metabolism. Barrier breakdown, changes in nutrient transport, such as decreased expression or deficiency of GLUT1, changes in active efflux of detrimental molecules, and disrupted angiogenesis can all require a change in ATP demand. There have been many studies regarding structural, transcriptional, and proteomic components of brain endothelial cells involved in NVU integrity and disruption. However, the bioenergetic characteristics of brain endothelial cells have not been investigated. It is imperative then, to investigate brain endothelial cell

bioenergetics to understand differences in energetic needs and metabolic processes, both in healthy and diseased states.

Studying cellular bioenergetics of brain endothelial cells can be achieved through the use of extracellular flux analysis. Measuring oxygen consumption rates (OCRs) and acidification of media, in real-time, in conjunction with various compound injections that alter or inhibit metabolic pathways, can reveal insights toward brain endothelial cell bioenergetics. These real-time measurements can be quantified and used to characterize energy producing pathways and metabolic flexibility of brain endothelial cells. Glycolysis is associated with the production of lactate, which is then exported from the cytosol with a proton via MCTs. Therefore, in order to quantify glycolytic rates, extracellular acidification measurements can be used. If pyruvate is not converted into lactate and exported, it then enters the TCA cycle and fuels OXPHOS, hence, oxygen consumption measurements can then be used to measure mitochondrial respiration rates.

This study provides a unique insight to the metabolic properties and bioenergetics of immortalized, as well as primary, human capillary microvascular endothelial cells. The immortalized hCMEC/D3 cell line has been extensively characterized and represents a promising NVU model *in vitro*. Therefore, through the use of the Seahorse XFe96 Bioanalyzer, OCRs, extracellular acidification rates (ECAR), and proton efflux rates (PER) of hCMEC/D3 cells were recorded, in real-time, and quantified to calculate glycolytic and mitochondrial characteristics. Using these recordings, we were able to develop a basic understanding of the typical energetic characteristics of hCMEC/D3 cells. We also observed the effects of MCT, MPC, GLS, and GLUT1 inhibition on energy production to observe the metabolic flexibility and ability to utilize different metabolites

of hCMEC/D3 cells. Glucose, pyruvate, and glutamine preference and utilization was also studied in hCMEC/D3 cells.

Endothelial cells in other tissues of the body contain very little mitochondria and exploit glycolysis as a primary source of ATP [37,69,70]. However, brain endothelial cells have approximately double the number of mitochondria than other tissues [37,70]. This phenomenon was also observed by Oldendorf and Brown in 1976, as they detected that rat brain endothelial cells contained more mitochondria than skeletal muscle cells. This led us to hypothesize that brain endothelial cells would have a considerable high rate of OXPHOS to meet energy demands. Although brain endothelial cells may contain more mitochondria than endothelial cells of different tissues, hCMEC/D3 cells and primary human brain microvascular endothelial cells exhibited a primarily glycolytic mode of metabolism, where a majority of protons produced are from glycolysis, and relatively little utilization of mitochondrial respiration. This is further supported as glycolytic ATP production rates were higher than mitochondrial ATP production rates.

We then hypothesized that changing the composition of available metabolites would alter the metabolic phenotype of hCMEC/D3 cells. Cells were presented with glucose, glutamine, pyruvate, a combination of two, or all three to test the effect of metabolite composition on hCMEC/D3 energy production. Metabolite composition in the extracellular space showed to significantly alter glycolytic and mitochondrial energy production in cells. With glucose present, the cells favored glycolysis and little glucose was shunted to OXPHOS. When presented with pyruvate and/or glutamine, cells increased mitochondrial activity to meet energy demands. When presented with an equal concentration of either metabolite or a combination, the total ATP production rates of

hCMEC/D3 cells also remained relatively consistent, with the exception of glutamine alone.

We then hypothesized that disrupting glucose transport, pyruvate transport into the mitochondria, conversion of glutamine into glutamate, or a combination of two or all three would alter energy production in hCMEC/D3 cells. To disrupt glucose and pyruvate transport, we utilized small molecule inhibitors BAY876 and UK5099, respectively. Glutamine conversion into glutamate was inhibited by using the small molecule inhibitor BPTES. We also tested inhibition of MCT1 or dual inhibition of MCT1 and MCT4 via small molecule inhibitors AZD3965 and MD1, respectively. Disruption of glucose transport significantly altered glycolytic and mitochondrial energy production in hCMEC/D3 cells. Mitochondrial targeted disruption altered various mitochondrial characteristics and lactate transport did not alter hCMEC/D3 energy production.

Chapter 2: Materials and Methods

Cell Culture

hCMEC/ D3 immortalized human brain microvascular cells were purchased from Millipore® (Cat. No. SCC066). Primary human brain microvascular endothelial cells were purchased from Cell Systems® (Cat. No. ACBRI 376). 1 mL aliquots of cells in growth medium were prepared and stored in liquid nitrogen. Cells were thawed with, and cultured, in growth medium containing 45% Ham's F10 (Gibco, Cat. No. 12390-027), 45% alpha MEM (Gibco, Cat. No. 12561-023), 10% fetal bovine serum, and 1.74 mM L-glutamine (Sigma, Cat. No. G 7513). The growth media was also supplemented with 0.5 mL Gentamicin (Gibco, Cat. No. 15710-015), and 500 ng of fibroblast growth factor β. Cells were incubated at 37°C and 5% CO_2 on rat tail collagen type I coated T75 cell

culture flasks. To passage cells, cells were washed with PBS and trypsin was added to the culture flask and cells incubated at 37°C and 5% CO_2 for 3-5 minutes. Growth media was then added to the cell-trypsin mixture to inactivate the effects of trypsin. The cell mixture was then centrifuged at 1000 rpm for 5 minutes to create a cell pellet. The resulting supernatant was then discarded and the cell pellet was resuspended in fresh growth media. A hemocytometer was then used to count cells and cell density was calculated to reseed culture flasks. Immortalized cells were then discarded after 20 passages due to possibility of losing unique brain endothelial cell properties. Primary cells were discarded after 4-6 passages.

Extracellular Flux Analysis

Extracellular flux analysis was performed using the Seahorse Xf96 Bioanalyzer (Agilent Technologies, Santa Clara, CA). This instrument is able to measure oxygen consumption, in real-time, by using sensitive fiber optic probes. These probes create a sealed environment in each well of a 96-well microplate to measure both oxygen levels and acidification of media within the wells (Figure 1). Using this technology, cells can be added to wells, where they would then adhere to the bottom and perform metabolism, consuming both oxygen, from OXPHOS, and producing lactic acid, from glycolysis. The probes would then measure oxygen and pH levels to later quantify respiration and glycolytic rates, respectively. These measurements can be taken in conjunction with timed injections of metabolic inhibitors in order to determine several metabolic characteristics, such as basal OCR, ATP coupled OCR, maximal respiration rates, non-mitochondrial OCR, basal PER, glycolytic PER, compensatory glycolysis, glycolytic ATP production rates, and mitochondrial ATP production rates. Injections are achieved

by utilizing four injection ports surrounding the probe, labeled A-D. Injections are done in a step-wise manner, where port A is injected first, then ports B, C, then D. Compounds within injection ports can be injected at desired times and mixed in wells by agitation of probes moving up and down. Oxygen and pH measurements can then be done for a desired amount of time as well.

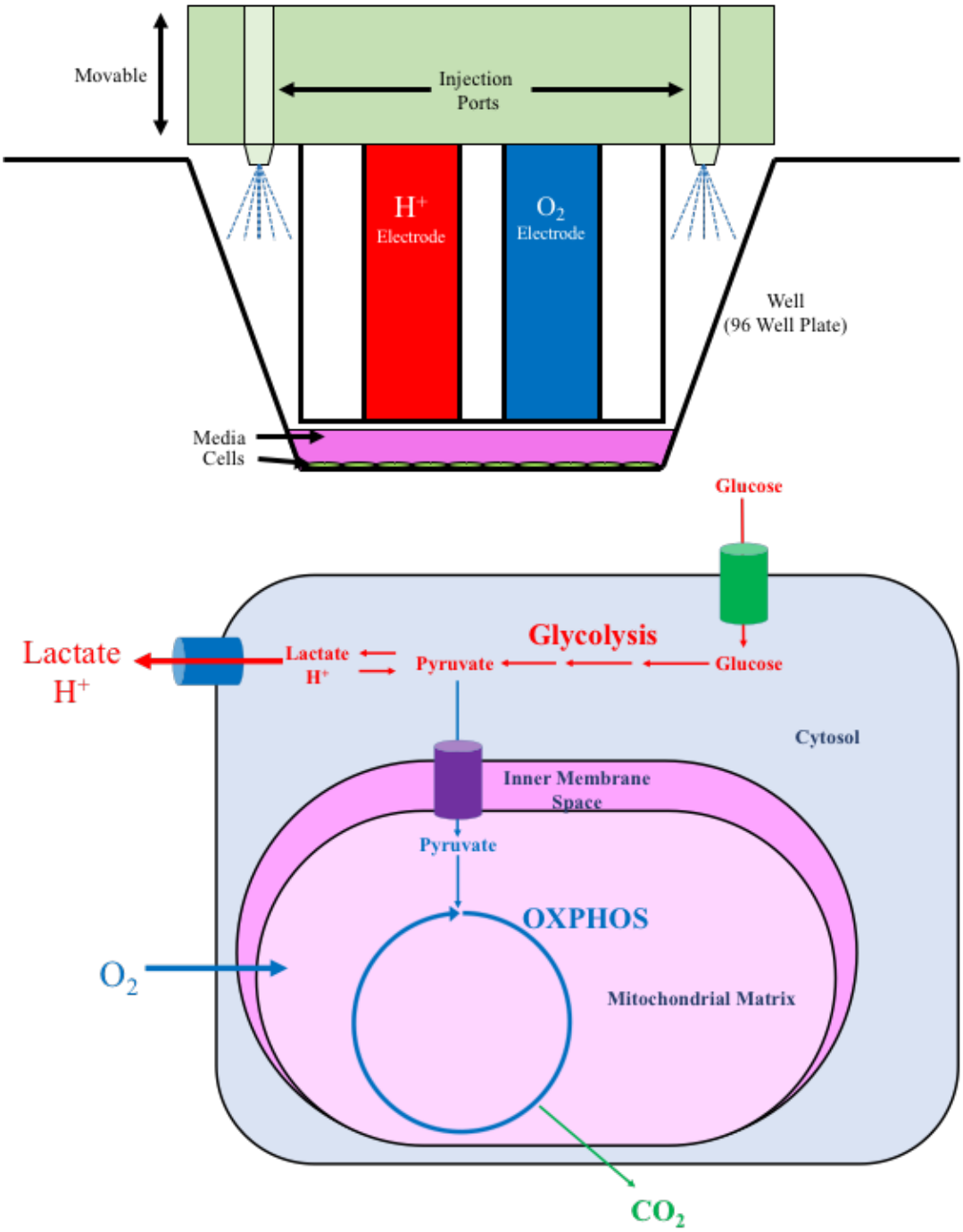

Figure 1: EXTRACELLULAR FLUX ANALYSIS CONFIGURATION AND ECAR/OCR CONTRIBUTIONS Extracellular flux analysis is achieved by utilizing sensitive optic probes, that measure changes in pH and oxygen levels of media, in a sealed environment where cells, adhered to the bottom of the well, perform glycolysis and mitochondrial respiration. Drug delivery ports surrounding the probe allow timed injections of various drugs to measure glycolytic and mitochondrial characteristics (Top). Glycolysis that leads to the conversion of pyruvate into lactic acid, which is then

exported, is the primary contributor to ECAR measurements. The TCA cycle and OXPHOS is the primary contributor to OCR measurements (Below).

Day prior to assay:

Cells were grown to 80-100% confluency, in a T75 cell culture flask, and seeded at 11.5 x 10^3 cells per well in a rat tail type I collagen coated Seahorse XFe96 Spheroid Microplate (Part No. 101085-004). Rat tail type I collagen was purchased from Corning (No. 354236). Cells incubated in the microplate for 20-24 hours at 37°C and 5% CO_2 prior to assays. A sensor cartridge was also hydrated with 200 μL of sterile water, per well, in a non-CO_2 incubator 20-24 hours at 37°C.

Day of Assay:

At least an hour prior to assay, water was replaced with 200 μL of XF calibrant in the sensor cartridge. After the overnight incubation period, growth media was removed by respiration and cells were washed twice with assay media consisting of Seahorse XF minimal base medium supplemented with 5.83 mM glucose, 1.5 mM glutamine, 1 mM pyruvate, pH adjusted to 7.4, and filtered to sterilize. For metabolite studies, an assay media consisting of 5 mM glucose, 5 mM glutamine, 5 mM pyruvate, a combination of two metabolites, or a combination of all three metabolites was used. A total of 175 μL assay media was then added to the wells and cells were incubated at 37°C in assay media, non-CO_2 incubator, one hour prior to the assay. Oligomycin, trifluoromethoxy carbonylcyanide phenylhydrazone (FCCP), rotenone, and antimycin A, for mito stress test and ATP rate studies, were synthesized by the Mereddy Lab at the University of Minnesota, Duluth Campus.

Mito Stress Test:

1 μM oligomycin, 0.5 μM FCCP, and 0.5 μM rotenone/antimycin A were prepared, using assay media, and 25 μL was added to ports A, B, and C in the sensor cartridge, respectively, to be injected into wells at designated times. After one hour of incubation, the 96-well microplate was placed in the Seahorse Bioanalyzer to begin oxygen consumption measurements. Oligomycin, FCCP, and rotenone/antimycin A were injected following three measurements prior to injection (Figure 2). For measurements, three minutes of mixing occurred prior to three minutes of measuring. Oligomycin inhibits ATP synthase, FCCP uncouples the proton gradient between the inter-membrane space and the mitochondrial matrix, and rotenone/antimycin A inhibit complexes I/III of the electron transport chain. Using the differences in measurements following the injection of these compounds, basal, ATP coupled, maximal respiration, spare respiratory capacity, proton leak, and non-mtochondrial OCR values can be calculated (Figure 2).

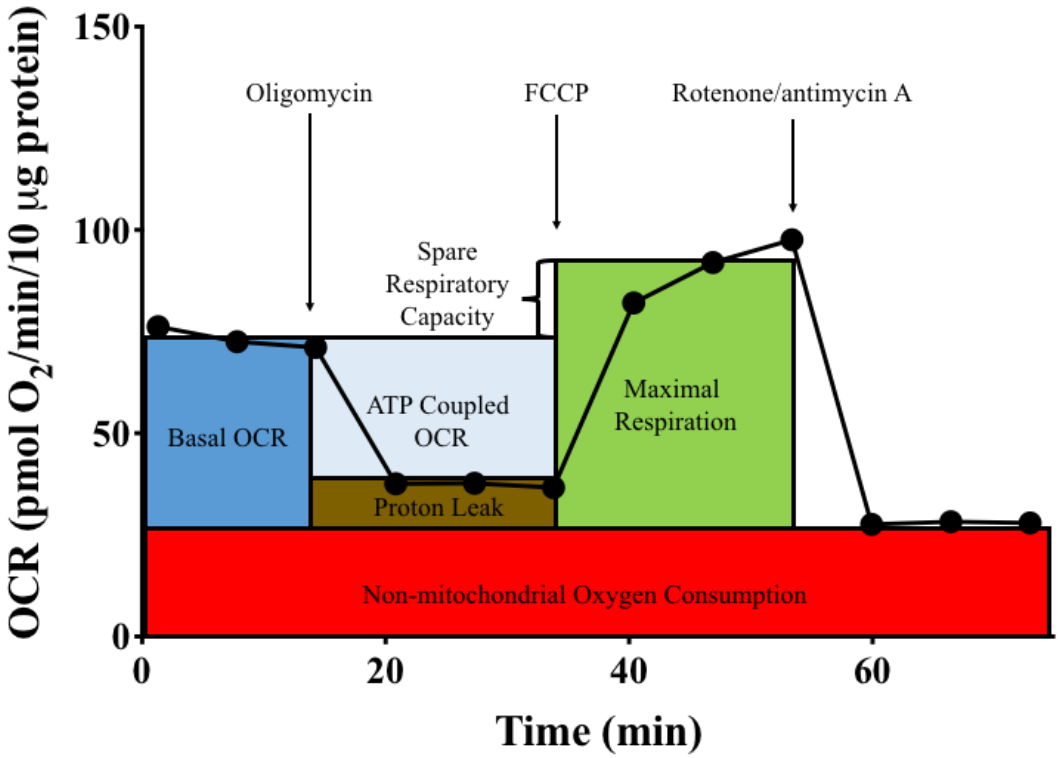

Figure 2: MITO STRESS TEST PROTOCOL A representation of real-time OCR measurements from a mito stress test. Timed injections of oligomycin, FCCP, and rotenone/antimycin A inhibit ATP synthase, uncouple the proton gradient between the inner mitochondrial membrane and the mitochondrial matrix, and inhibit complexes I/III of the mitochondria, respectively. From real-time measurements and timed injections of these compounds, basal OCR, ATP coupled OCR, maximal respiration OCR, spare respiratory capacity OCR, proton leak OCR, and non-mitochondrial OCR can be calculated.

Glycolytic Rate Assay:

50 mM 2-deoxyglucose (2-DG) (Agilent, No. 103344-100) and 0.5 μM rotenone/antimycin A were prepared, using assay media, and 25 μL was added to ports A and B in the sensor cartridge, respectively, to be injected into wells at designated times. Following one hour of incubation, assay media was removed by respiration and fresh assay media was added to cells. The 96-well microplate was then placed in the Seahorse Bioanalyzer to begin extracellular acidification measurements. Rotenone/antimycin A and 2-DG were injected following three measurements prior to injection (Figure 3). For measurements, three minutes of mixing occurred prior to three minutes of measuring. Using real-time ECAR measurements following injection of these compounds, basal, glycolytic, compensatory, and post 2-DG PER values can be calculated (Figure 3).

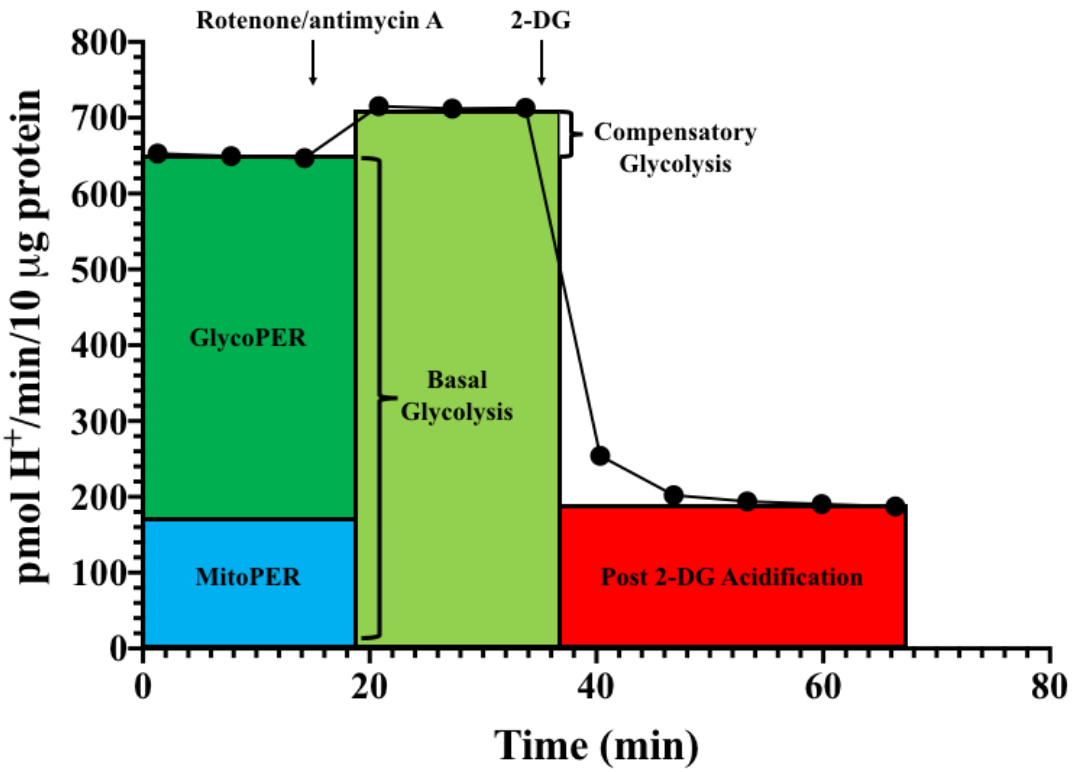

Figure 3: GLYCOLYTIC RATE ASSAY PROTOCOL A representation of real-time PER measurements of a glycolytic rate assay. Timed injections of rotenone/antimycin A and 2-DG inhibit mitochondrial complexes I/III and hexokinase, respectively. From real-time measurements and timed injections of these compounds, basal PER, glycoPER, compensatory glycolyric PER, and post 2-DG acidification can be quantified.

ATP Rate Assays:

For inhibitor assays, 50 nM BAY876 (MedChem Express, Cat. HY-100017), 10 µM AZD3965 (MedKoo Biosciences, Cat. 206040), 10 µM MD1 (University of Minnesota, Duluth Campus, Mereddy Lab), 5 µM UK5099 (MedChem Express, Cat. HY-15475), and 5 µM BPTES (Cayman Chemical Cat. 19284) were prepared, using assay media, and added to designated wells in 96 well plated for the one-hour incubation period at 37°C in a non-CO_2 incubator. 1 µM oligomycin, 0.5 µM FCCP, and 0.5 µM rotenone/antimycin A were prepared, using assay media, and 25 µL was added to ports A, B, and C in the sensor cartridge, respectively, to be injected into wells at designated times to observe

respiratory and glycolytic characteristics. Following the one-hour incubation period, assay media was removed by respiration from each well and fresh assay media, and inhibitors (for inhibitor studies), was added to designated wells. The microplate was then immediately placed in the Seahorse bioanalyzer to begin extracellular flux analysis. Oligomycin was injected following six measurements. Following oligomycin injection, FCCP and rotenone/antimycin A were subsequently injected and allowed three measurements following injection (Figure 4).

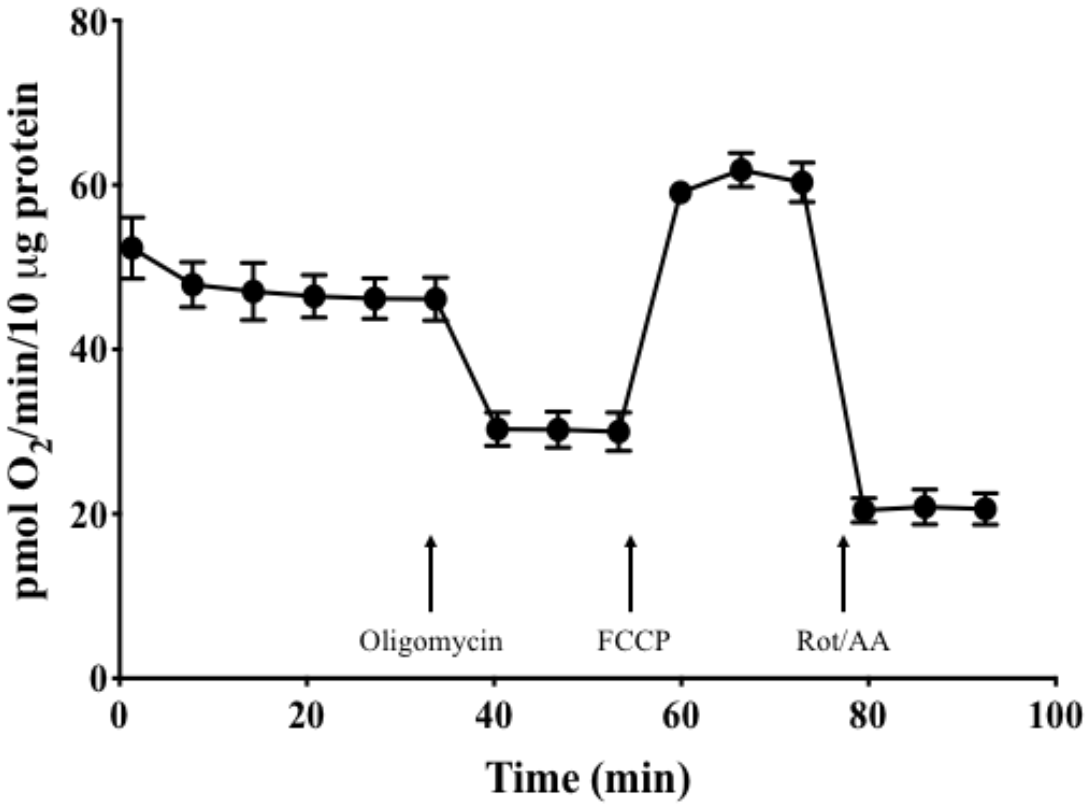

Figure 4: ATP RATE ASSAY PROTOCOL A modified ATP-rate assay was used to measure mitochondrial and glycolytic characteristics of hCMEC/D3 cells by utilizing real-time OCR and ECAR measurements paired with sequential injections of oligomycin, FCCP, and rotenone/antimycin A. Using these real-time measurements, mitochondrial respiration, glycolytic, and ATP production rates were quantified using calculations from mito stress test, glycolytic rate, and ATP production rate equations. OCR measurements were used to calculate basal, ATP coupled, maximal respiration, spare respiratory capacity, proton leak, and non-mitochondrial OCR values along with mitochondrial ATP production rates. ECAR measurements were used to calculate basal PER, glycolytic PER, compensatory glycolytic PER, and glycolytic ATP production rates.

Microscopy

A laser confocal microscope was used to image cells along with mitochondria and DNA. Cultured cells were taken from culture flasks by trypsinization and seeded in 35 mm collagen coated glass bottom (No. 0) petri dishes purchased from MatTek (Part No. P35GCOL-0-10-C). Cells incubated at 37°C and 5% CO_2 for at least 2 days and allowed at least one media change. 150 nM MitoTracker Red CMXRos, purchased from Cell Signaling, (No. 9082S) and 300 nM DAPI, purchased from Thermo Fisher (No. D1306), was prepared in Seahorse minimal basal medium containing 5.83 mM glucose, 1.5 mM glutamine, 1 mM pyruvate, and pH to 7.4. Seahorse minimal basal medium with supplemented metabolites was added to cells, which then incubated at 37°C and 5% CO_2 for one hour. Media was then discarded from cells and 4 mL of the MitoTracker/DAPI basal media solution was added to cells. Cells were then incubated at 37°C and 5% CO_2 for 15-30 minutes. Media and dyes were then discarded and cells were washed with PBS and fixed with cold methanol/1% acetic acid. Cells were then stored in -20°C for at least four hours. Methanol/acetic acid was then discarded and cells were washed with PBS then distilled water. Petri plates were then allowed to dry and then were imaged using the laser confocal microscope.

Data Normalization and Statistical Analysis

To normalize OCR, ECAR, and PER values obtained from real-time measurements, media from wells was discarded immediately following assays, leaving ~20 µL left, and 150 µL of cold methanol/1% acetic acid was added to wells to fix cells. Cells were then stored in -20°C for at least four hours. Methanol/1% acetic acid was then discarded, wells were washed twice with cold PBS, and plates were allowed to air-dry. A BCA protein

assay was then performed on the fixed cells to determine the amount of protein in each well. The protein amount was then used to normalize OCR, ECAR, and PER data to 10 μg of protein. ATP production calculations were done using equations provided by Romero *et al.* (2018) [71]. For hCMEC/D3 and hMVEC comparisons, statistical analysis was not performed because hMVEC came from one individual. For inhibitor and metabolite studies, one-way ANOVA analysis paired with Tukey's method was used to determine statistical significance of data between treatment groups. GraphPad by Prism was the software used for graph construction and statistical analysis. All experiments and treatment groups include a sample size of n=3.

Chapter 3: hCMEC/D3 Cells as a Model for Bioenergetic Studies

hCMEC/D3 cells were chosen as a model for these experiments because of their similarities with primary human brain endothelial cells, ease of culturing, and inexpensiveness. The hCMEC/D3 cell line is extensively characterized and has shown to represent a promising model of the NVU for various studies. Though hCMEC/D3 do not express high trans-endothelial electrical resistance values [5], which is a defining characteristic of the NVU, there are other similarities in tight junction, efflux transporters, surface receptors, and solute carrier expression. A comparative study performed by Eigenmann *et al.* (2013) showed that hCMEC/D3 cells exhibit high expression of brain endothelial cell tight junction proteins zonula occludin-1, VE-cadherin, and claudin-5. Furthermore, Weksler, Romero, and Couraud (2013) show that hCMEC/D3 cells express other brain endothelial cell markers such as CD34, CD31, CD40, CD105, CD144, and von Willebrand factor. hCMEC/D3 cells do not express CD36, which is not present in human brain endothelial cells as well. Weksler *et al.*

(2005) show that hCMEC/D3 cells exhibit similar permeability coefficients to hydrophilic molecules, such as sucrose and inulin, when compared to a bovine co-culture model. There is also decreased permeability to hydrophilic molecules when compared to rat brain endothelial cell lines RBE4 and GPNT. hCMEC/D3 cells express defining human brain endothelial ABC transporters such as P-gp, MDR1, MRPs, and BCRP [72,73]. Ohtsuki *et al.* (2013) show that hCMEC/D3 cells have similar proteomic expression of the transporters Na^+/K^+ ATPase, MCT1, and GLUT1 when compared to human brain microvessels. These defining characteristics of brain endothelial cells are maintained, in culture, until the 35th passage [72]. This allows for various experiments to be performed on these cells over an extended period of time. Extracellular flux analysis of primary human brain microvascular endothelial cells showed similar results to hCMEC/D3 cells (Figure 9 and 10). Therefore, all of the similarities with primary human brain endothelial cells described, culturing simplicity, and extensive characterization, hCMEC/D3 cells are represented as an optimal model for human brain endothelial cell bioenergetic studies. hCMEC/D3 cells create monolayers when in culture and appear to have a flat and thin structure when viewed under DIC microscopy (Figure 5).

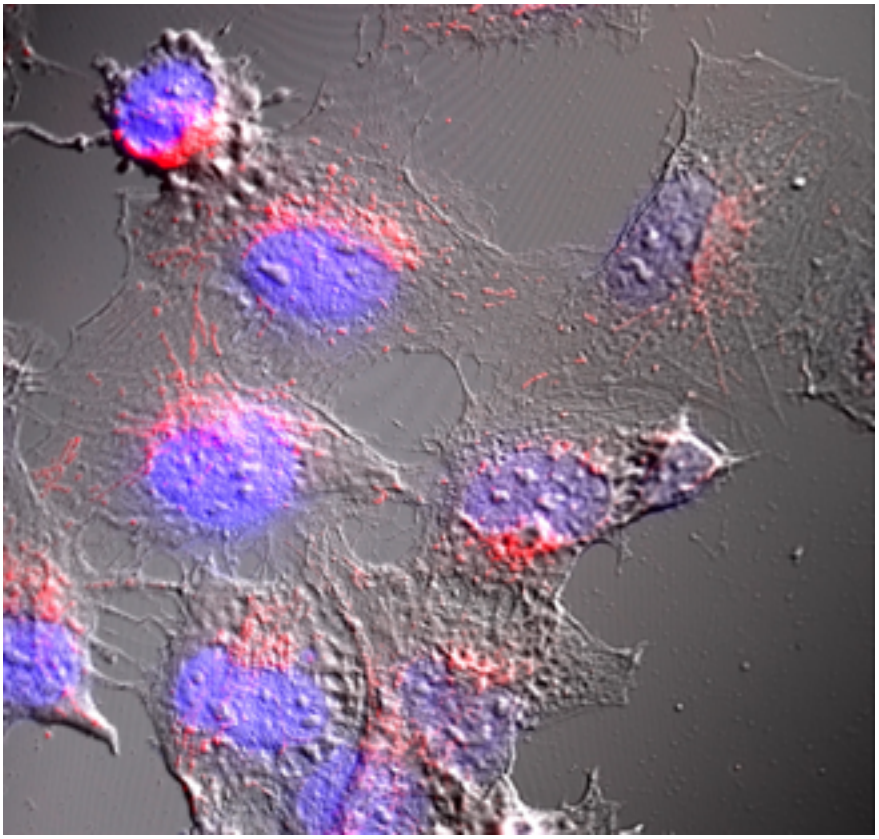

Figure 5: HCMEC/D3 CELL PHOTOMICROGRAPH A photomicrograph of hCMEC/D3 cells at 6300X magnification and differential interference contrast (DIC). Cells were also exposed to MitoTracker Red and DAPI to fluorescently stain mitochondria (red) and nuclei (blue), respectively.

Chapter 4: OCR and ECAR

OXPHOS generates considerably many more ATP molecules (~33) than glycolysis (2) per glucose molecule. ATP synthase exploits the electrical-chemical gradient of protons, produced from the ETC, as a driving force to convert ADP into ATP. This process involves the consumption of oxygen as oxygen acts as a final electron acceptor for the ETC and is converted into H_2O. The Cell Mito Stress test was performed in order to measure mitochondrial characteristics and quantify respiration rates of hCMEC/D3 cells. This assay measures oxygen consumption, in real-time, in conjunction with stepwise additions of oligomycin, FCCP, and Rotenone/Antimycin A in order to calculate various respiratory values and characteristics (Figure 6). Using this test, we were able to

calculate basal respiration, ATP coupled respiration, maximum respiration, spare respiratory capacity, proton leak, and non-mitochondrial oxygen consumption rates of hCMEC/D3 cells. From these oxygen consumption measurements, in real-time, hCMEC/D3 cells exhibited a basal mitochondrial OCR of 44.0, ATP-linked OCR of 34.9, proton leak OCR of 9.1, maximum respiration OCR of 70.8, and non-mitochondrial OCR of 27.6 pmol O_2/min/10μg protein (Figure 7). hCMEC/D3 cells were also able to increase oxygen consumption by 26.7% and couple 79.3% of oxygen consumption to ATP production (Figure 7).

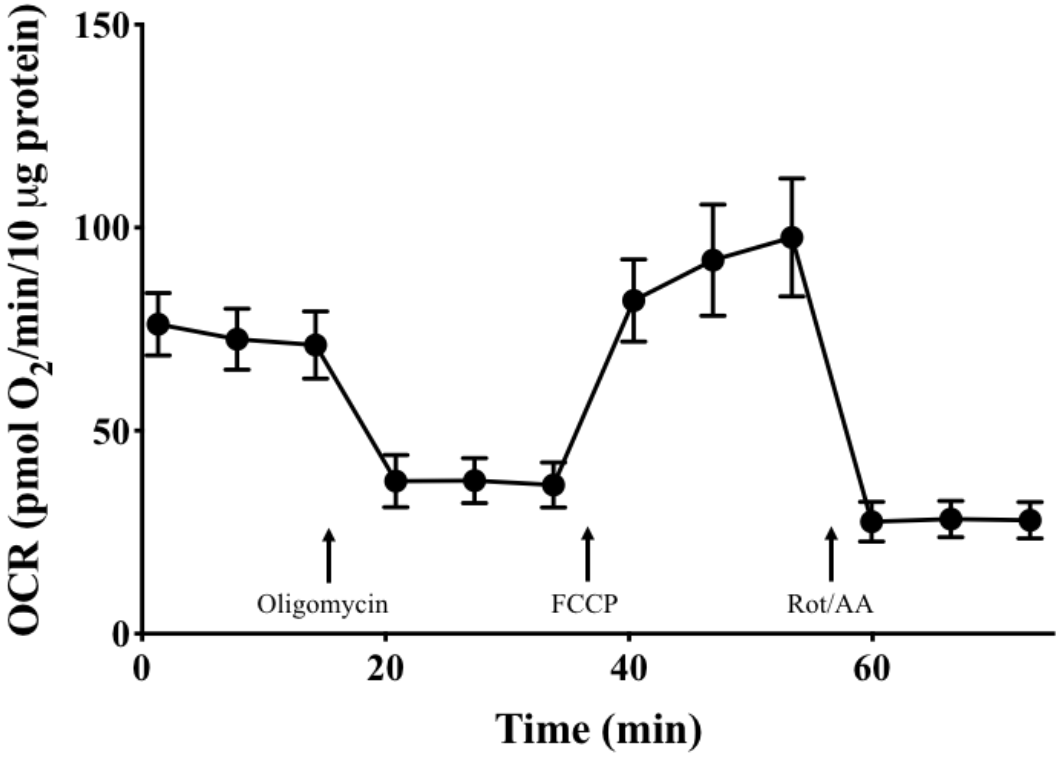

Figure 6: HCMEC/D3 CELL OCR TRACE OCR measurements were taken in-real time in conjunction with step-wise injections of oligomycin, FCCP, and rotenone/antimycin A to characterize mitochondrial respiration values of hCMEC/D3 cells. Real-time OCR measurements were used to calculate basal, ATP coupled, maximal respiration, spare respiratory capacity, proton leak, and non-mitochondrial OCR and were normalized to 10 μg protein. Each point represents a mean measurement of n=3 samples. Error bars represent the SEM.

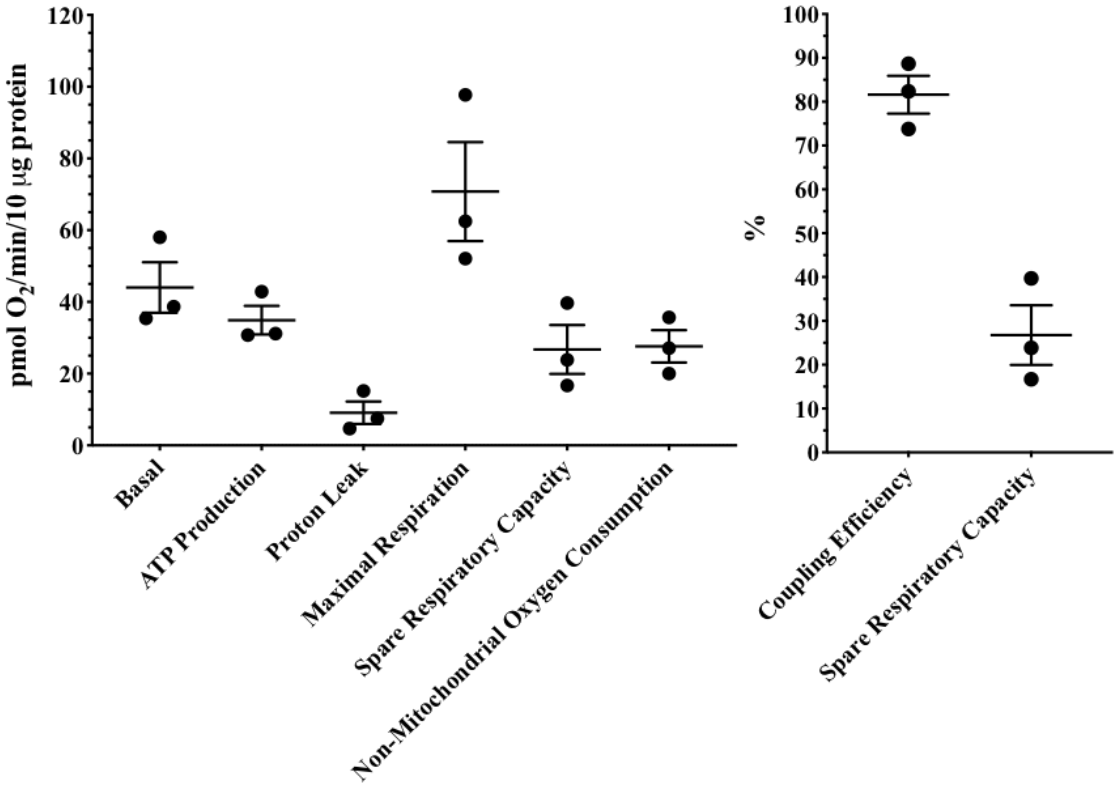

Figure 7: HCMEC/D3 CELL OCR VALUES A scatter dot plot of basal, ATP coupled, maximal respiration spare respiratory capacity, and non-mitochondrial OCR values of hCMEC/D3 cells were calculated, using real-time OCR measurements with injections of oligomycin, FCCP, and rotenone/antimycin A (Left). The coupling efficiency and spare respiratory capacity percentage were also calculated for hCMEC/D3 cells (Right). All measurements were normalized to 10 μg protein. Each point represents one assay. Middle bars and error bars represent the mean and SEM of n=3 measurements, respectively.

By measuring extracellular acidification, the rate of glycolysis in hCMEC/D3 cells could be calculated. To measure glycolytic flux, a glycolytic rate assay was performed. This assay involves measuring extracellular acidification, in real-time, in conjunction with step-wise additions of Rotenone/Antimycin A and 2-deoxyglucose (2-DG) (Figure 3). ECAR can be converted into PER by measuring the buffering capacity of the assay media. PER is considered the rate in which protons are being produced by either glycolysis, CO_2 production, or other cellular processes. Using these measurements and calculations, the basal PER, glycolytic PER (glycoPER), compensatory glycolytic PER, and post 2-DG acidification was calculated for hCMEC/D3 cells. Cells exhibited a basal

PER of 498.9, glycoPER of 483.6, compensatory glycolytic PER of 566.3, and post 2-DG acidification of 55.0 pmol H^+/min/10μg protein (Figure 8). hCMEC/D3 cells are able to increase glycolytic flux by 114%. Furthermore, based on basal PER and glycoPER values, 97.2 % of proton production is attributed to glycolysis (Figure 8).

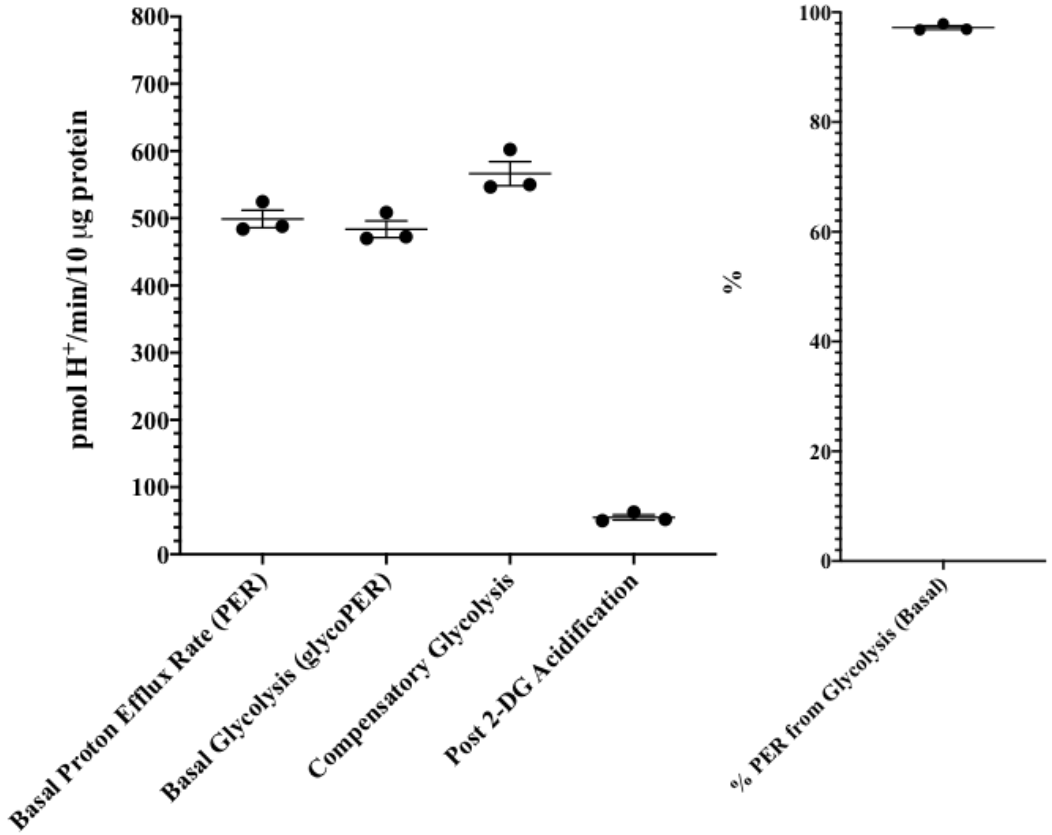

Figure 8: HCMEC/D3 PER VALUES Real-time measurements of extracellular acidification, in conjunction with sequential injections of rotenone/antimycin A and 2-DG, were used to calculate glycolytic characteristics of hCMEC/D3 cells. Basal, glycolytic, compensatory, and post 2-DG acidification PER values (Left), along with % PER from glycolysis (Right), were quantified. All measurements were normalized to 10 μg protein. Each point represents one assay. Middle bars and error bars represent the mean and SEM of n=3 measurements, respectively.

Given these values of mitochondrial and glycolytic characteristics, there was still the question of whether hCMEC/D3 cells could be used as a model for brain endothelial cell bioenergetic analysis. Because there are no known studies regarding brain endothelial cell bioenergetics via extracellular flux analysis, human primary brain microvascular

endothelial cell (hMVEC) bioenergetics was also analyzed. When compared to the measurements of hCMEC/D3 cells, hMVECs showed similar values for mitochondrial characteristics (Figure 9). hMVECs also exhibited similar values for glycolytic measurements as well (Figure 10). This further supports the use of hCMEC/D3 cells for bioenergetic studies of human brain microvascular endothelial cells.

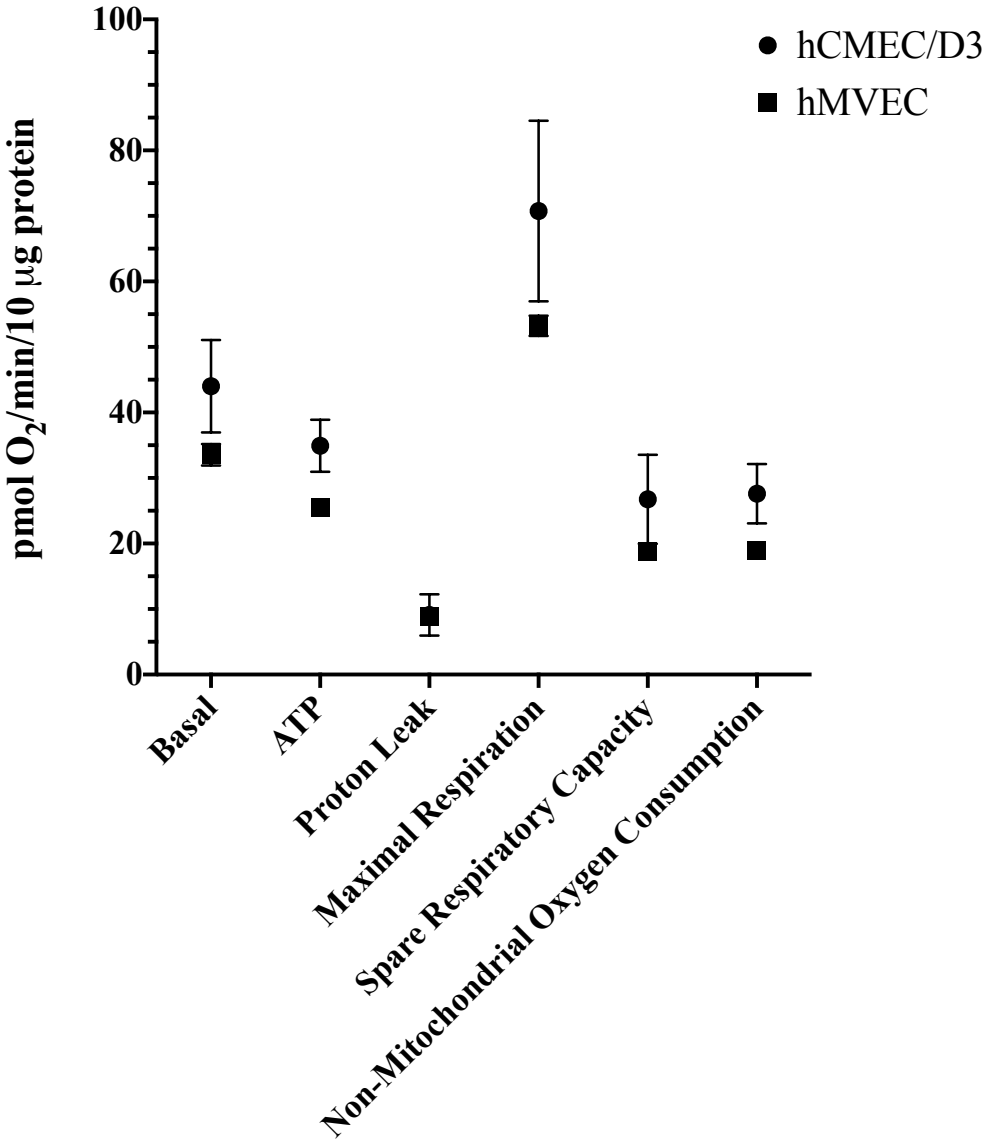

Figure 9: HCMEC/D3 VS. HMVEC OCR VALUES Basal, ATP coupled, proton leak, maximal respiration, spare respiratory capacity, and non-mitochondrial OCR values were measured and compared between hCMEC/D3 cells and hMVECs. All measurements were normalized to 10 μg protein. Each point represents the mean value of three experiments. Error bars represent the SEM of n=3 experiments for hCMEC/D3 cells.

SEM for hMVEC cells could not be measured as three experiments were taken from one sample.

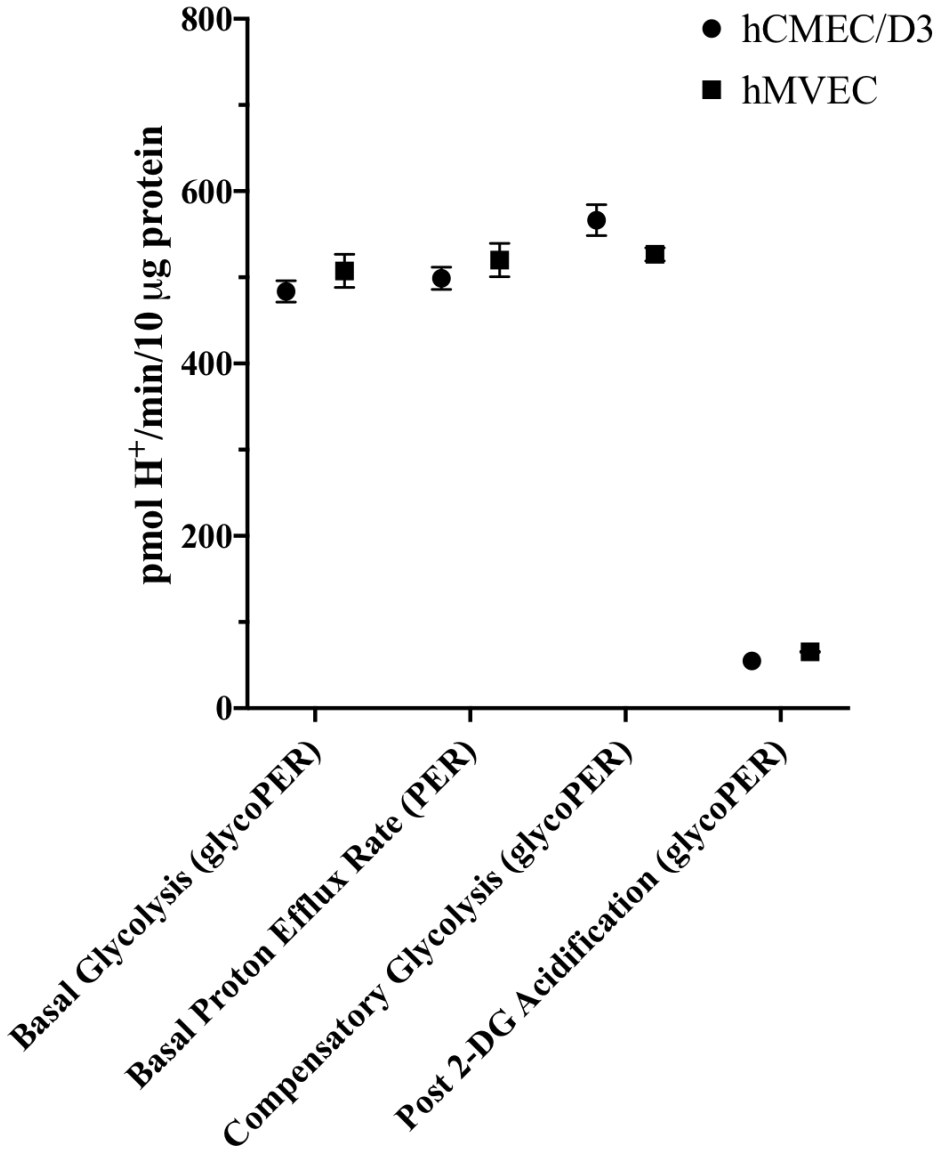

Figure 10: HCMEC/D3 VS. HMVEC PER VALUES Basal, glycolytic, compensatory, and post 2-DG PER values were calculated and compared between hCMEC/D3 cells and hMVECs. All measurements were normalized to 10 μg protein. Each point represents the mean value of three experiments. Error bars represent the SEM of n=3 experiments for hCMEC/D3 cells. SEM for hMVEC cells could not be measured as three experiments were taken from one sample.

Chapter 5: ATP Production Rates

Many cellular processes require ATP to fuel metabolic and signaling pathways. Two main ATP producing pathways are glycolysis and OXPHOS. Brain endothelial cells use

ATP to perform and maintain many cellular functions, transportation, and signaling important for NVU integrity and function. Using equations provided by Romero *et al.* (2018), OCR and PER measurements can be used to calculate the ATP production rate from the mitochondria or glycolysis, respectively. Equations 1-7, below, were used to calculate mitochondrial and glycolytic ATP production rates for hCMEC/D3 cells. OCR values are in pmol O_2/min, PER values are in pmol H^+/min, and ATP production rates are in pmol/min/10 μg protein. Vol_{XF} represents the geometric volume of the sealed microplate well and is 2.28 μL (Equation 3). The buffer factor is calculated for each assay media and each assay media has a unique buffer factor. Kvol represents the volume scaling factor and is 1.6 for the XFe96 (Equation 3). CCF represents the CO_2 Contribution Factor, in which how much CO_2 contributes to ECAR measurements, and has a value of 0.61 for the XFe96 (Equation 4). Equations are provided by Romero *et al.* (2018).

Equation 1	Glycolytic ATP production rate = GlycoPER
Equation 2	glycoPER = PER - mitoPER
Equation 3	PER = ECAR x Buffer Factor x $Vol_{XF\ microchamber}$ x Kvol
Equation 4	mitoPER = mitoOCR x CCF
Equation 5	mitoOCR = OCR_{basal} - $OCR_{rot/AA}$
Equation 6	OCR_{ATP} = OCR_{basal} - OCR_{oligo}
Equation 7	Mitochondrial ATP production rate = OCR_{ATP} x 2 x P/O

The difference in OCR between basal measurements and following addition of oligomycin, an ATP synthase inhibitor, is proportional to the amount of OCR coupled

with ATP production. This value is then multiplied by two, to convert to O atoms, and also multiplied by the number of molecules of ATP synthesized per atom of O (P/O value). The P/O ratio values may differ slightly based on cell types and metabolite composition. However, a P/O ratio value of 2.75 seemed to be the most fitting for multiple cell types, according to Romero *et al.* (2018). Given this information, a P/O value of 2.75 was used for hCMEC/D3 cells [71]. Glycolytic ATP rates can be calculated by using glycoPER values. Glycolysis produces two ATP molecules and two lactate molecules, which are subsequently exported with a proton, therefore, proton production from glycolysis is directly proportional to glycolytic ATP production. OCR and PER measurements of hCMEC/D3 revealed that the ATP production rates from glycolysis and OXPHOS are 527.8 and 88.4 pmol ATP/min/10 µg protein, respectively (Figure 11). Therefore, the total ATP production rate of hCMEC/D3 cells is 616.2 pmol ATP/min/10µg protein (Figure 11), where 85.7% is contributed from glycolysis and 14.3% is contributed from OXPHOS. The glycolytic ATP production rate of these cells is significantly higher than the mitochondrial ATP production rate.

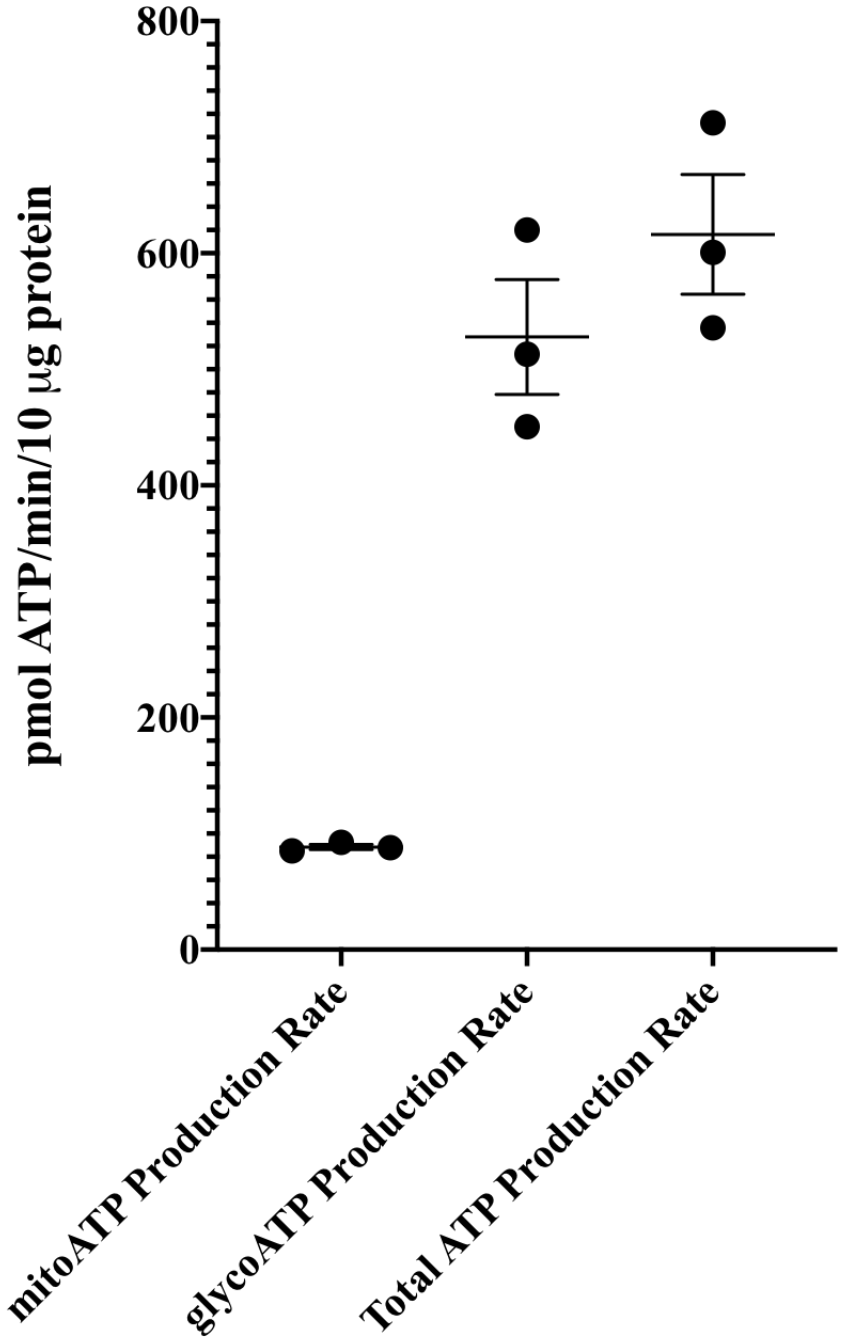

Figure 11: HCMEC/D3 CELL ATP PRODUCTION RATES Mitochondrial, glycolytic, and total ATP production rates were calculated, using equations provided in Table 1, for hCMEC/D3 cells. All measurements were normalized to 10 μg protein. Each point represents a single measurement and error bars represent SEM of n=3 samples.

Chapter 6: Metabolite Effect on Bioenergetics

There are a variety of molecules that are able to fuel cellular metabolism, such as glucose, glutamine, and pyruvate (Figure 12). The most considerable of these molecules is glucose. Glucose acts as the main source of energy for cellular metabolism for many tissues, and cell types, and is the most abundant metabolite in blood serum [74]. Many molecules are also able to fuel the TCA cycle through a wide range of enzymatic reactions. Of these metabolites, glutamine and pyruvate are two metabolic substrates that are able to enter the TCA cycle with ease and are readily available in blood serum [48,74,75]. Utilizing glucose, glutamine, and pyruvate allows cells to generate molecules necessary for macromolecules, amino acids, nucleic acids, various cellular compartments, and to maintain cellular ATP production [37,44,56,57]. Based on the availability of these metabolites, distinct cell types may be able to utilize different metabolites to fuel ATP production. hCMEC/D3 cells were presented with 5 mM of glucose, glutamine, pyruvate, glucose + glutamine, glucose + pyruvate, glutamine + pyruvate, and all three metabolites. Using timed injections of oligomycin, FCCP, and rotenone/antimycin A (Figures 13 and 14), oxygen consumption, glycolysis, and ATP production rates were measured, using extracellular flux analysis, based on these metabolites and combinations. An equal concentration (5 mM) of each metabolite was used to eliminate preference based on concentration.

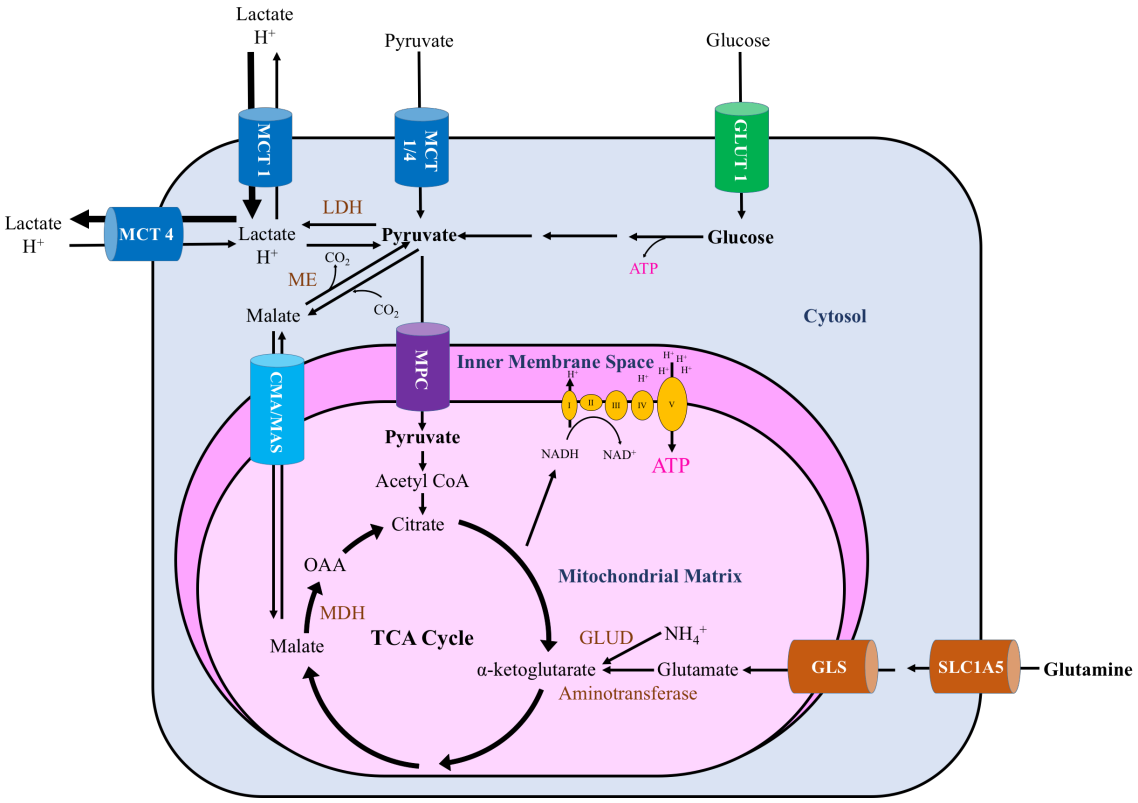

Figure 12: CELLULAR METABOLITE PATHWAYS A schematic representation of common cellular energy producing pathways of glucose, pyruvate, and glutamine. LDH=lactate dehydrogenase, GLS=glutaminase, GLUD=glutamate dehydrogenase, ME= malic enzyme, MDH= malate dehydrogenase, and CMA/MAS= citrate malate antiporter/malate aspartate shuttle.

Complete Media:

In the presence of assay media containing all three metabolites, at 5 mM concentrations, the basal OCR of hCMEC/D3 cells was 57.6 pmol O_2/min/10 µg protein (Figure 15). Mitochondrial respiration values calculated from OCR measurements, in real-time, displayed ATP coupled OCR of 44.7 pmol O_2/min/10 µg protein, resulting in 77.8% of basal oxygen being coupled with ATP production (Figures 16 and 17). Maximal respiration and spare respiratory capacity OCR values were 90.2 and 32.6 pmol O_2/min/10 µg protein, respectively (Figures 18 and 19). Lastly, proton leak and non-mitochondrial OCR values were calculated to be 12.8 and 21.9 pmol O_2/min/10 µg

protein, respectively (Figures 20 and 21). From PER measurements, the compensatory PER was calculated as 244.6 pmol H^+/min/ 10 μg protein (Figure 22). Using OCR and PER measurements, we were able to also calculate mitochondrial and glycolytic ATP production rates, respectively. Calculated mitochondrial and glycolytic ATP production rates were 246.1 and 199.5 pmol ATP/min/10 μg protein, respectively (Figures 23 and 24). Therefore, the total ATP production rate was 445.6 pmol ATP/min/10 μg protein (Figure 25).

Glucose Media:

When 5 mM glucose was the only available metabolite, Basal OCR showed to be significantly lower than cells in the complete media (Figure 15). Basal OCR of hCMEC/D3 cells in glucose only media was calculated to be 34.2 pmol O_2/min/10 μg protein (Figure 15). ATP coupled OCR was also lowered in glucose compared to complete media (Figure 16). However, the coupling efficiency was not affected (Figure 17). Mitochondrial respiration values calculated from OCR measurements, in real-time, displayed ATP coupled OCR of 25.0 pmol O_2/min/10 μg protein, resulting in 72.9% of basal oxygen being coupled with ATP production (Figures 16 and 17). Maximal respiration and, subsequently, spare respiratory capacity were also significantly lower compared to cells in complete media (Figures 18 and 19). Maximal respiration and spare respiratory capacity OCR values were 19.2 and -15.0 pmol O_2/min/10 μg protein, respectively (Figures 18 and 19). Both proton leak and non-mitochondrial OCR did not change in cells with only glucose as a metabolite (Figures 20 and 21). Proton leak and non-mitochondrial OCR values were calculated to be 9.2 and 20.7 pmol O_2/min/10 μg protein, respectively (Figures 20 and 21). From PER measurements, the compensatory

PER was calculated as 90.7 pmol H^+/min/ 10 μg protein (Figure 22). The mitochondrial ATP production rate in hCMEC/D3 cells was lowered with glucose as the only available metabolite (Figure 23). However, the glycolytic ATP production rate increased compared to cell in complete media (Figure 24). Calculated mitochondrial and glycolytic ATP production rates were 137.4 and 323.6 pmol ATP/min/10 μg protein, respectively (Figures 23 and 24). However, total ATP production rates did not change compared to the complete media (Figure 25). The total ATP production rate in hCMEC/D3 cells in glucose only media, therefore, was 461.0 pmol ATP/min/10 μg protein (Figure 25).

Glutamine Media:

When in the presence of assay media containing 5 mM glutamine only, the basal OCR of hCMEC/D3 cells was significantly higher than cells in complete media (Figure 15). Basal OCR of cells in glutamine was calculated as 82.7 pmol O_2/min/10 μg protein (Figure 15). Similarly, ATP coupled OCR in cells with glutamine only was also higher than cells in complete media (Figure 16). However, the coupling efficiency did not change (Figure 17). Mitochondrial respiration values calculated from OCR measurements, in real-time, displayed ATP coupled OCR of 61.5 pmol O_2/min/10 μg protein (Figure 16), resulting in 74.3% of basal oxygen being coupled with ATP production (Figure 17). Calculated maximal respiration and spare respiratory capacity OCR values were lower than values of cells in complete media (Figures 18 and 19). Maximal respiration and spare respiratory capacity OCR values were 65.3 and -17.4 pmol O_2/min/10 μg protein, respectively (Figures 18 and 19). Cells in media with glutamine alone showed higher proton leak OCR than cells in complete media (Figure 20). However, non-mitochondrial OCR was not changed (Figure 21). Proton leak and non-

mitochondrial OCR values were calculated to be 21.2 and 25.0 pmol O_2/min/10 μg protein, respectively (Figures 20 and 21). From PER measurements, the compensatory PER was calculated as -23.1 pmol H^+/min/ 10 μg protein (Figure 22). Calculated mitochondrial ATP production rates of cells in glutamine media were higher than cells in complete media (Figure 23). However, glycolytic ATP production rates were much lower than cells in complete media (Figure 24). Calculated mitochondrial and glycolytic ATP production rates were 338.4 and 9.2 pmol ATP/min/10 μg protein, respectively (Figures 23 and 24). The total ATP production rate was 347.6 pmol ATP/min/10 μg protein, which showed to be lower than cells in the complete media (Figure 25).

Pyruvate Media:

In the presence of assay media containing 5 mM pyruvate, hCMEC/D3 cells displayed higher basal OCR values than cells in complete media (Figure 15). Basal OCR of hCMEC/D3 cells in pyruvate media was calculated as 76.7 pmol O_2/min/10 μg protein (Figure 15). ATP coupled OCR values was also higher in cells with pyruvate as an only metabolite than cells in complete media (Figure 16). Coupling efficiency, however, was not altered compared to cells in complete media (Figure 17). Mitochondrial respiration values calculated from OCR measurements, in real-time, displayed ATP coupled OCR of 65.0 pmol O_2/min/10 μg protein (Figure 16), resulting in 84.7% of basal oxygen being coupled with ATP production (Figure 17). Maximal respiration OCR did not show any difference compared to cells in complete media (Figure 18). However, spare respiratory capacity OCR values was significantly lower than complete media (Figure 19). Maximal respiration and spare respiratory capacity OCR values were 74.3 and -2.4 pmol O_2/min/10 μg protein, respectively (Figures 18 and 19). Proton leak and non-

mitochondrial OCR values of cells with pyruvate alone showed to be higher than complete media cells (Figures 20 and 21). Calculated proton leak and non-mitochondrial OCR values were calculated to be 11.7 and 28.3 pmol O_2/min/10 μg protein, respectively (Figures 20 and 21). From PER measurements, the compensatory PER was calculated as -37.9 pmol H^+/min/ 10 μg protein (Figure 22). Mitochondrial ATP production rates were significantly higher in cells treated with pyruvate (Figure 23). Contrarily, glycolytic ATP production rates were lower for cells with pyruvate media compared to complete media (Figure 24). Calculated mitochondrial and glycolytic ATP production rates were 357.7 and 26.4 pmol ATP/min/10 μg protein, respectively (Figures 23 and 24). Total ATP production rates, however, did not change for cells in pyruvate media in comparison to complete media (Figure 25). The total ATP production rate was 384.0 pmol ATP/min/10 μg protein (Figure 25).

Glucose + Glutamine Media:

hCMEC/D3 cells, when treated with 5 mM glucose and glutamine, exhibited basal OCR values that were significantly lower than cells in complete media (Figure 15). The calculated basal OCR of hCMEC/D3 cells in glucose + glutamine media was 41.5 pmol O_2/min/10 μg protein (Figure 15). ATP coupled OCR was also lower in cells with glucose and glutamine as metabolites in comparison to cells in complete media (Figure 16). The coupling efficiency, however, was not different than complete media cells (Figure 17). OCR measurements, in real-time, displayed ATP coupled OCR of 30.1 pmol O_2/min/10 μg protein (Figure 16), resulting in 72.5% of basal oxygen being coupled with ATP production (Figure 17). Maximal respiration and spare respiratory capacity OCR values in cells with glucose and glutamine were also lower than cells in complete media

(Figures 18 and 19). Calculated maximal respiration and spare respiratory capacity OCR values were 45.4 and 3.9 pmol O_2/min/10 μg protein, respectively (Figures 18 and 19). Proton leak and non-mitochondrial oxygen consumption values of cells, in glucose and glutamine media, did not exhibit a significant difference when compared to cells in complete media (Figures 20 and 21). Proton leak and non-mitochondrial OCR values were calculated to be 11.4 and 20.3 pmol O_2/min/10 μg protein, respectively (Figures 20 and 21). From PER measurements, the compensatory PER was calculated as 168.5 pmol H^+/min/ 10 μg protein (Figure 22). Mitochondrial ATP production rates in cells with glucose and glutamine as metabolites was lower than cells in complete media (Figure 23). In contrast, glycolytic ATP production rates were significantly higher compared to cells in complete media (Figure 24). Calculated mitochondrial and glycolytic ATP production rates were 165.7 and 327.3 pmol ATP/min/10 μg protein, respectively (Figures 23 and 24). The total ATP production rates, for cells in glucose + glutamine media, remained unchanged from cells in complete media (Figure 25). The total ATP production rate was 493.0 pmol ATP/min/10 μg protein (Figure 25).

Glucose + Pyruvate Media:

hCMEC/D3 cells, in the presence of assay media containing 5 mM glucose and pyruvate, showed lower basal OCR values than cells in complete media (Figure 15). The calculated basal OCR of cells in glucose + pyruvate media was 42.9 pmol O_2/min/10 μg protein (Figure 15). Cells in glucose + pyruvate media also had decreased ATP coupled OCR values in comparison to cells in complete media (Figure 16). Coupling efficiency remained statistically unchanged compared to cells in complete media (Figure 17). Mitochondrial respiration values calculated from OCR measurements, in real-time,

displayed ATP coupled OCR of 33.4 pmol O_2/min/10 μg protein (Figure 16), resulting in 77.8% of basal oxygen being coupled with ATP production (Figure 17). Cells treated with glucose and pyruvate displayed maximal respiration and spare respiratory capacity OCR values lower than cells in complete media (Figures 18 and 19). Calculated maximal respiration and spare respiratory capacity OCR values were 41.0 and -2.0 pmol O_2/min/10 μg protein, respectively (Figures 18 and 19). Cells in glucose + pyruvate did not exhibit changes in either proton leak or non-mitochondrial oxygen consumption when compared to cells in complete media (Figures 20 and 21). Proton leak and non-mitochondrial OCR values were calculated to be 9.5 and 20.5 pmol O_2/min/10 μg protein, respectively (Figures 20 and 21). From PER measurements, the compensatory PER was calculated as 117.1 pmol H^+/min/ 10 μg protein (Figure 22). Mitochondrial ATP production rates of cells in glucose + pyruvate media decreased in comparison to cells in complete media, while glycolytic ATP production rates increased (Figures 23 and 24). Calculated mitochondrial and glycolytic ATP production rates were 183.7 and 235.5 pmol ATP/min/10 μg protein, respectively (Figures 23 and 24). Total ATP production rates did not change between the two media groups (Figure 25). Total ATP production rate was 419.2 pmol ATP/min/10 μg protein (Figure 25).

Glutamine + Pyruvate Media:

Lastly, cells in the presence of assay media containing 5 mM glutamine and pyruvate displayed higher basal OCR values compared to cells in complete media (Figure 15). The basal OCR of hCMEC/D3 cells was calculated as 86.9 pmol O_2/min/10 μg protein (Figure 15). Similarly, ATP coupled OCR values were significantly higher than those of complete media (Figure 16). Coupling efficiency was not different between the two

media groups, though (Figure 17). OCR measurments, in real-time, revealed ATP coupled OCR of 67.8 pmol O_2/min/10 μg protein (Figure 16), resulting in 78.0% of basal oxygen being coupled with ATP production (Figure 17). Cells in glutamine + pyruvate media showed lower maximal respiration and spare respiratory values than cells in complete media (Figures 18 and 19). Maximal respiration and spare respiratory capacity OCR values were calculated to be 66.5 and -20.4 pmol O_2/min/10 μg protein, respectively (Figures 18 and 19). Cells in glutamine + pyruvate media exhibited higher proton leak and non-mitochondrial OCR values than complete media cells (Figures 20 and 21). Proton leak and non-mitochondrial OCR values were calculated to be 19.1 and 29.1 pmol O_2/min/10 μg protein, respectively (Figures 20 and 21). From PER measurements, the compensatory PER was calculated as -33.6 pmol H^+/min/ 10 μg protein (Figure 22). Calculated mitochondrial and glycolytic ATP production rates were higher and lower, respectively, compared to complete media (Figures 23 and 24). Mitochondrial and glycolytic ATP production rates were 372.8 and 29.9 pmol ATP/min/10 μg protein, respectively (Figures 23 and 24). The total ATP production rate was 402.7 pmol ATP/min/10 μg protein, which was not significantly different than cells in complete media (Figure 25).

Interestingly, though mitoATP and glycoATP production rates of hCMEC/D3 cells increased or decreased based on media composition, the total ATP production rate was able to be maintained for all, besides glutamine, metabolite groups. hCMEC/D3 cells in all media groups also showed lower total ATP production rates than cells in assay media containing glucose, glutamine, and pyruvate at concentrations of 5.83 mM, 1.5 mM, and 1 mM, respectively.

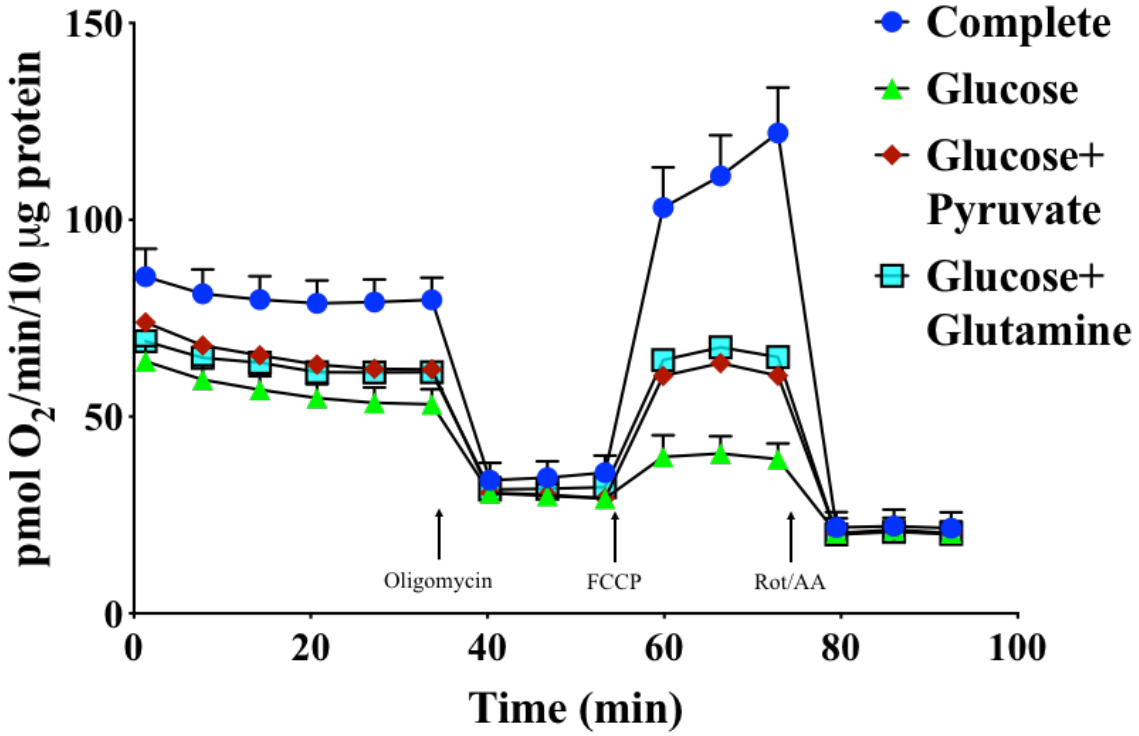

Figure 13: HCMEC/D3 CELL METABOLITE OCR TRACE (A) OCR and ECAR (not shown) measurements were taken in-real time and in conjunction with step-wise injections of oligomycin, FCCP, and rotenone/antimycin A to characterize mitochondrial respiration, glycolytic, and ATP production rate values of hCMEC/D3 cells. Real-time measurements shown are from cells treated with a complete media consisting of 5 mM glucose + 5 mM glutamine + 5 mM pyruvate, 5 mM glucose, 5 mM glucose + 5 mM pyruvate, or 5 mM glucose + 5 mM glutamine. Measurements were normalized to 10 µg protein. Each point represents a mean measurement and error bars represent SEM of n=3 samples.

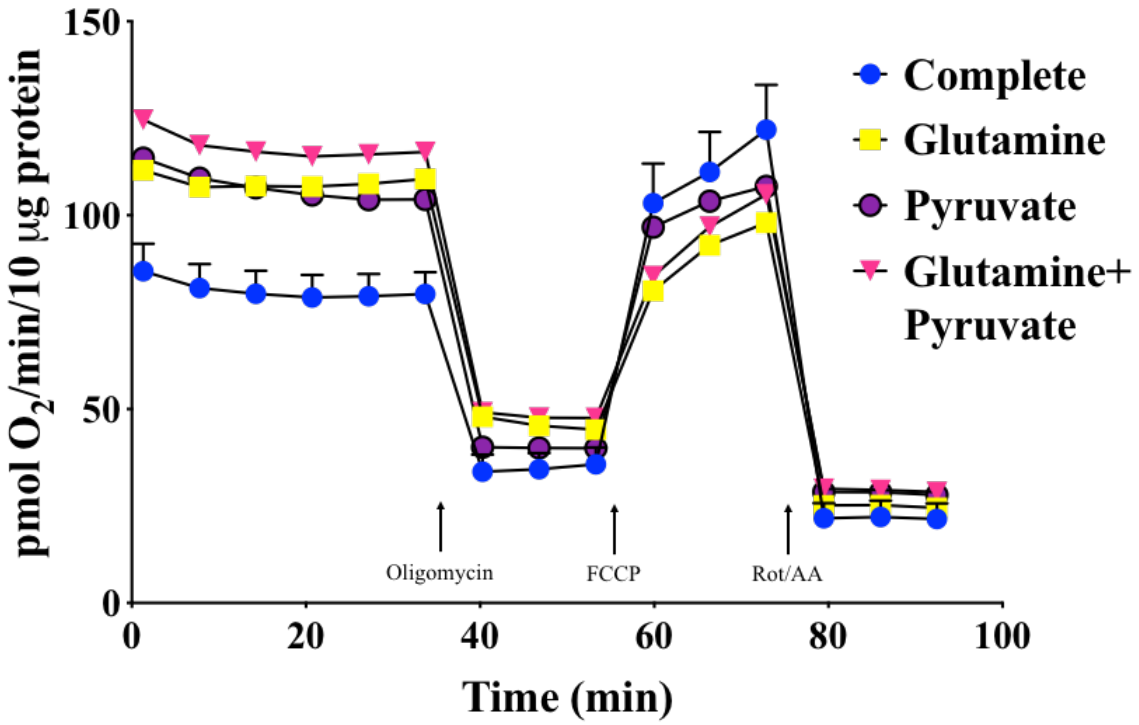

Figure 14: HCMEC/D3 CELL METABOLITE OCR TRACE (B) OCR and ECAR (not shown) measurements were taken in-real time and in conjunction with step-wise injections of oligomycin, FCCP, and rotenone/antimycin A to characterize mitochondrial respiration, glycolytic, and ATP production rate values of hCMEC/D3 cells. Real-time measurements shown are from cells treated with a complete media consisting of 5 mM glucose + 5 mM glutamine + 5 mM pyruvate, 5 mM glutamine, 5 mM pyruvate, or 5 mM glutamine + 5 mM pyruvate. Measurements were normalized to 10 µg protein. Each point represents a mean measurement and error bars represent SEM of n=3 samples.

Table 1: HCMEC/D3 CELL METABOLITE ENERGETIC VALUES OCR, Compensatory PER (Comp PER), mitochondrial ATP production rate (mitoATP), glycolytic ATP production rate (glycoATP), and total ATP production rate values were calculated for cells treated with each media type. OCR, PER, and ATP production rate values are expressed as pmol O_2, H^+, and ATP/min/10 µg protein, respectively

	Basal OCR	ATP coupled OCR	Coupling Efficiency (%)	Maximal Respiration OCR	Spare Respiratory Capacity OCR	Proton Leak OCR
Complete Media	57.6	44.7	77.8	90.2	32.6	12.8
Glucose Media	34.2	25.0	72.9	19.2	-15.0	9.2
Glucose + Glutamine Media	41.5	30.1	72.5	45.4	3.9	11.4
Glucose + Pyruvate Media	42.9	33.4	77.8	41.0	-2.0	9.5
Pyruvate Media	76.7	65.0	84.7	74.3	-2.4	11.7
Glutamine Media	82.7	61.5	74.3	65.3	-17.4	21.2
Glutamine + Pyruvate Media	86.9	67.8	78.0	66.5	-20.4	19.1

	Non-mito OCR	Comp PER	mitoATP	glycoATP	Total ATP
Complete Media	21.9	244.6	246.1	199.5	445.6
Glucose Media	20.7	90.7	137.4	323.6	461.0
Glucose + Glutamine Media	20.3	168.5	165.7	327.3	493.0
Glucose + Pyruvate Media	20.5	117.1	183.7	235.5	419.2
Pyruvate Media	28.3	-37.9	357.7	26.4	384.0
Glutamine Media	25.0	-23.1	338.4	9.2	347.6
Glutamine + Pyruvate Media	29.1	-33.6	372.8	29.9	402.7

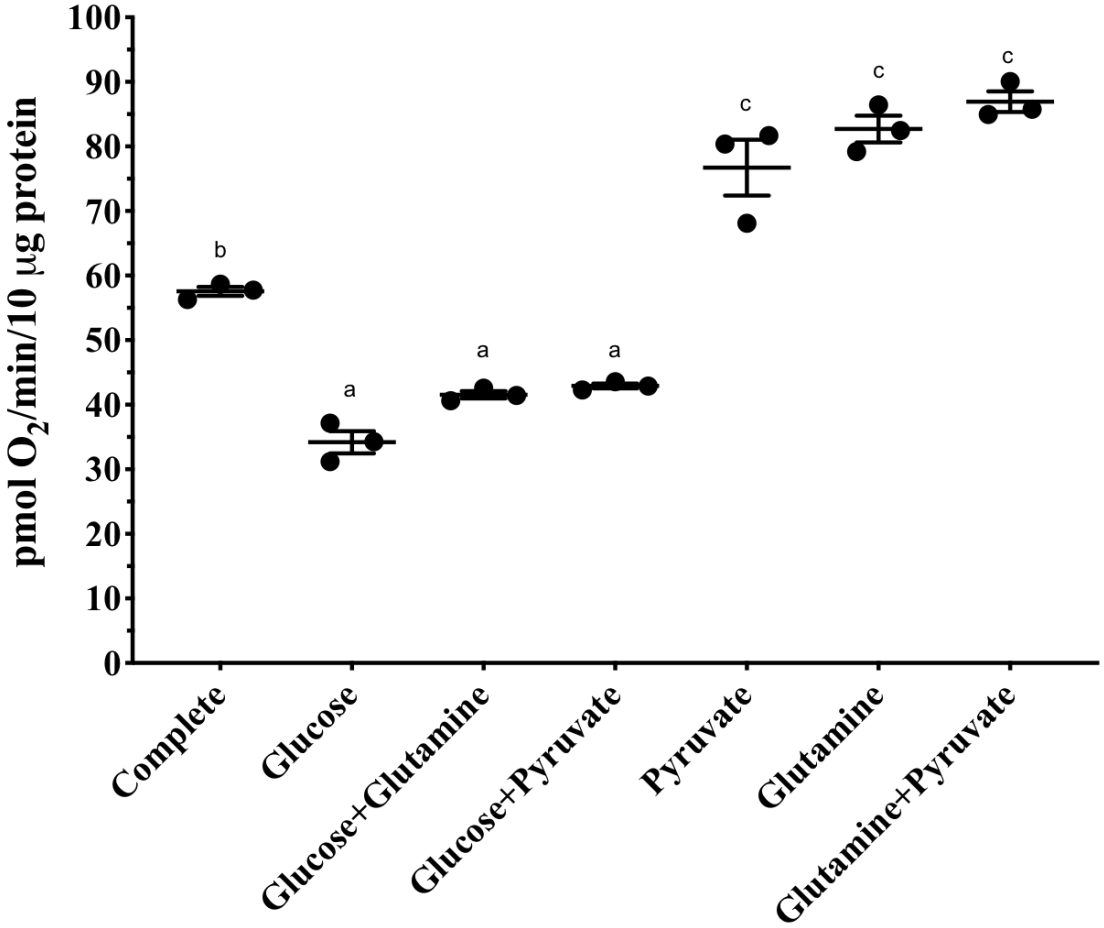

Figure 15: HCMEC/D3 METABOLITE BASAL OCR Basal OCR values of hCMEC/D3 cells were calculated, based on real-time OCR measurements, for each metabolite group. Values from each metabolite group were compared to each other group. All measurements were normalized to 10 µg protein. Each point represents a single measurement and error bars represent SEM of n=3 samples. Shared letters indicate no significant difference. Absence of a shared letter indicates a significant difference between groups.

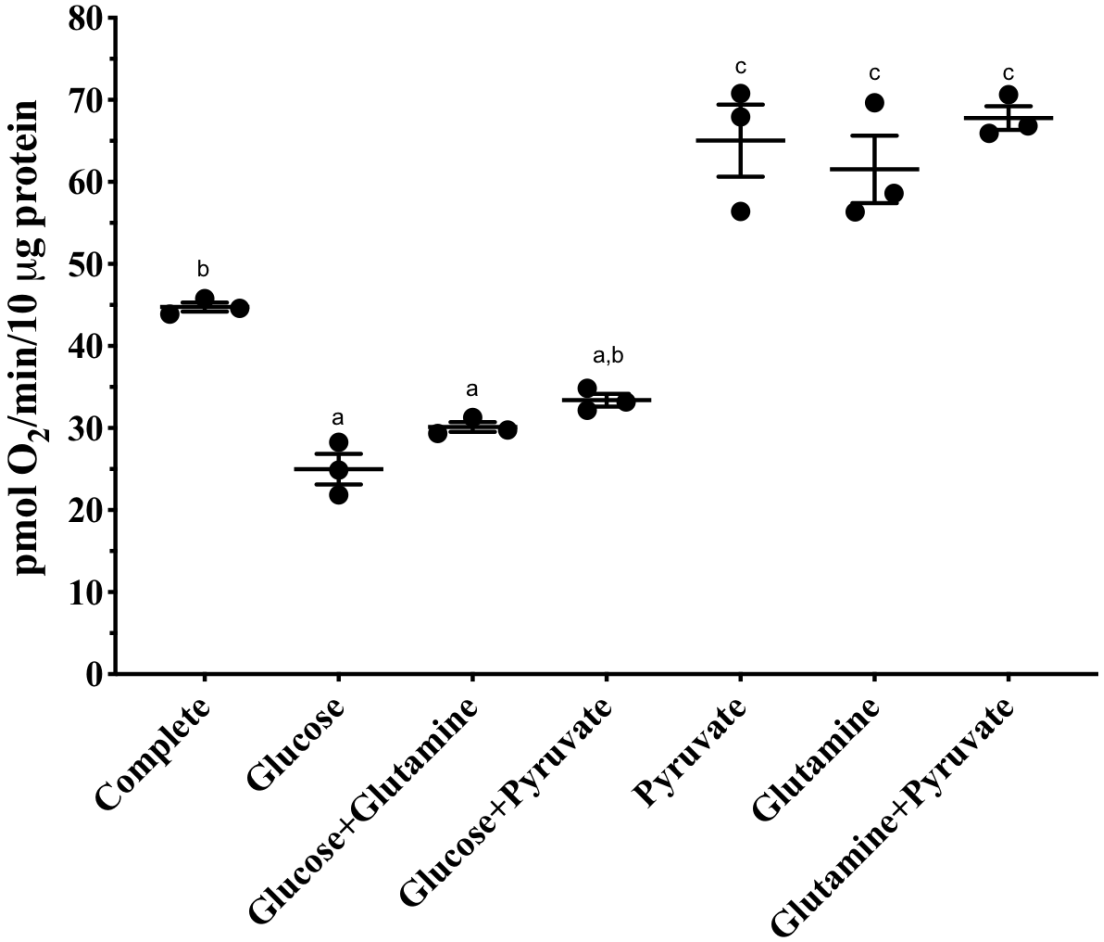

Figure 16: HCMEC/D3 METABOLITE ATP COUPLED OCR ATP coupled OCR values of hCMEC/D3 cells were calculated, based on real-time OCR measurements, for each metabolite group. Values from each metabolite group were compared to each other group. All measurements were normalized to 10 µg protein. Each point represents a single measurement and error bars represent SEM of n=3 samples. Shared letters indicate no significant difference. Absence of a shared letter indicates a significant difference between groups.

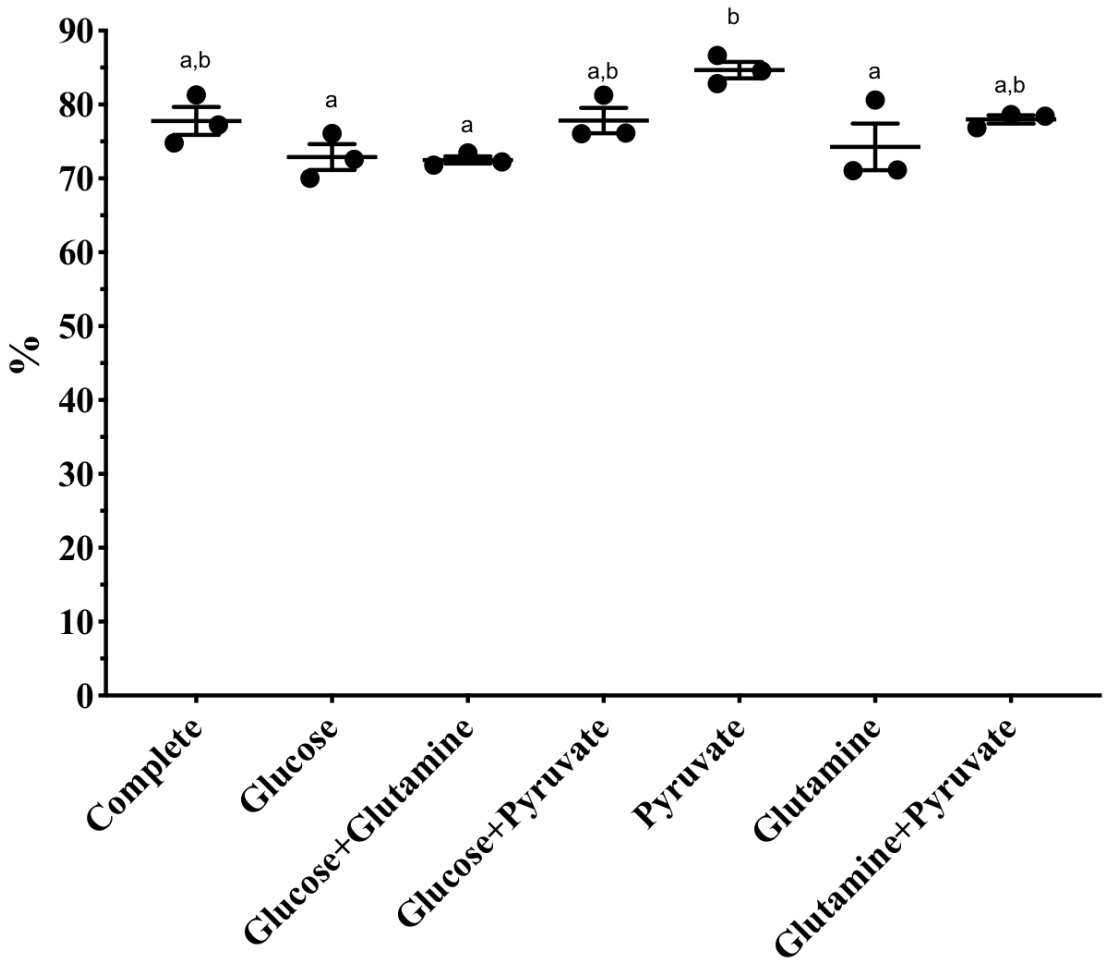

Figure 17: HCMEC/D3 METABOLITE COUPLING EFFICIENCY Coupling efficiency of hCMEC/D3 cells were calculated, based on real-time OCR measurements, for each metabolite group. Values from each metabolite group were compared to each other group. All measurements were normalized to 10 µg protein. Each point represents a single measurement and error bars represent SEM of n=3 samples. Shared letters indicate no significant difference. Absence of a shared letter indicates a significant difference between groups.

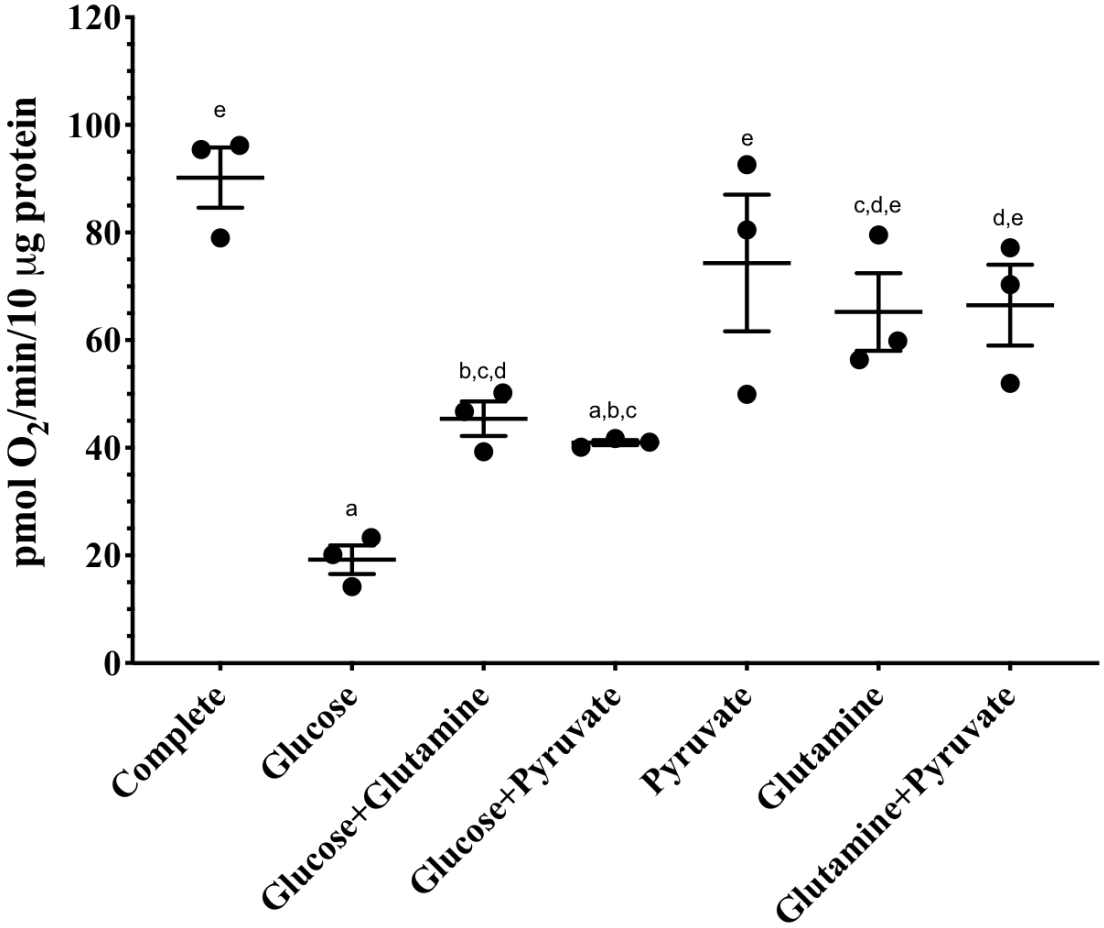

Figure 18: HCMEC/D3 METABOLITE MAXIMAL RESPIRATION Maximal respiration OCR values of hCMEC/D3 cells were calculated, based on real-time OCR measurements, for each metabolite group. Values from each metabolite group were compared to each other group. All measurements were normalized to 10 µg protein. Each point represents a single measurement and error bars represent SEM of n=3 samples. Shared letters indicate no significant difference. Absence of a shared letter indicates a significant difference between groups.

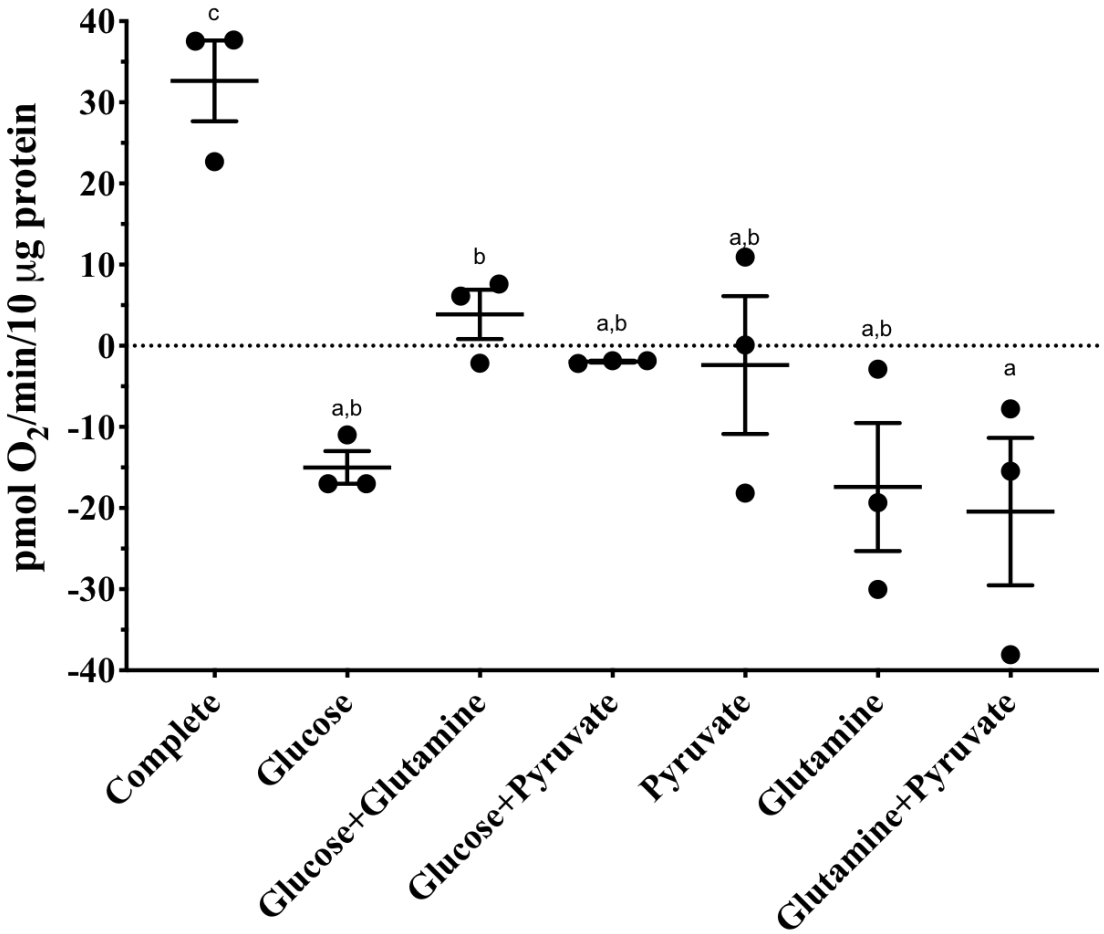

Figure 19: HCMEC/D3 METABOLITE SPARE RESPIRATORY CAPACITY
Spare respiratory capacity OCR values of hCMEC/D3 cells were calculated, based on real-time OCR measurements, for each metabolite group. Values from each metabolite group were compared to each other group. All measurements were normalized to 10 µg protein. Each point represents a single measurement and error bars represent SEM of n=3 samples. Shared letters indicate no significant difference. Absence of a shared letter indicates a significant difference between groups.

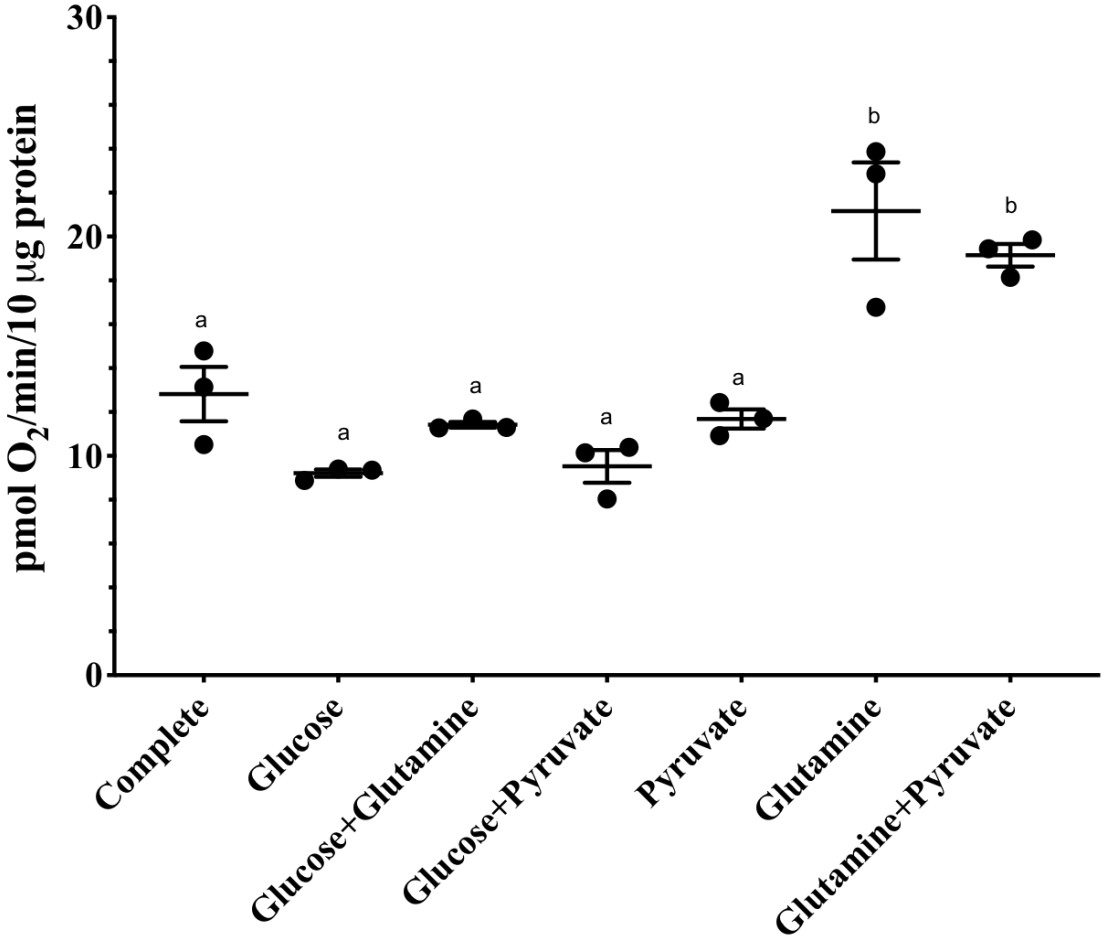

Figure 20: HCMEC/D3 METABOLITE PROTON LEAK Proton leak OCR values of hCMEC/D3 cells were calculated, based on real-time OCR measurements, for each metabolite group. Values from each metabolite group were compared to each other group. All measurements were normalized to 10 µg protein. Each point represents a single measurement and error bars represent SEM of n=3 samples. Shared letters indicate no significant difference. Absence of a shared letter indicates a significant difference between groups.

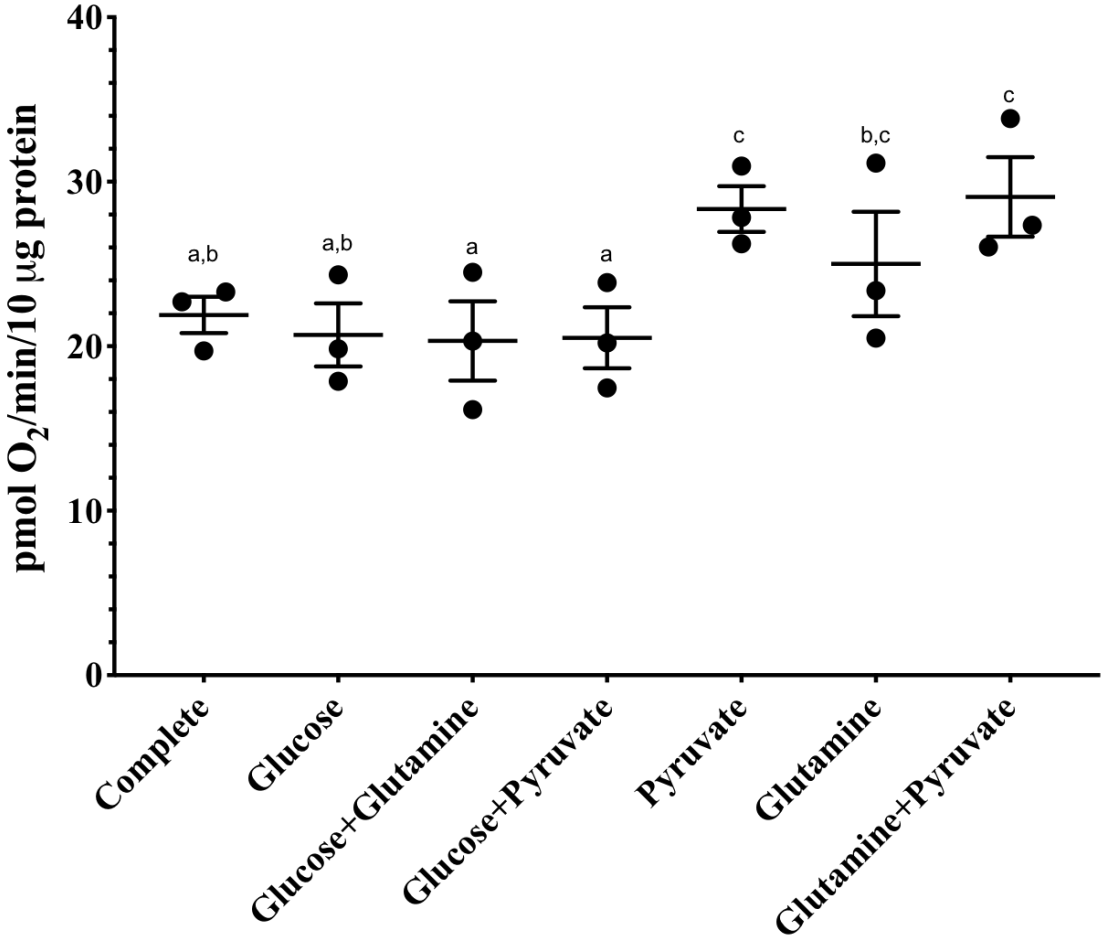

Figure 21: HCMEC/D3 METABOLITE NON-MITOCHONDRIAL OCR Non-mitochondrial OCR values of hCMEC/D3 cells were calculated, based on real-time OCR measurements, for each metabolite group. Values from each metabolite group were compared to each other group. All measurements were normalized to 10 μg protein. Each point represents a single measurement and error bars represent SEM of n=3 samples. Shared letters indicate no significant difference. Absence of a shared letter indicates a significant difference between groups.

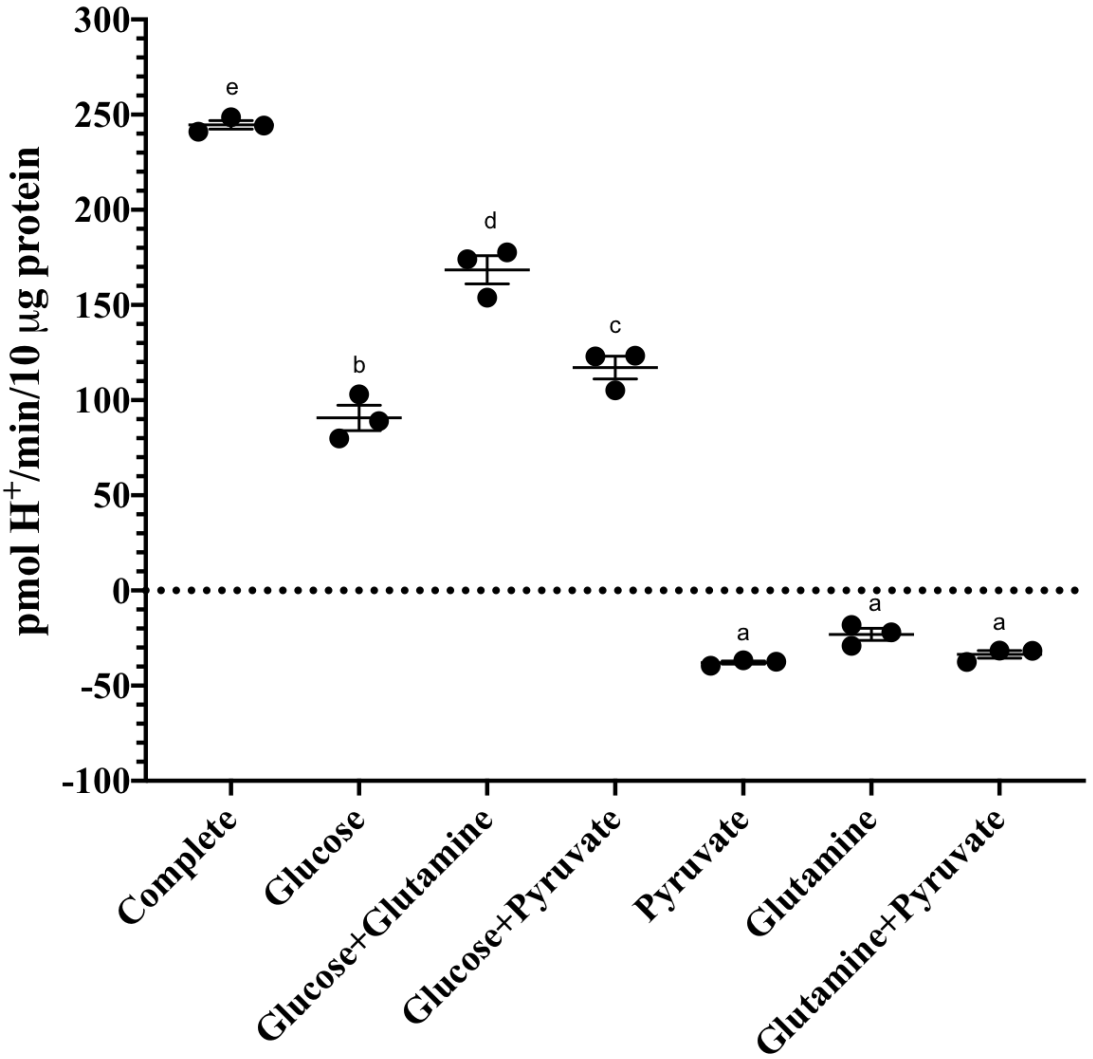

Figure 22: HCMEC/D3 METABOLITE COMPENSATORY PER Compensatory PER values of hCMEC/D3 cells were calculated, based on real-time PER measurements, for each metabolite group. Values from each metabolite group were compared to each other group. All measurements were normalized to 10 µg protein. Each point represents a single measurement and error bars represent SEM of n=3 samples. Shared letters indicate no significant difference. Absence of a shared letter indicates a significant difference between groups.

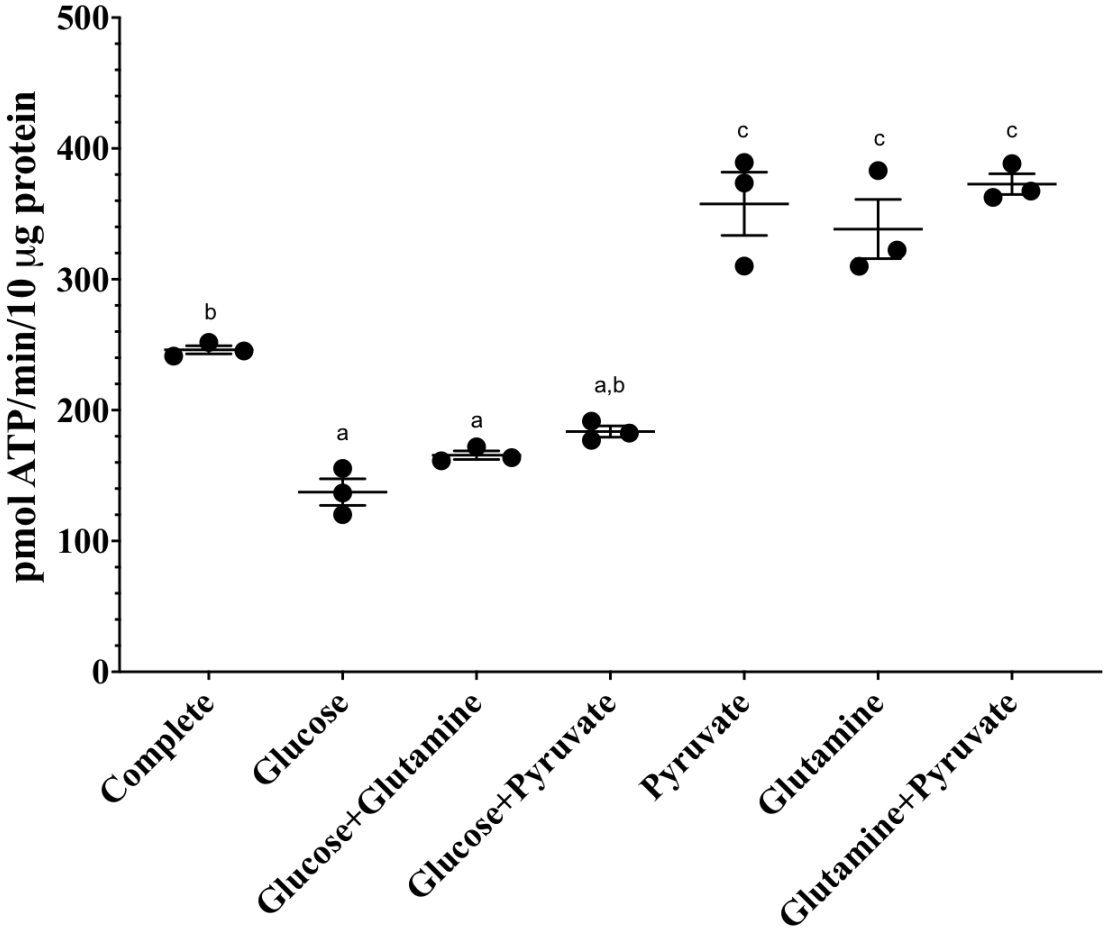

Figure 23: HCMEC/D3 METABOLITE MITOCHONDRIAL ATP PRODUCTION RATES Mitochondrial ATP production rates values of hCMEC/D3 cells were calculated, based on real-time OCR measurements, for each metabolite group. Values from each metabolite group were compared to each other group. All measurements were normalized to 10 μg protein. Each point represents a single measurement and error bars represent SEM of n=3 samples. Shared letters indicate no significant difference. Absence of a shared letter indicates a significant difference between groups.

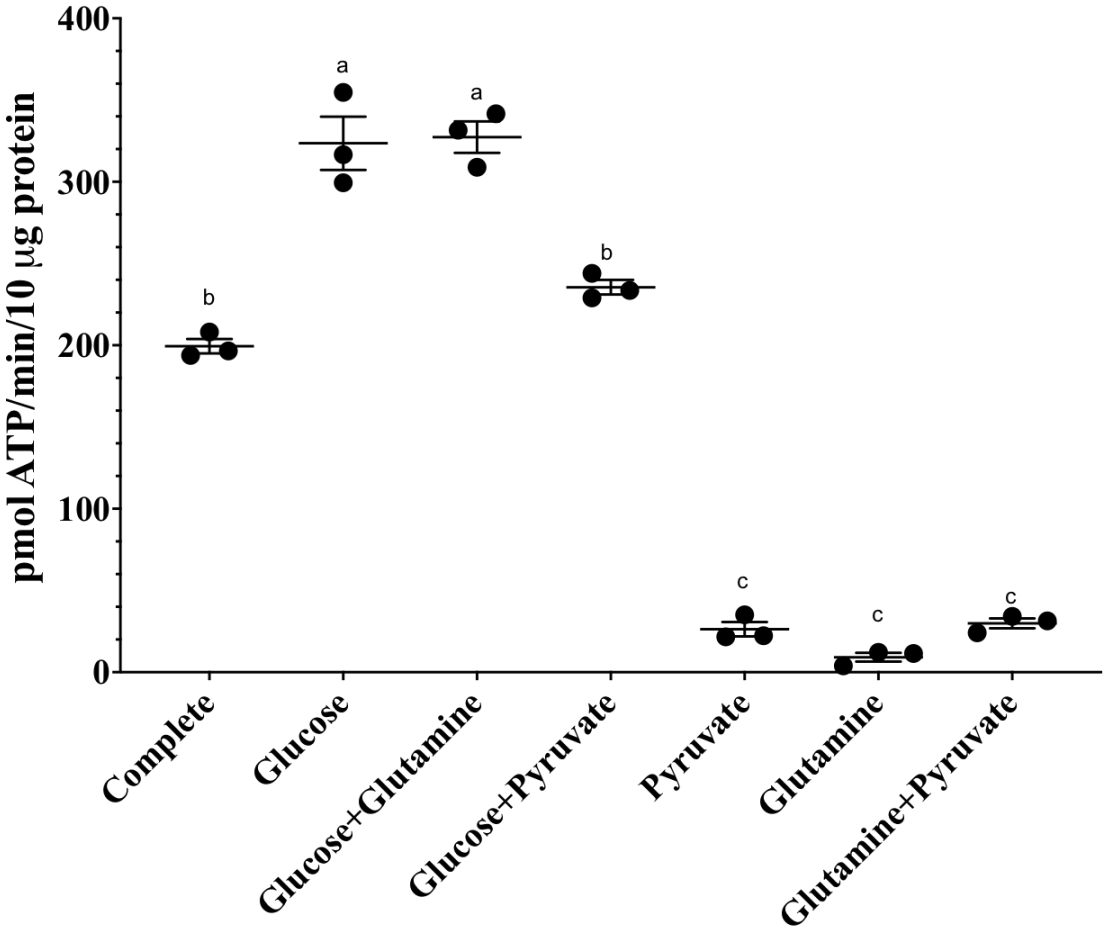

Figure 24: HCMEC/D3 METABOLITE GLYCOLYTIC ATP PRODUCTION RATES Glycolytic ATP production rates values of hCMEC/D3 cells were calculated, based on real-time PER measurements, for each metabolite group. Values from each metabolite group were compared to each other group. All measurements were normalized to 10 μg protein. Each point represents a single measurement and error bars represent SEM of n=3 samples. Shared letters indicate no significant difference. Absence of a shared letter indicates a significant difference between groups.

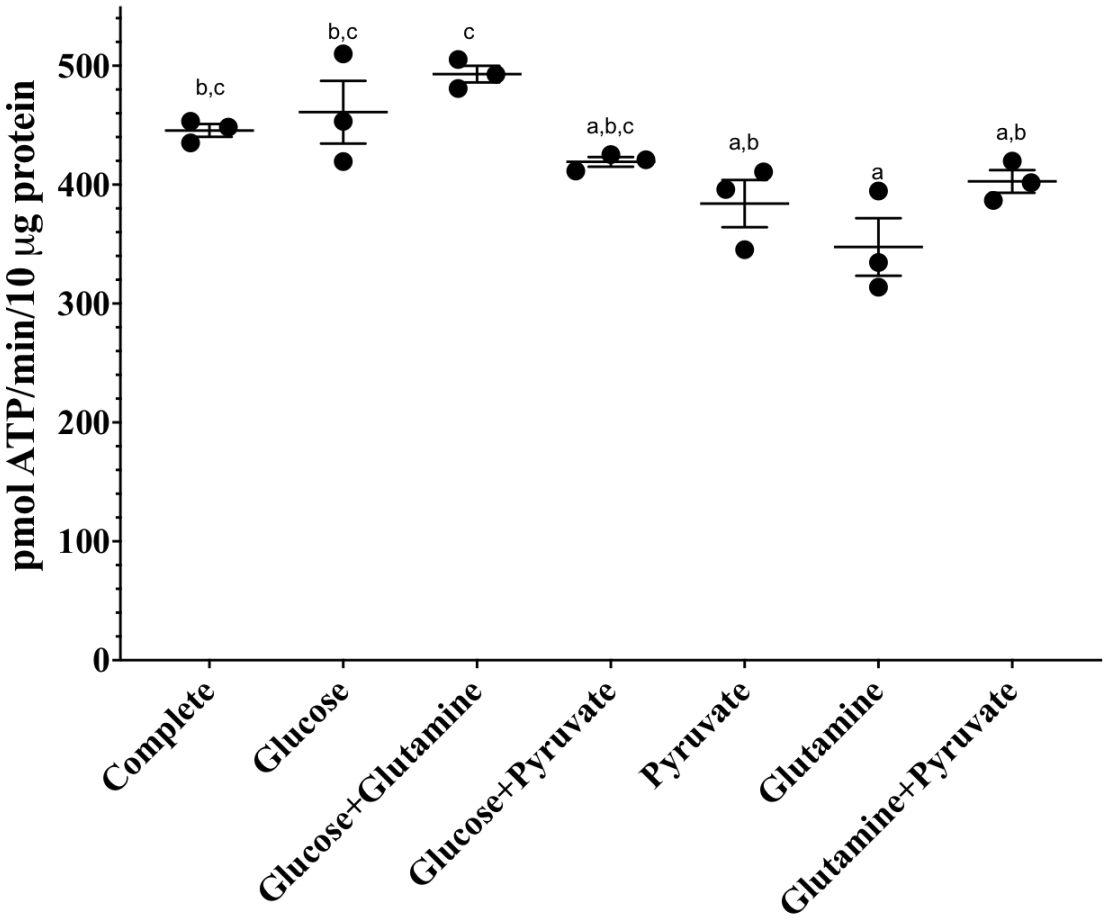

Figure 25: HCMEC/D3 METABOLITE TOTAL ATP PRODUCTION RATES
Total ATP production rates values of hCMEC/D3 cells were calculated, by adding mitochondrial and glycolytic ATP production rates, for each metabolite group. Values from each metabolite group were compared to each other group. All measurements were normalized to 10 μg protein. Each point represents a single measurement and error bars represent SEM of n=3 samples. Shared letters indicate no significant difference. Absence of a shared letter indicates a significant difference between groups.

Chapter 7: Inhibitor Effect on Bioenergetics

Transport proteins are essential in cellular metabolism. In order to utilize various molecules for cellular metabolism, the cells should be able to transport those metabolites, via transmembrane proteins, into the cytoplasm from the extracellular space or from the cytoplasm to the mitochondrial matrix (Figure 26). Depending on expression levels, kinetics, and location, both passive and active transport mechanisms can dictate the rate

of which metabolites may enter, or exit, the cellular compartment. Transport mechanisms may also dictate the rate of TCA cycle reactions and OXPHOS, as well as glycolytic rates. These metabolic pathways, in turn, may dictate the rate in which ATP is produced within the cell. Important metabolite transporters include GLUT1, a primary glucose transporter, and those of the solute carrier family. Solute carrier proteins for pyruvate, lactate, and glutamine include SLC16A1 (MCT1), SLC16A3 (MCT4), and SLC1A5 (ACST2) [8,53,76]. Pyruvate and lactate, both monocarboxylates, import or export is governed by MCTs 1 and 4, which act as symporters with H^+ ions [8,41]. ACST2 is mainly responsible for glutamine transport and acts as an antiporter with Na^+ ions [53,76]. Pyruvate is transported into the mitochondria, to fuel the TCA cycle, by MPC [58,77,78]. Glutamine is converted to glutamate, via glutaminase (GLS), which then enters the TCA cycle by being converted into alpha-ketoglutarate [44,45].

Inhibiting GLUT1, MCT1, MPC, and GLS revealed insights for hCMEC/D3 metabolic plasticity and ability to compensate for metabolic pathway disruption. In order to inhibit GLUT1, MCT1, MPC, and GLS, small molecule inhibitors were used. These inhibitors are named BAY876, AZD3965, UK5099, and BPTES, respectively (Figure 25). An experimental small molecule inhibitor, named MD1, was also tested. MD1 is an experimental duo MCT1/MCT4 inhibitor developed by the lab of Dr. Venkatram Mereddy at the University of Minnesota, Duluth Campus. Concentrations used for inhibitors were determined based on experiments performed by other investigators in literature and extracellular flux analysis assays. Concentrations that exhibited a robust response in PER or OCR were used for final ATP rate assays. Extracellular flux analysis was performed, using individual inhibitors and combinations, to determine OCR, PER,

and ATP production rate plasticity in hCMEC/D3 cells. Inhibitor combinations used were BAY876 + UK5099, BAY876 + BPTES, BAY876 + MD1, and BAY876 + UK5099 + BPTES.

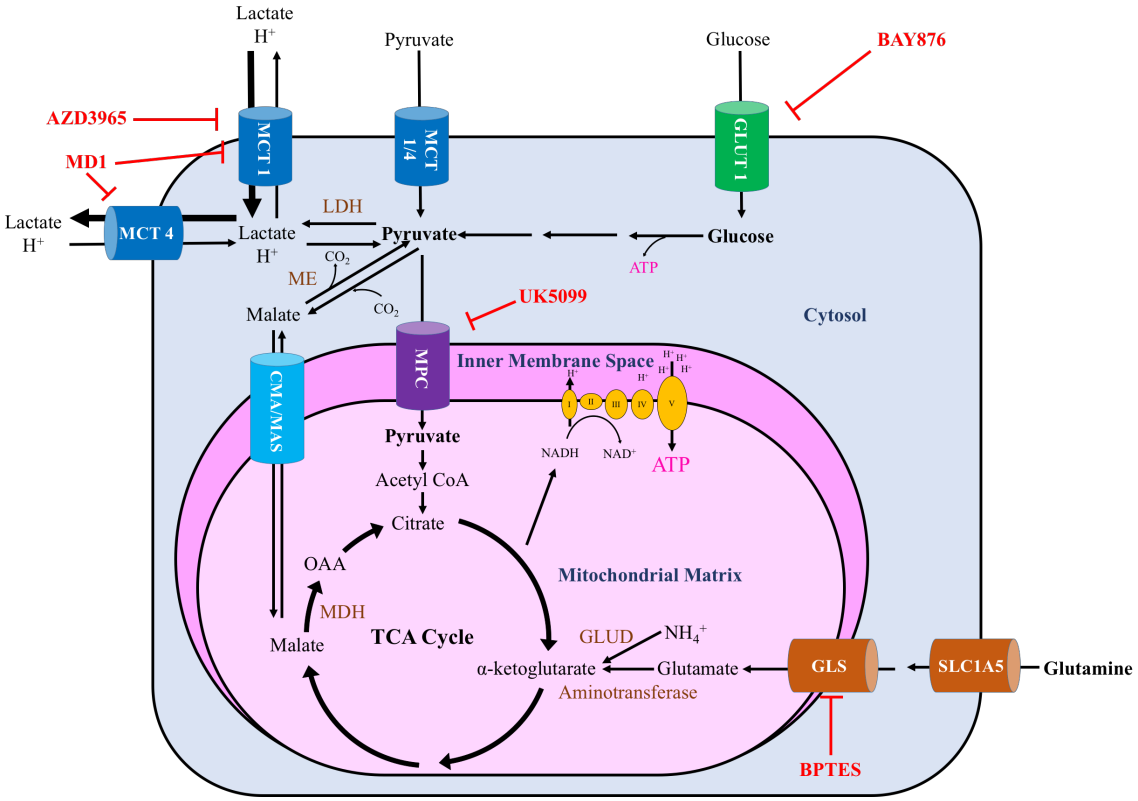

Figure 26: INHIBITOR TARGETS A schematic representation of common cellular energy producing pathways of glucose, pyruvate, and glutamine. Inhibitors tested include BAY876, AZD3965, MD1, UK5099, and BPTES. These inhibit glucose transporter 1 (GLUT1), monocarboxylate transporter 1 (MCT1), mitochondrial pyruvate carrier (MPC), and glutaminase (GLS), respectively. LDH=lactate dehydrogenase, GLUD=glutamate dehydrogenase, ME= malic enzyme, MDH= malate dehydrogenase, and CMA/MAS= citrate malate antiporter/malate aspartate shuttle.

Control:

Unlike complete media, control media consisted of 5.83 mM glucose, 1.5 mM glutamine, and 1 mM pyruvate. With no inhibitors present, hCMEC/D3 cells exhibited a basal OCR value of 25.6 and an ATP coupled OCR value of 16.1 pmol O_2/min/10 µg protein (Figures 29 and 30). Given these measurements, the coupling efficiency was calculated and showed that hCMEC/D3 cells were able to couple 62.9% of the OCR with

ATP production (Figure 31). Maximal respiration and spare respiratory capacity OCR values were 39.8 and 14.2 pmol O_2/min/10 μg protein, respectively (Figure 32 and 33). Proton leak and non-mitochondrial OCR measurements for hCMEC/D3 cells were also calculated as 9.5 and 20.6 pmol O_2/min/10 μg protein, respectively (Figures 34 and 35). PER measurements indicated a compensatory PER of 38.2 pmol H^+/min/10 μg protein (Figure 36). Using OCR and PER measurements, mitochondrial and glycolytic ATP production rates were also calculated for hCMEC/D3 cells. The mitochondrial and glycolytic ATP production rates were 88.4 and 527.8 pmol ATP/min/10 μg protein, respectively (Figures 37 and 38). Therefore, the total ATP production rate of hCMEC/D3 cells was 616.2 pmol ATP/min/10 μg protein (Figure 39).

BAY876 Treated Cells:

Inhibition of GLUT1 in hCMEC/D3 cells, by the small molecule inhibitor BAY876, increased both basal and ATP coupled OCR values compared to the control (Figures 29 and 30). Calculated basal and ATP coupled OCR values for BAY876 treated cells were 55.7 and 41.7 pmol O_2/min/10 μg protein, respectively (Figures 29 and 30). Given these values, 74.9% of the basal OCR is able to be coupled with ATP production (Figure 31). This coupling efficiency is also significantly higher than control cells (Figure 31). Cells treated with BAY876 also exhibited an increase in maximal respiration and spare respiratory capacity (Figures 32 and 33). Calculated maximal respiration and spare respiratory capacity values were 78.6 and 22.9 pmol O_2/min/10 μg protein, respectively (Figures 32 and 33). The proton leak OCR values of cells treated with BAY876 showed to be higher than control cells (Figure 34). The calculated proton leak OCR was 13.9 pmol O_2/min/10 μg protein (Figure 34). Non-mitochondrial OCR, calculated to be 23.2

pmol O_2/min/10 μg protein, was not significantly different than the control (Figure 35). PER measurements indicated a compensatory PER of -3.6 pmol H^+/min/10 μg protein (Figure 36). Treatment with BAY876 increased the mitochondrial ATP production rate in hCMEC/D3 cells, but in contrast, decreased the glycolytic ATP production rate significantly (Figures 37 and 38). Mitochondrial and glycolytic ATP production rates were calculated as 229.6 and 103.9 pmol ATP/min/10μg protein, respectively (Figures 37 and 38). BAY876 showed to significantly decrease the total ATP production rate in hCMEC/D3 cells (Figure 39). The total ATP production rate was calculated as 333.5 pmol/min/10 μg protein (Figure 39).

AZD3965 Treated Cells:

MCT1 inhibition by AZD3965 exhibited no change in basal OCR or ATP coupled OCR in hCMEC/D3 cells (Figures 29 and 30). Calculated basal and ATP coupled OCR values for AZD3965 treated cells were 30.4 and 19.5 pmol O_2/min/10 μg protein, respectively (Figures 29 and 30). The coupling efficiency of cells treated with AZD3965 did not change as well (Figure 31). It was calculated that 64.1% of the basal OCR was able to be coupled with ATP production (Figure 31). Cells treated with AZD3965 also did not exhibit any significant change in maximal respiration and spare respiratory capacity compared to control cells (Figures 32 and 33). Calculated maximal respiration and spare respiratory capacity values were 48.8 and 18.4 pmol O_2/min/10 μg protein, respectively (Figures 32 and 33). There was also no change in proton leak and non-mitochondrial OCR values, of cells treated with AZD3965, compared to the control (Figures 34 and 35). The calculated proton leak and non-mitochondrial OCR was 10.9 and 22.5 pmol O_2/min/10 μg protein (Figures 34 and 35). PER measurements indicated a

compensatory PER of 47.5 pmol H^+/min/10 μg protein (Figure 36). Treatment with AZD3965 did not significantly alter the mitochondrial or glycolytic ATP production rate in hCMEC/D3 cells (Figures 37 and 38). Mitochondrial and glycolytic ATP production rates were calculated as 107.0 and 438.8 pmol ATP/min/10μg protein, respectively (Figures 37 and 38). AZD3965 treatment also did not alter the total ATP production rate in hCMEC/D3 cells (Figure 39). The total ATP production rate was calculated as 545.9 pmol/min/10 μg protein (Figure 39).

MD1 Treated Cells:

Using the experimental small molecule inhibitor, MD1, treated cells did not show a significant difference in either basal or ATP coupled OCR values, compared to control cells (Figures 29 and 30). Calculated basal and ATP coupled OCR values for cells treated with MD1 were 29.2 and 13.3 pmol O_2/min/10 μg protein, respectively (Figures 29 and 30). Coupling efficiency of cells treated with MD1 was significantly lower than control cells as 45.5% of basal OCR was calculated to be for ATP production (Figure 31). Maximal respiration and spare respiratory capacity OCR values of treated cells were significantly lower than control cells (Figures 32 and 33). Calculated maximal respiration and spare respiratory capacity values were 17.5 and -11.7 pmol O_2/min/10 μg protein, respectively (Figures 32 and 33). Proton leak of cells treated with MD1 was shown to be significantly higher than the control (Figure 34). Non-mitochondrial OCR values remained unchanged compared to the control (Figure 35). The calculated proton leak and non-mitochondrial OCR values were 15.9 and 22.9 pmol O_2/min/10 μg protein, respectively (Figures 34 and 35). PER measurements indicated a compensatory PER of 17.1 pmol H^+/min/10 μg protein (Figure 36). Mitochondrial and glycolytic ATP

production rate in hCMEC/D3 cells treated with MD1 did not show a significant difference than the control cells (Figures 37 and 38). Mitochondrial and glycolytic ATP production rates were calculated as 73.4 and 574.3 pmol ATP/min/10μg protein, respectively (Figures 37 and 38). The total ATP production rate in hCMEC/D3 cells treated with MD1 was, therefore, not different than control cells (Figure 39). The total ATP production rate was calculated as 647.7 pmol/min/10 μg protein (Figure 39).

UK5099 Treated Cells:

Inhibiting MPC, via UK5099, in hCMEC/D3 cells did not significantly alter either basal and ATP coupled OCR values compared to the control (Figures 29 and 30). Calculated basal and ATP coupled OCR values for cells exposed to UK5099 were 23.8 and 14.1 pmol O_2/min/10 μg protein, respectively (Figures 29 and 30). Coupling effiency of cells treated with UK5099 did not change compared to the control (Figure 31). Basal OCR coupled with ATP production was calculated as 58.2% (Figure 31). Cells treated with UK5099 displayed a decrease in maximal respiration and spare respiratory capacity. Calculated maximal respiration and spare respiratory capacity values were 16.9 and -6.5 pmol O_2/min/10 μg protein, respectively. There was no significant difference in proton leak and non-mitochondrial OCR values of cells treated with UK5099 compared to control cells. The calculated proton leak and non-mitochondrial OCR values were 9.8 and 18.3 pmol O_2/min/10 μg protein, respectively. PER measurements indicated a compensatory PER of 17.3 pmol H^+/min/10 μg protein. Inhibition of MPC by UK5099 did not display a significant change in mitochondrial and glycolytic ATP production rate in hCMEC/D3 cells. Mitochondrial and glycolytic ATP production rates were calculated as 77.3 and 507.1 pmol ATP/min/10μg protein, respectively. MPC inhibition did not alter

total ATP production rate in hCMEC/D3 cells. The total ATP production rate was calculated as 584.4 pmol/min/10 μg protein.

BPTES Treated Cells:

hCMEC/D3 cells treated with BPTES, a glutaminase inhibitor, did not show a significant change in both basal and ATP coupled OCR values compared to the control (Figures 29 and 30). Calculated basal and ATP coupled OCR values for BPTES treated cells were 14.2 and 8.3 pmol O_2/min/10 μg protein, respectively (Figures 29 and 30). The coupling efficiency of BPTES treated cells was not significantly altered compared to control cells (Figure 31). The coupling efficiency of BPTES treated cells was calculated as 58.5% (Figure 31). Maximal respiration and spare respiratory capacity OCR values were significantly lower in BPTES treated cells compared to control cells (Figures 32 and 33). Calculated maximal respiration and spare respiratory capacity values were 13.0 and -1.2 pmol O_2/min/10 μg protein, respectively (Figures 32 and 33). Proton leak and non-mitochondrial OCR values of cells treated with BPTES exhibited no significant change compared to control cells (Figures 34 and 35). The calculated proton leak and non-mitochondrial OCR values were 5.9 and 15.3 pmol O_2/min/10 μg protein (Figures 34 and 35). PER measurements indicated a compensatory PER of -32.5 pmol H^+/min/10 μg protein (Figure 36). Mitochondrial and glycolytic ATP production rates were not significantly different, than control cells, in cells treated with BPTES (Figures 37 and 38). Mitochondrial and glycolytic ATP production rates were calculated as 45.9 and 490.3 pmol ATP/min/10μg protein, respectively (Figures 37 and 38). The total ATP production rate in hCMEC/D3 cells was also not significantly different in BPTES treated

cells (Figure 39). The total ATP production rate was calculated as 536.2 pmol/min/10 μg protein (Figure 39).

BAY876 + UK5099 Treated Cells:

Inhibition of GLUT1 and MPC in hCMEC/D3 cells, by the small molecule inhibitors BAY876 and UK5099, increased both basal and ATP coupled OCR values compared to the control (Figures 29 and 30). Calculated basal and ATP coupled OCR values for BAY876 treated cells were 50.7 and 38.2 pmol O_2/min/10 μg protein, respectively (Figures 29 and 30). The calculated coupling efficiency is also significantly higher than control cells (Figure 31). hCMEC/D3 cells are able to couple 75.3% of their basal OCR to ATP production (Figure 31). Maximal respiration OCR was also increased in cells treated with BAY876 and UK5099 (Figure 32). However, spare respiratory capacity did not significantly change (Figure 33). Calculated maximal respiration and spare respiratory capacity values were 71.8 and 21.1 pmol O_2/min/10 μg protein, respectively (Figures 32 and 33). Both proton leak and non-mitochondrial OCR values of cells treated with BAY876 and UK5099 were not significantly different than control cells (Figures 34 and 35). The calculated proton leak and non-mitochondrial OCR was 12.4 and 24.1 pmol O_2/min/10 μg protein, respectively (Figures 34 and 35). PER measurements indicated a compensatory PER of 10.9 pmol H^+/min/10 μg protein (Figure 36). Treatment with BAY876 and UK5099 significantly increased the mitochondrial ATP production rate in hCMEC/D3 cells (Figures 37). However, the glycolytic ATP production rate significantly decreased as well (Figure 38). Mitochondrial and glycolytic ATP production rates were calculated as 210.2 and 134.1 pmol ATP/min/10μg protein, respectively (Figures 37 and 38). BAY876 combined with UK5099 showed to significantly decrease the total ATP

production rate in hCMEC/D3 cells, compared to control cells (Figure 39). The total ATP production rate was calculated as 344.4 pmol/min/10 μg protein (Figure 39).

BAY876 + BPTES Treated Cells:

Inhibiting GLUT1 and GLS, via BAY876 and BPTES combined, increased both basal and ATP coupled OCR values compared to the control (Figures 29 and 30). Calculated basal and ATP coupled OCR values for BAY876 + BPTES treated cells were 40.3 and 31.2 pmol O_2/min/10 μg protein, respectively (Figures 29 and 30). Coupling efficiency of cells treated with BAY876 and BPTES was also significantly higher than control cells (Figure 31). The coupling efficiency revealed that cells were able to utilize 77.4% of the basal OCR for ATP production (Figure 31). Maximal respiration and spare respiratory capacity, in cells treated with BAY876 + BPTES, did not show a significant difference compared to control cells (Figures 32 and 33). Maximal respiration and spare respiratory capacity values were calculated as 59.4 and 19.1 pmol O_2/min/10 μg protein, respectively (Figures 32 and 33). Proton leak and non-mitochondrial OCR values were not significantly different, in BAY876 + BPTES treated cells, than control cells (Figures 34 and 35). Proton leak and non-mitochondrial OCR values were calculated as 9.0 and 21.4 pmol O_2/min/10 μg protein, respectively (Figures 34 and 35). PER measurements indicated a compensatory PER of -10.4 pmol H^+/min/10 μg protein (Figure 36). Mitochondrial ATP production rate, in hCMEC/D3 cells treated with BAY876 + BPTES, was significantly higher than control cells (Figure 37). Subsequently, the glycolytic ATP production rate was significantly lower than control cells (Figure 38). Mitochondrial and glycolytic ATP production rates were calculated as 171.8 and 131.2 pmol ATP/min/10μg protein, respectively (Figures 37 and 38). The total ATP production rate, of cells treated

with BAY876 + BPTES, was significantly lower than control cells (Figure 39). The total ATP production rate was calculated as 302.9 pmol/min/10 μg protein (Figure 39).

BAY876 + MD1 Treated Cells:

Using BAY876 and MD1, inhibition of GLUT1 and MCT1/MCT4 in hCMEC/D3 cells exhibited a significant increase in both basal and ATP coupled OCR values compared to the control (Figures 29 and 30). Calculated basal and ATP coupled OCR values for BAY876 + MD1 treated cells were 49.6 and 31.4 pmol O_2/min/10 μg protein, respectively (Figures 29 and 30). The coupling efficiency, however, was not significantly altered (Figure 31). BAY876 + MD1 treated cells were able to couple 63.3% of their basal OCR to ATP production (Figure 31). Maximal respiration OCR values were higher in BAY876 + MD1 treated cells than control cells (Figure 32). However, the spare respiratory capacity remained unchanged, statistically (Figure 33). Calculated maximal respiration and spare respiratory capacity values were 62.3 and 12.6 pmol O_2/min/10 μg protein, respectively (Figures 32 and 33). Proton leak OCR values, of cells treated with BAY876 + MD1, were significantly higher than control cells (Figure 34). The non-mitochondrial OCR was not altered in treated cells compared to control cells (Figure 35). Proton leak and non-mitochondrial OCR values were calculated as 18.2 and 24.0 pmol O_2/min/10 μg protein, respectively (Figures 34 and 35). PER measurements indicated a compensatory PER of 37.1 pmol H^+/min/10 μg protein (Figure 36). Treatment with BAY876 + MD1 significantly increased the mitochondrial ATP production rate in hCMEC/D3 cells, however, decreased the glycolytic ATP production rate significantly (Figures 37 and 38). Mitochondrial and glycolytic ATP production rates were calculated as 172.8 and 149.1 pmol ATP/min/10μg protein, respectively (Figures 37 and 38).

BAY876 + MD1 showed to significantly decrease the total ATP production rate in hCMEC/D3 cells (Figure 39). The total ATP production rate was calculated as 321.9 pmol/min/10 μg protein (Figure 39).

BAY876 + UK5099 + BPTES Treated Cells:

Basal and ATP coupled OCR values in cells treated with BAY876, UK5099, and BPTES were significantly higher than control cells (Figures 29 and 30). Calculated basal and ATP coupled OCR values for BAY876 + UK5099 + BPTES treated cells were 38.5 and 28.1 pmol O_2/min/10 μg protein, respectively (Figures 29 and 30). The coupling efficiency of cells treated with BAY876 + UK5099 + BPTES was significantly higher than control cells (Figure 31). The coupling efficiency was calculated as 73.0% of basal OCR being coupled to ATP production (Figure 31). The maximal respiration OCR for cells treated with BAY876 + UK5099 + BPTES was not different than control cells (Figure 32). However, the spare respiratory capacity was significantly lower than control cells (Figure 33). Calculated maximal respiration and spare respiratory capacity values were 40.6 and 2.1 pmol O_2/min/10 μg protein, respectively (Figures 32 and 33). Proton leak and non-mitochondrial OCR values of cells treated with BAY876 + UK5099 + BPTES were not significantly altered compared to control cells (Figures 34 and 35). The calculated proton leak and non-mitochondrial OCR values were 10.4 and 18.9 pmol O_2/min/10 μg protein (Figures 34 and 35). PER measurements indicated a compensatory PER of -5.0 pmol H^+/min/10 μg protein (Figure 36). Mitochondrial ATP production rates in cells treated with BAY876 + UK5099 + BPTES were lower than control cells (Figure 37). The glycolytic ATP production rate of treated cells, in contrast, was lower than control cells (Figure 38). Mitochondrial and glycolytic ATP production rates were

calculated as 154.6 and 134.8 pmol ATP/min/10µg protein, respectively (Figures 37 and 38). The total ATP production rate in BAY876 + UK5099 + BPTES treated hCMEC/D3 cells was lower than control cells (Figure 39). The total ATP production rate was calculated as 289.4 pmol/min/10 µg protein (Figure 39).

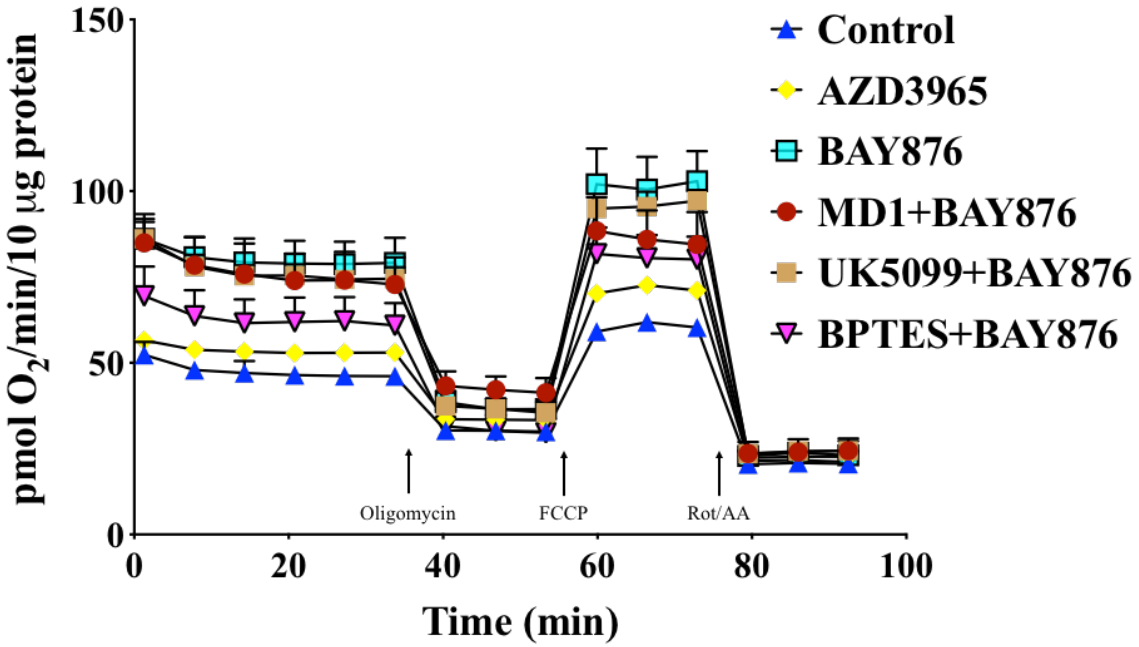

Figure 27: HCMEC/D3 CELL INHIBITOR OCR TRACE (A) OCR and ECAR (not shown) measurements were taken in-real time and in conjunction with step-wise injections of oligomycin, FCCP, and rotenone/antimycin A to characterize mitochondrial respiration, glycolytic, and ATP production rate values of hCMEC/D3 cells. Real-time measurements shown are from cells treated with no inhibitors (control), AZD3965, BAY876, MD1 + BAY876, UK5099 + BAY876, and BPTES + BAY876. Measurements were normalized to 10 µg protein. Each point represents a mean measurement and error bars represent SEM of n=3 samples.

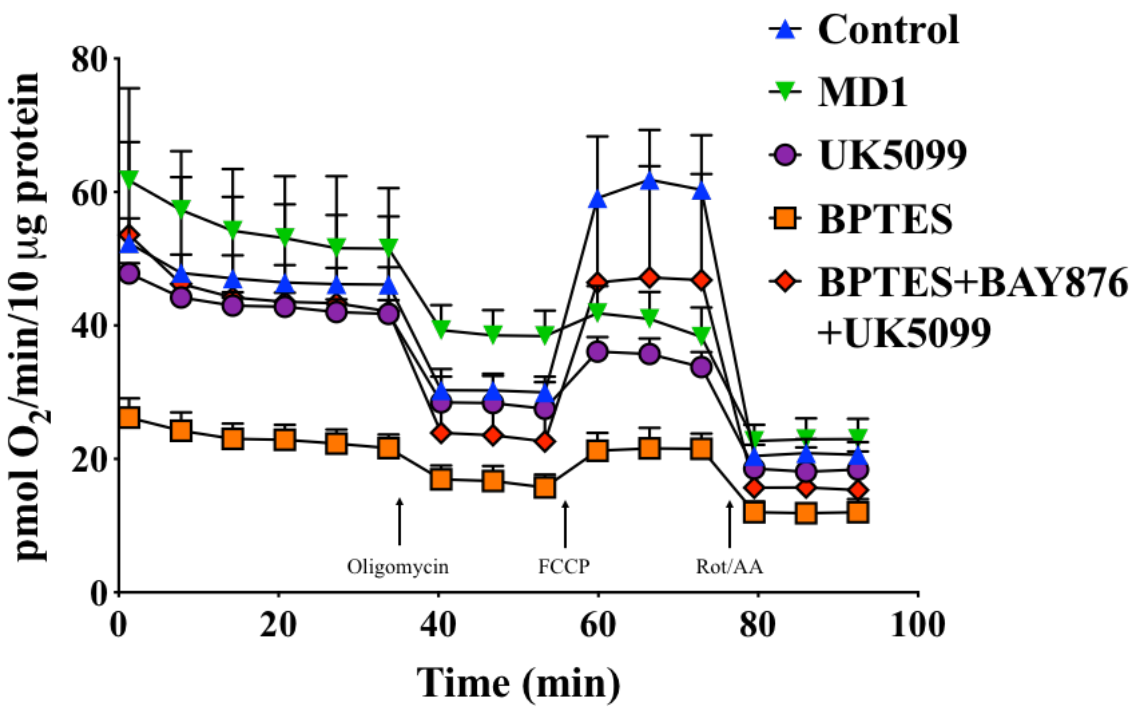

Figure 28: HCMEC/D3 INHIBITOR OCR TRACE (B) OCR and ECAR (not shown) measurements were taken in-real time and in conjunction with step-wise injections of oligomycin, FCCP, and rotenone/antimycin A to characterize mitochondrial respiration, glycolytic, and ATP production rate values of hCMEC/D3 cells. Real-time measurements shown are from cells treated with no inhibitors (control), MD1, UK5099, BPTES, and BPTES + BAY876 + UK5099. Measurements were normalized to 10 µg protein. Each point represents a mean measurement and error bars represent SEM of n=3 samples.

Table 2: HCMEC/D3 INHIBITOR ENERGETIC VALUES OCR, compensatory PER (Comp PER), mitochondrial ATP production rate (mitoATP), glycolytic ATP production rate (glycoATP), and total ATP production rate values were calculated for cells treated with each inhibitor or combination. OCR, PER, and ATP production rate values are expressed as pmol O_2, H^+, and ATP/min/10 µg protein, respectively

	Basal OCR	ATP coupled OCR	Coupling efficiency (%)	Maximal Respiration OCR	Spare Respiratory Capacity OCR	Proton Leak OCR
Control	25.6	16.1	62.9	39.8	14.2	9.5
BAY876	55.7	41.7	74.9	78.6	22.9	13.9
UK5099 + BAY876	50.7	38.2	75.3	71.8	21.1	12.4
MD1 + BAY876	49.6	31.4	63.3	62.3	12.7	18.2
BPTES + BAY876	40.3	31.2	77.4	59.4	19.1	9.0
BPTES + UK5099 + BAY876	38.5	28.1	73.0	40.6	2.1	10.4
AZD3965	30.4	19.5	64.1	48.8	18.4	10.9
MD1	29.2	13.3	45.5	17.5	-11.7	15.9
UK5099	23.8	14.1	59.2	16.9	-6.9	9.8
BPTES	14.2	8.3	58.5	13.0	-1.2	5.9

	Non-mito OCR	Comp PER	mitoATP	glycoATP	Total ATP
Control	20.6	38.2	88.4	527.8	616.2
BAY876	23.2	-3.6	229.6	103.9	333.5
UK5099 + BAY876	24.1	10.9	210.2	134.1	344.4
MD1 + BAY876	24.0	37.1	172.8	149.1	321.9
BPTES + BAY876	21.4	-10.4	171.8	131.2	302.9
BPTES + UK5099 + BAY876	18.9	-5.0	154.6	134.8	289.4
AZD3965	22.5	47.5	107.0	438.8	545.9
MD1	22.9	17.1	73.4	574.3	647.7
UK5099	18.3	17.3	77.3	507.1	584.4
BPTES	15.3	-32.5	45.9	490.3	536.2

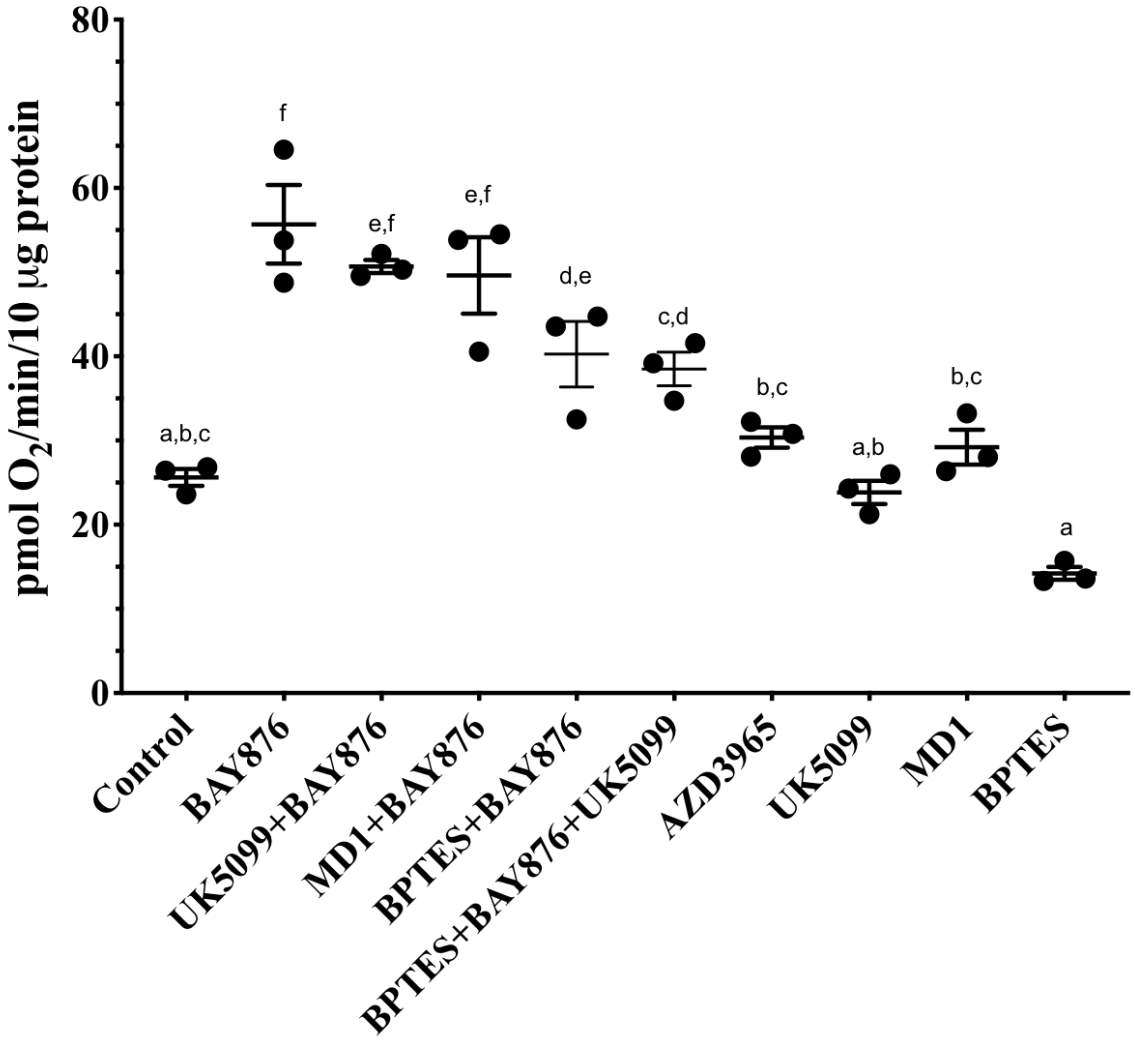

Figure 29: HCMEC/D3 INHIBITOR BASAL OCR Basal OCR values of hCMEC/D3 cells were calculated, based on real-time OCR measurements, for each inhibitor treatment group. Values from each inhibitor group were compared to each other group. All measurements were normalized to 10 µg protein. Each point represents a single measurement and error bars represent SEM of n=3 samples. Shared letters indicate no significant difference. Absence of a shared letter indicates a significant difference between groups.

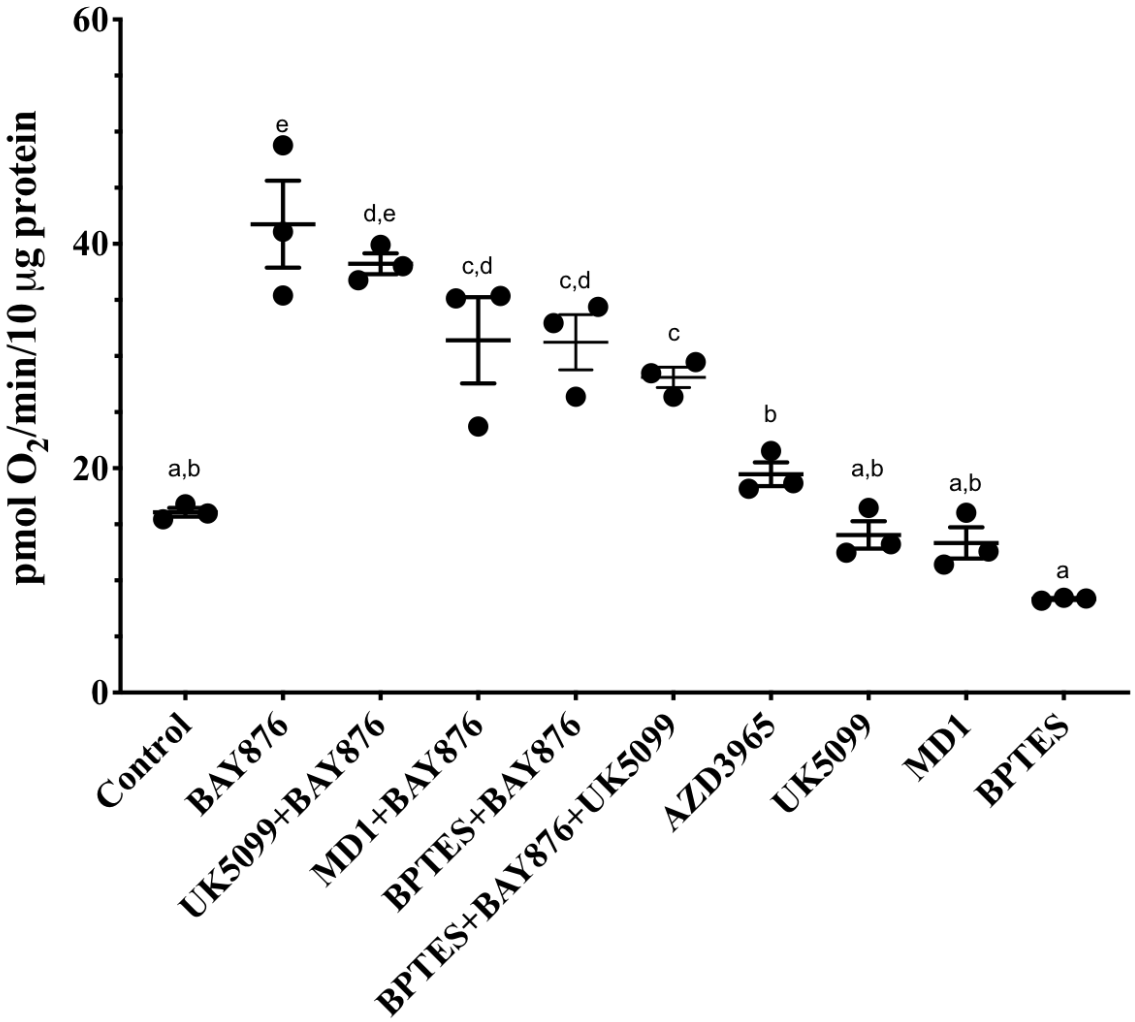

Figure 30: HCMEC/D3 INHIBITOR ATP COUPLED OCR ATP coupled OCR values of hCMEC/D3 cells were calculated, based on real-time OCR measurements, for each inhibitor treatment group. Values from each inhibitor group were compared to each other group. All measurements were normalized to 10 µg protein. Each point represents a single measurement and error bars represent SEM of n=3 samples. Shared letters indicate no significant difference. Absence of a shared letter indicates a significant difference between groups.

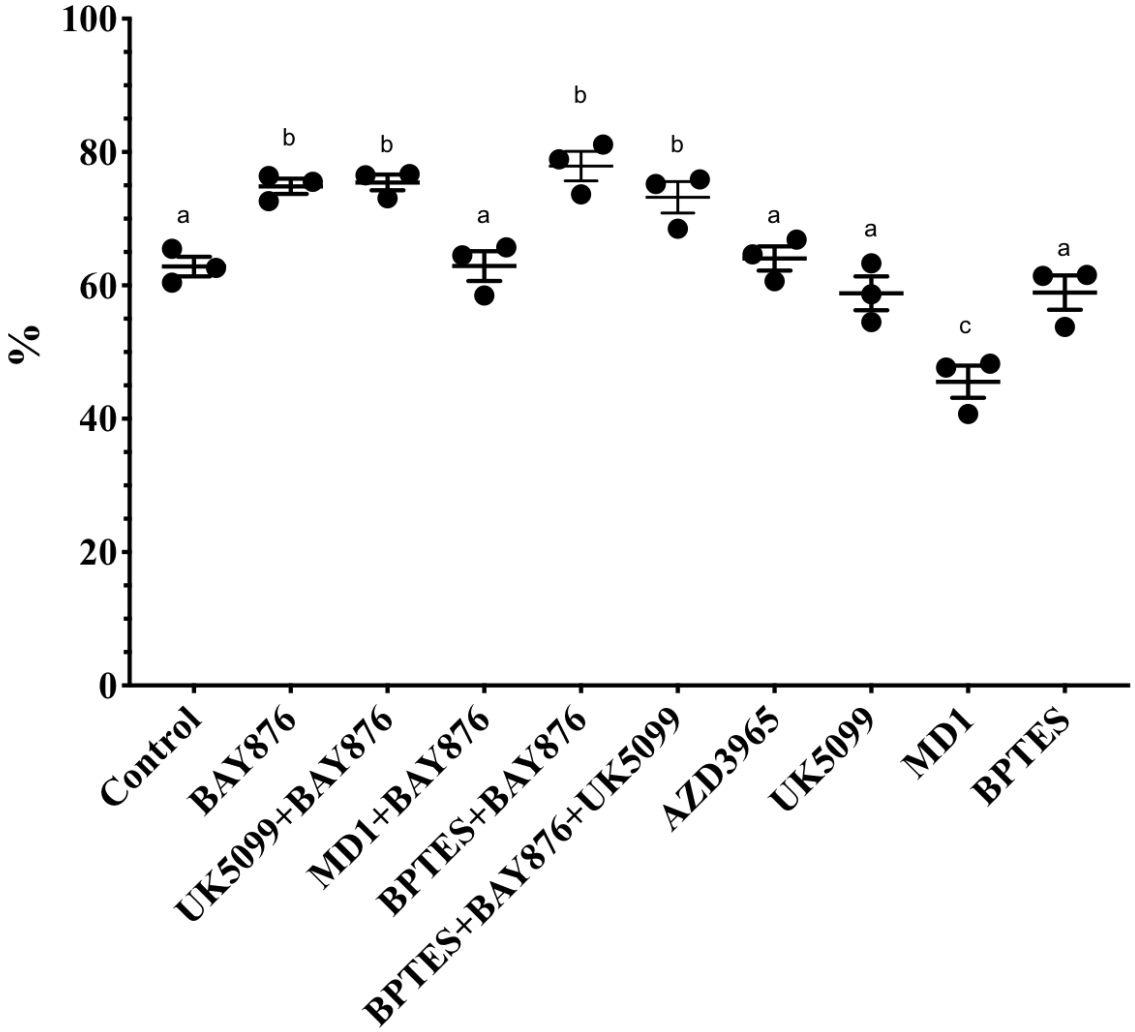

Figure 31: HCMEC/D3 INHIBITOR COUPLING EFFICIENCY Coupling efficiencies of hCMEC/D3 cells were calculated, based on real-time OCR measurements, for each inhibitor treatment group. Values from each inhibitor group were compared to each other group. All measurements were normalized to 10 μg protein. Each point represents a single measurement and error bars represent SEM of n=3 samples. Shared letters indicate no significant difference. Absence of a shared letter indicates a significant difference between groups.

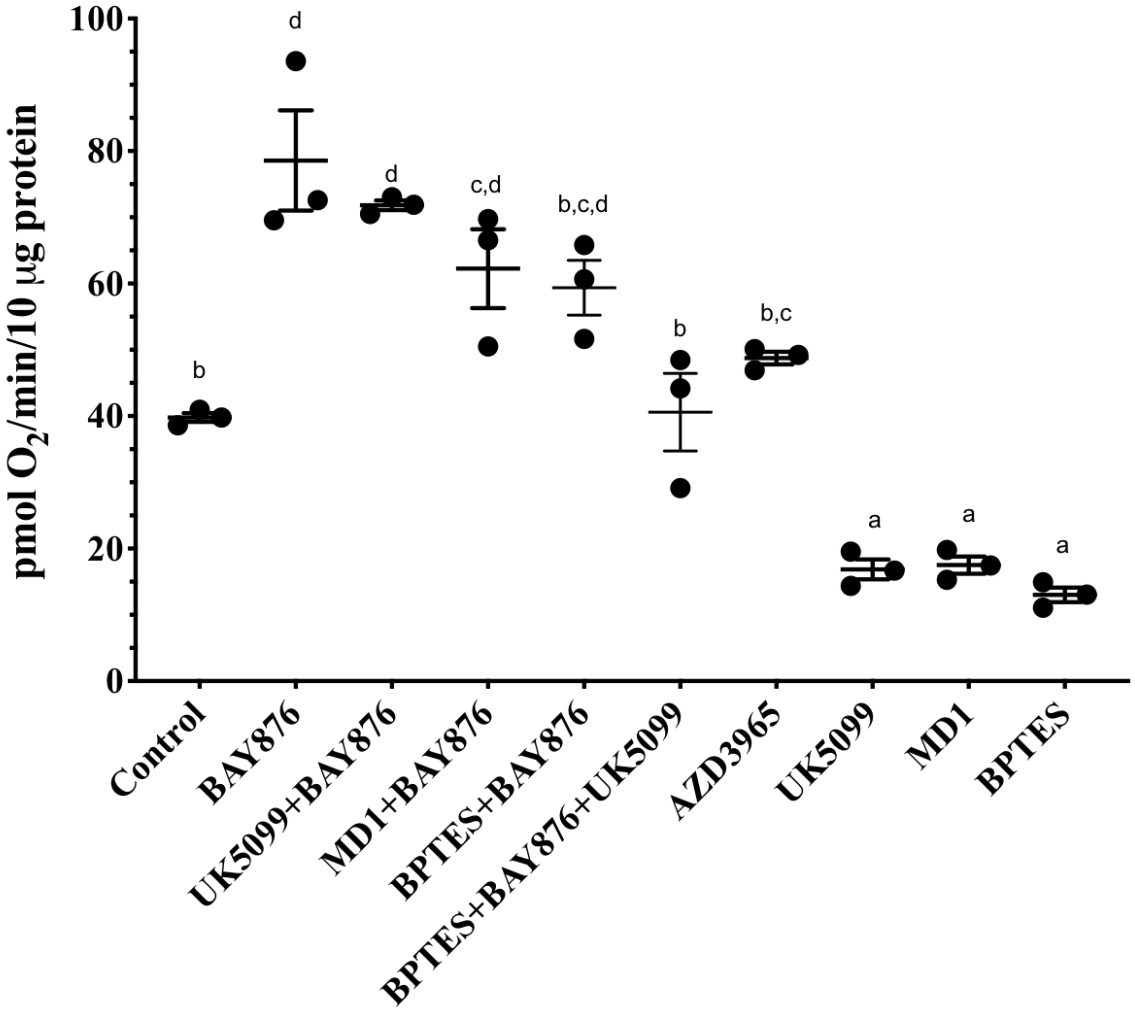

Figure 32: HCMEC/D3 INHIBITOR MAXIMAL RESPIRATION Maximal respiration OCR values of hCMEC/D3 cells were calculated, based on real-time OCR measurements, for each inhibitor treatment group. Values from each inhibitor group were compared to each other group. All measurements were normalized to 10 μg protein. Each point represents a single measurement and error bars represent SEM of n=3 samples. Shared letters indicate no significant difference. Absence of a shared letter indicates a significant difference between groups.

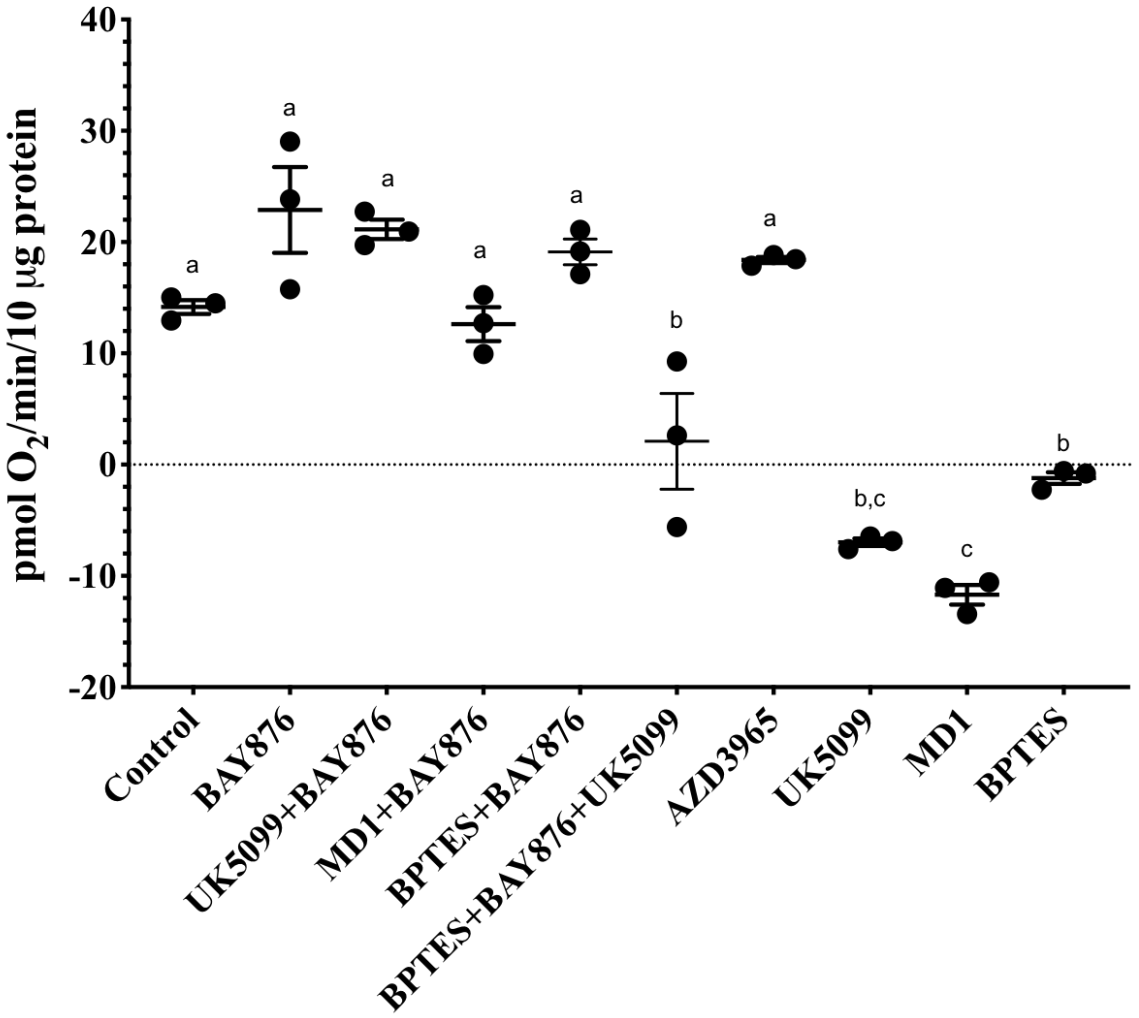

Figure 33: HCMEC/D3 INHIBITOR SPARE RESPIRATORY CAPACITY Spare respiratory capacity OCR values of hCMEC/D3 cells were calculated, based on real-time OCR measurements, for each inhibitor treatment group. Values from each inhibitor group were compared to each other group. All measurements were normalized to 10 µg protein. Each point represents a single measurement and error bars represent SEM of n=3 samples. Shared letters indicate no significant difference. Absence of a shared letter indicates a significant difference between groups.

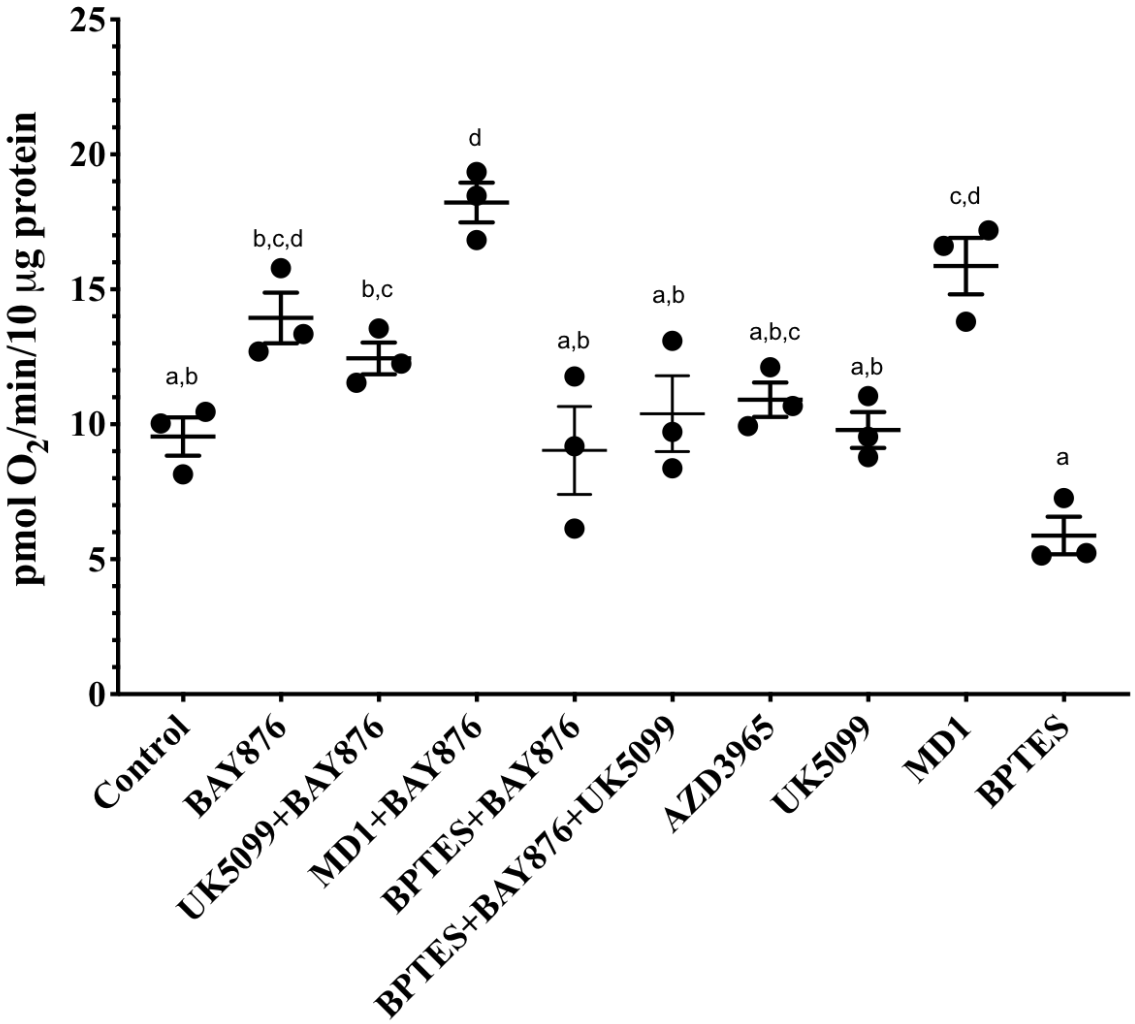

Figure 34: HCMEC/D3 INHIBITOR PROTON LEAK Proton leak OCR values of hCMEC/D3 cells were calculated, based on real-time OCR measurements, for each inhibitor treatment group. Values from each inhibitor group were compared to each other group. All measurements were normalized to 10 µg protein. Each point represents a single measurement and error bars represent SEM of n=3 samples. Shared letters indicate no significant difference. Absence of a shared letter indicates a significant difference between groups.

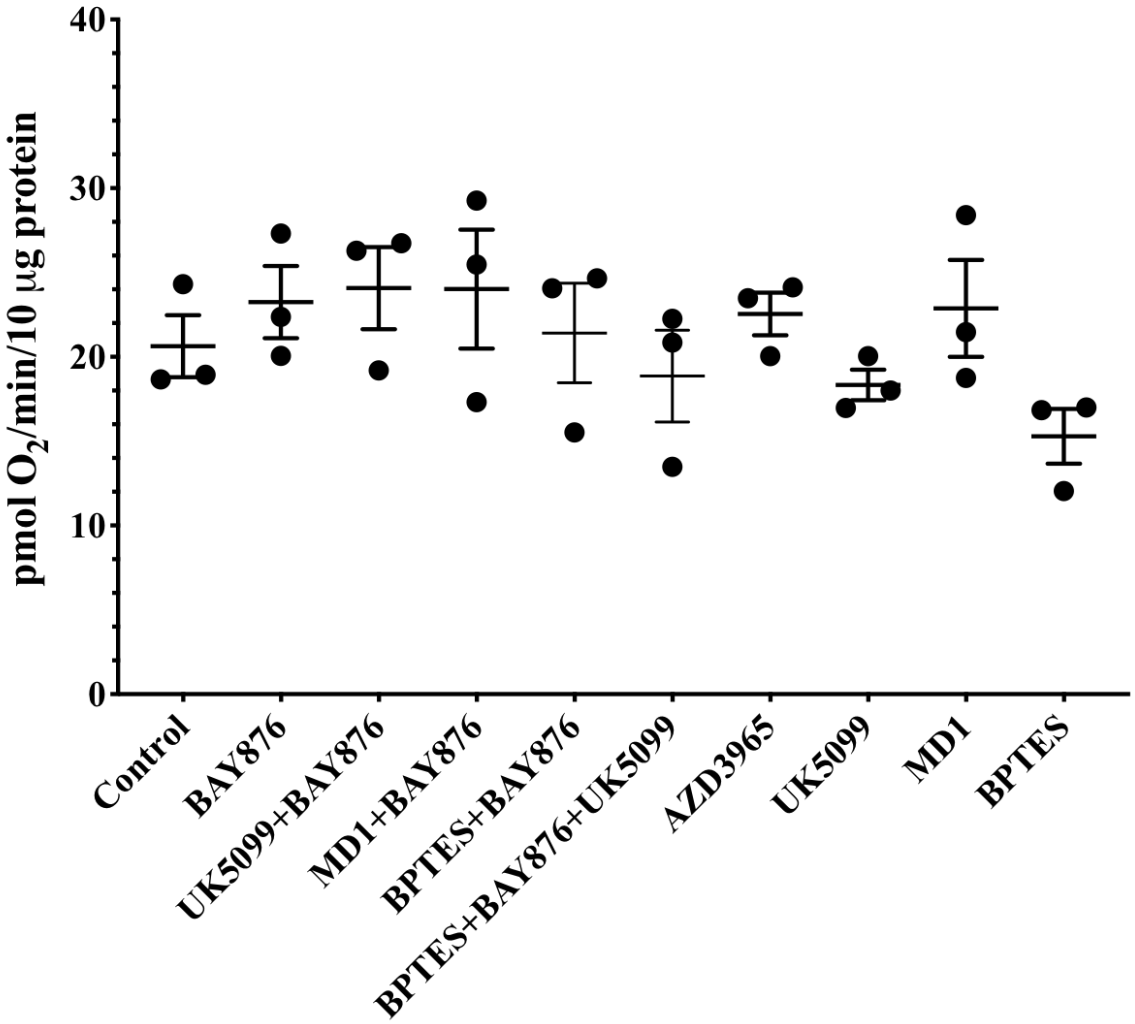

Figure 35: HCMEC/D3 INHIBITOR NON-MITOCHONDRIAL OCR non-mitochondrial OCR values of hCMEC/D3 cells were calculated, based on real-time OCR measurements, for each inhibitor treatment group. Values from each inhibitor group were compared to each other group. All measurements were normalized to 10 μg protein. Each point represents a single measurement and error bars represent SEM of n=3 samples. Shared letters indicate no significant difference. Absence of a shared letter indicates a significant difference between groups.

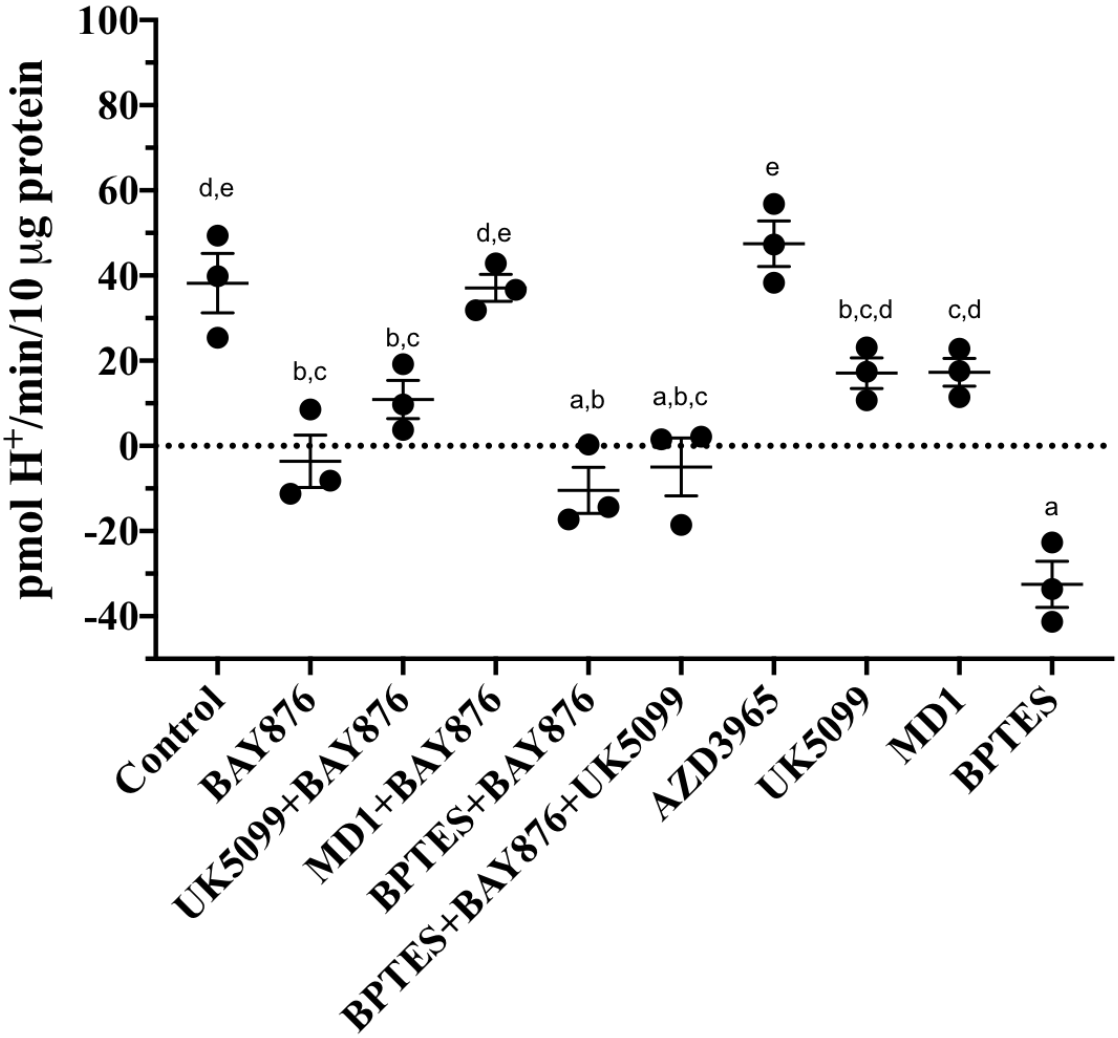

Figure 36: HCMEC/D3 INHIBITOR COMPENSATORY PER Compensatory PER values of hCMEC/D3 cells were calculated, based on real-time PER measurements, for each inhibitor treatment group. Values from each inhibitor group were compared to each other group. All measurements were normalized to 10 μg protein. Each point represents a single measurement and error bars represent SEM of n=3 samples. Shared letters indicate no significant difference. Absence of a shared letter indicates a significant difference between groups.

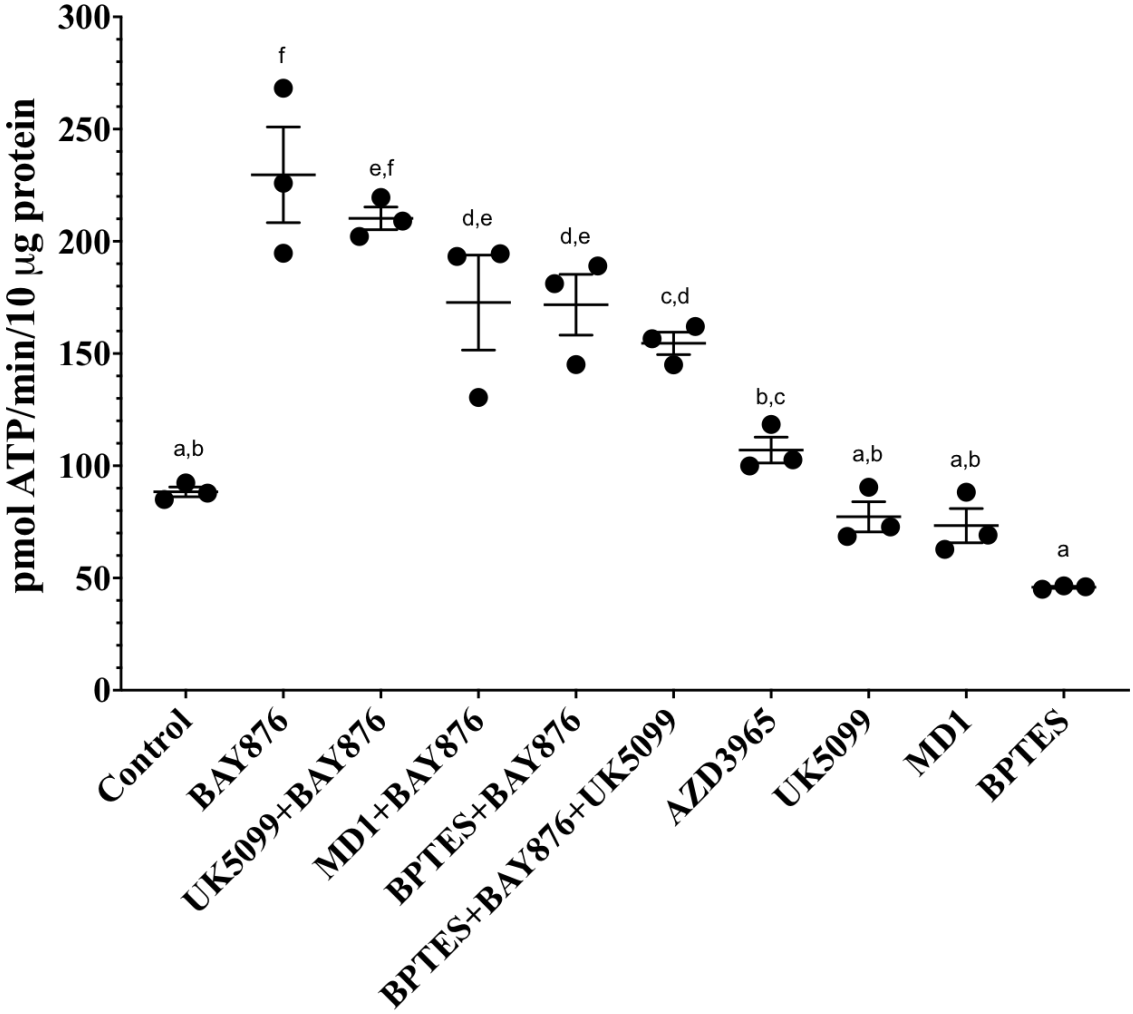

Figure 37: HCMEC/D3 INHIBITOR MITOCHONDRIAL ATP PRODUCTION RATES Mitochondrial ATP production rate values of hCMEC/D3 cells were calculated, based on real-time OCR measurements, for each inhibitor treatment group. Values from each inhibitor group were compared to each other group. All measurements were normalized to 10 μg protein. Each point represents a single measurement and error bars represent SEM of n=3 samples. Shared letters indicate no significant difference. Absence of a shared letter indicates a significant difference between groups.

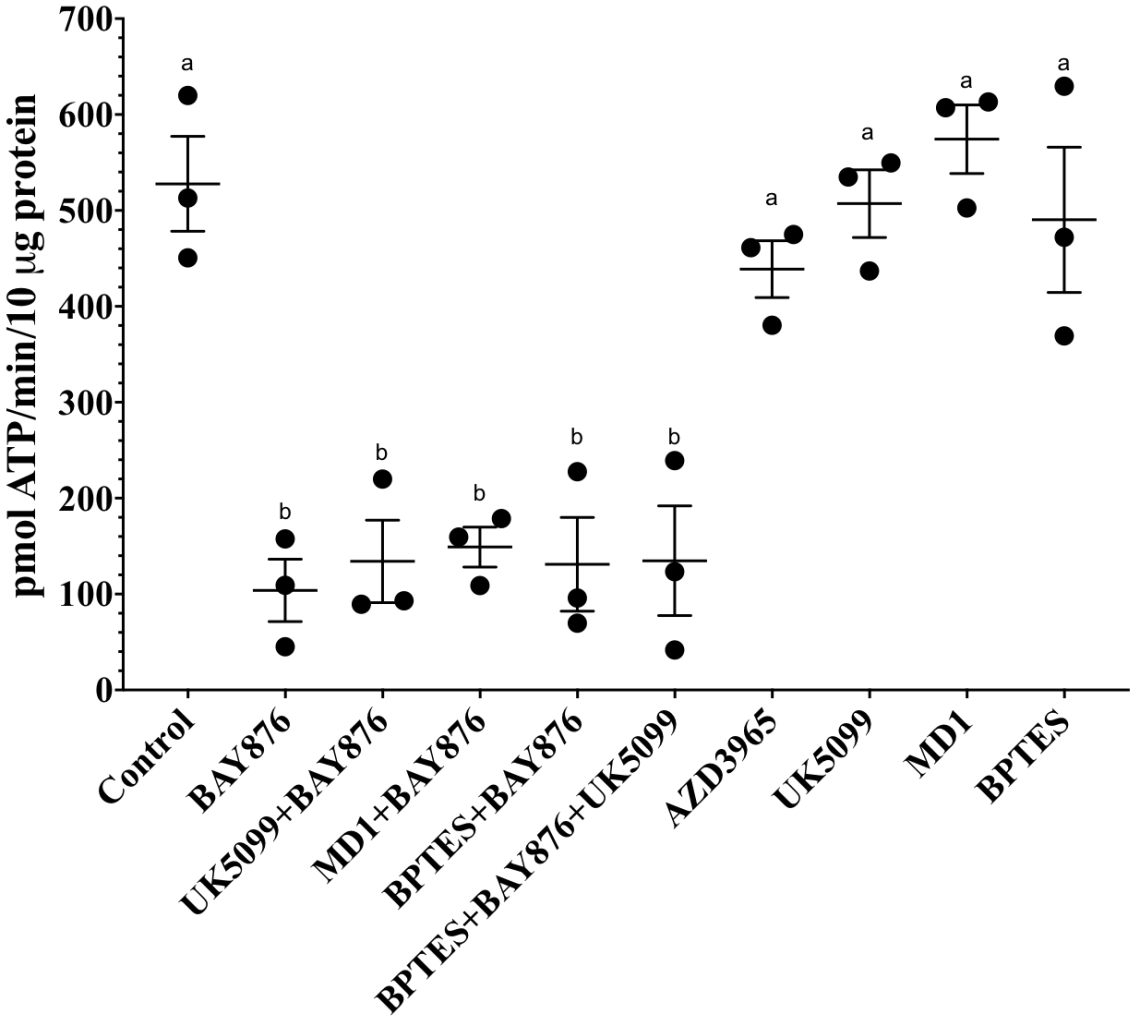

Figure 38: HCMEC/D3 INHIBITOR GLYCOLYTIC ATP PRODUCTION RATES Glycolytic ATP production rate values of hCMEC/D3 cells were calculated, based on real-time PER measurements, for each inhibitor treatment group. Values from each inhibitor group were compared to each other group. All measurements were normalized to 10 μg protein. Each point represents a single measurement and error bars represent SEM of n=3 samples. Shared letters indicate no significant difference. Absence of a shared letter indicates a significant difference between groups.

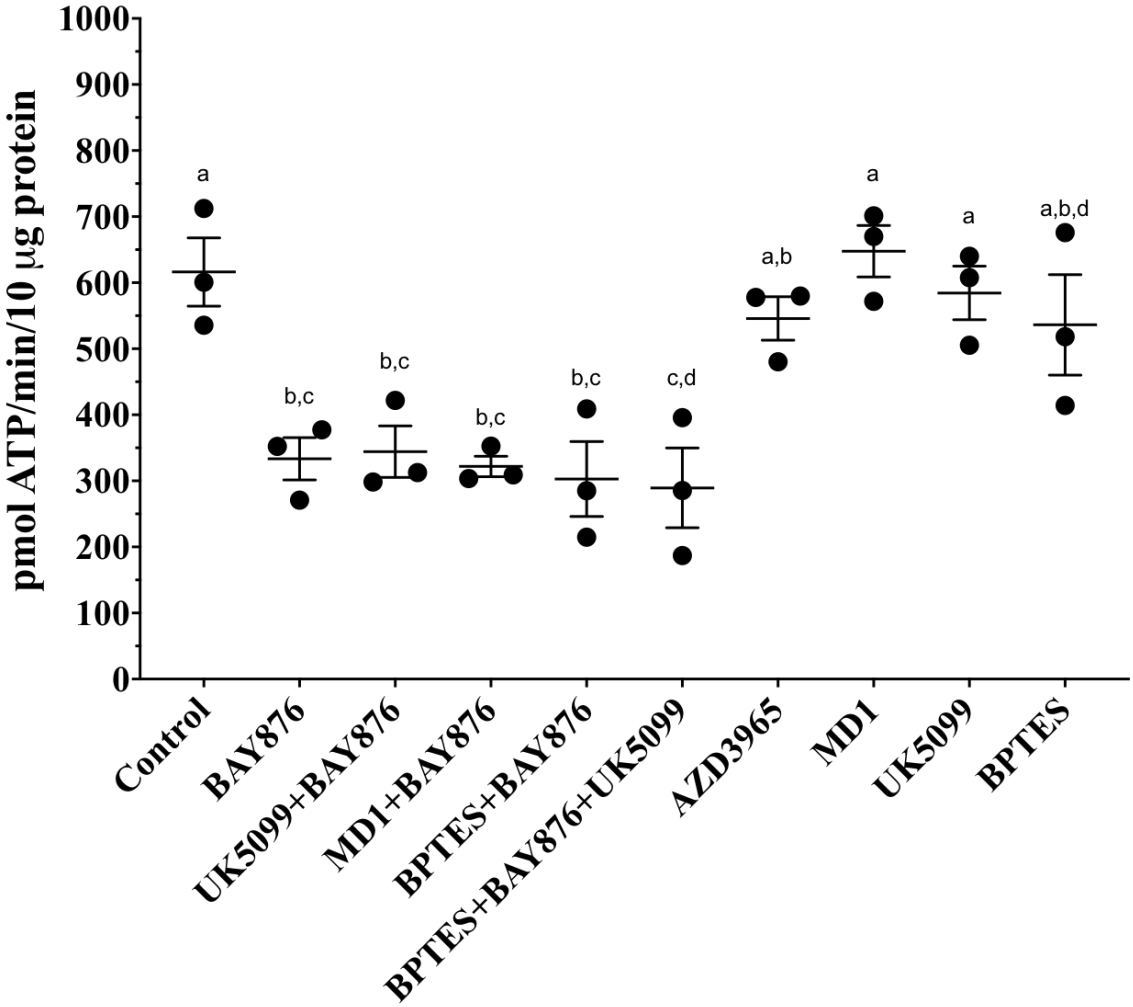

Figure 39: HCMEC/D3 INHIBITOR TOTAL ATP PRODUCTION RATES Total ATP production rate values of hCMEC/D3 cells were calculated, by adding mitochondrial and glycolytic ATP production rates, for each inhibitor treatment group. Values from each inhibitor group were compared to each other group. All measurements were normalized to 10 μg protein. Each point represents a single measurement and error bars represent SEM of n=3 samples. Shared letters indicate no significant difference. Absence of a shared letter indicates a significant difference between groups.

Chapter 8: Discussion

Using real-time measurements of OCR and ECAR, the mitochondrial respiration and glycolytic rates of hCMEC/D3 human immortalized microvascular endothelial cells were able to be quantified, respectively. Using this technology, we were able to reveal many insights into brain endothelial cell OCR, PER, and ATP production rates. After

characterizing mitochondrial respiration and glycolytic rates, we then tested metabolite preference of glucose, glutamine, pyruvate, or a combination of two or three metabolites. We were then able to test the metabolic plasticity of hCMEC/D3 cells by utilizing various nutrient transport inhibitors. These small molecule inhibitors targeted GLUT1, MCT1, MPC, and GLS. Inhibiting these transporters allowed us to observe how hCMEC/D3 cells are able to compensate in energy production with the disruption of different metabolic pathways.

Initial experiments revealed that hCMEC/D3 cells exhibit a metabolism driven majorly by glycolysis, as over 96% of protons exported were from glycolysis, via lactate production, rather than OXPHOS. This is further supported by results from ATP rate assays performed. These assays reveal that hCMEC/D3 cells display an 85.7% glycolytic ATP production rate, while mitochondrial ATP production is 14.3%. These results do not support our original hypothesis that hCMEC/D3 cells would have a primarily oxidative mode of metabolism.

There are advantages to a primarily glycolytic metabolism for brain endothelial cells. Increased glycolytic rates decreases the production of damaging reactive oxygen species (ROS) and also allows unused oxygen to be available in the surrounding tissue [37]. Therefore, it is important to reduce the amount of ROS within the CNS to prevent neural damage and dysfunction. Lactate produced via glycolysis can also act as a signaling molecule for active angiogenesis [79−81]. This can allow a large proportion of the brain and CNS to be vascularized to make nutrient, ion, and other molecules easily accessible from the blood. A glycolytic metabolism is furthermore said to precondition endothelial cells to sprout in avascular and hypoxic environments [82]. Therefore, it can be beneficial

for microvascular endothelial cells to express a highly glycolytic metabolic phenotype to encourage maximal vessel sprouting within the CNS and provide oxygen, nutrients, and other substances for neural function.

With the exception of glutamine alone, cells exposed to glucose, pyruvate, a combination of glucose and pyruvate or glucose and glutamine, or a combination of glutamine and pyruvate, are able to alter glycolytic or OXPHOS rates to maintain the total ATP production rate in hCMEC/D3 cells similarly to complete media. This can be accomplished by either increasing glycolytic or OXPHOS rates, based on available metabolites, to compensate for a loss in ATP production from OXPHOS or glycolytic rates, respectively. This supports the hypothesis that cells alter their metabolic phenotype, based on available metabolites, to maintain adequate energy production. It shall be noted, however, that mitochondrial and glycolytic ATP production rates remained unchanged in cells with glucose and pyruvate combined, in comparison to complete media. Therefore, pyruvate can act as a major contributor to OXPHOS with glucose present. Interestingly, with glucose as the only metabolite, hCMEC/D3 cells exhibit a lower glycolytic ATP production rate and higher mitochondrial ATP production rate than those of which are subject to a combination of 5.83 mM glucose, 1.5 mM glutamine, and 1 mM pyruvate. This suggests that the cells, when glucose is abundant, in comparison to pyruvate and glutamine, utilize pyruvate, glutamine, or both, to increase glycolytic ATP production rates. With an equal concentration of glucose, glutamine, and pyruvate in a single media, hCMEC/D3 cells are able to increase mitochondrial respiration and mitochondrial ATP production rates. Glycolysis and glycolytic ATP rates, in contrast, decrease for cells in this complete media compared to control media containing 5.83 mM glucose, 1.5 mM

glutamine, and 1 mM pyruvate. Although mitochondrial respiration increases, the total ATP production rate of cells in this complete media is lower than cells in control media. Since OXPHOS produces more ATP molecules, per molecule of glucose, than glycolysis, glycolytic and total ATP production rates could be lowered as the total available ATP amount within the cells can remain constant.

As these studies have shown, hCMEC/D3 cells are highly reliant on glycolysis as a mode of energy production. Inhibiting GLUT1, via BAY876, showed to significantly decrease glycolytic and total ATP production rates. However, inhibition of MCT1, MPC, and GLS had no effect on ATP production. UK5099, MD1, and BPTES did not affect basal respiration or glycolytic rates. However, UK5099, MD1, and BPTES decreased maximal respiration and spare respiratory capacity OCR. This suggests that the mitochondria of hCMEC/D3 cells are able to adequately fuel basal oxygen consumption, even with MPC or GLS inhibited. Pyruvate or glutamine alone can suffice to maintain the basal OCR in hCMEC/D3 cells. However, when subjected to FCCP, hCMEC/D3 cells are not able to respire as much as the control. This can be due to the lack of one metabolite, either pyruvate or glutamine, able to enter the TCA cycle and fuel OXPHOS. With one of the two metabolites unable to enter the TCA cycle, maximal respiration and spare respiratory capacity is significantly hindered. However, when MPC and GLS are inhibited along with GLUT1, these cells are able to maintain maximal respiration OCR. This suggests that cells are able to switch from pyruvate and glutamine metabolism to fatty acid, amino acid, or both metabolism to fuel OXPHOS. Inhibition of GLUT1 or GLS, via BAY876 or BPTES respectively, significantly decreased compensatory glycolysis in hCMEC/D3 cells as well. This further supports that glutamine is able to fuel

glycolytic rates. However, a combination of BAY876 and MD1 did not show to decrease compensatory glycolysis. These inhibition studies support our hypothesis that disruption of glucose transport, mitochondrial pyruvate transport, or conversion of glutamine into glutamate alter various aspects of glycolytic or mitochondrial energy production. Inhibition of lactate transport, however, did not alter cellular metabolism. Exposing cells to the small molecule inhibitor MD1 showed similar results of MPC inhibition. This suggests that MD1, at 10 μM concentration, acts as an MPC inhibitor rather than a dual MCT1 and MCT 4 inhibitor. Given these results, it is possible that inhibiting MCT1 did not affect cellular metabolism as cells were able to effectively export lactate at a consistent rate via MCT4.

These experiments show the rapid metabolic adaptation of hCMEC/D3 cells. These cells are able to alter their metabolic phenotype, in a short amount of time, in order to compensate for energy demands. Although these cells seem to favor glycolysis, with enough substrates to fuel OXPHOS, the cells are able to switch to, and rely on, mitochondrial respiration to generate energy. The same phenomenon can be seen with nutrient transport inhibition. Although the cells cannot maintain total ATP production, when glucose transport is inhibited, hCMEC/D3 cells increase OXPHOS in an attempt to meet energy demands. With glucose as an only substrate, hCMEC/D3 cells are able to utilize glycolysis while OXPHOS is decreased as a majority of glucose is shunted to lactate production.

Extracellular flux analysis reveals can reveal many insights of cellular energetic rates. There is supporting evidence that shows using this technology can allow quantification of glycolytic, OXPHOS, and ATP production rates accurately. Quantifying these rates can

reveal the metabolic phenotype and plasticity in various substrate compositions. Further analysis can also reveal how much certain metabolic substrates contribute to glycolysis and OXPHOS. Such studies have been performed by Mookerjee *et al.,* (2017), providing useful calculations and analyses of metabolic substrate contribution to cellular energetics. Though this indirect method of measuring cellular energetics is well supported and beneficial, it does not provide specific amounts of intracellular metabolites and ATP. In order to measure these parameters, mass spectrometry and a fluorescent, or radioactive, labeled ATP rate assay can be utilized. These experiments can reveal the intracellular amounts of metabolite intermediates and ATP, respectively.

Metabolomics is gaining attention in cancer treatment, stem cell biology, and immunology. These results can contribute to furthering research in CNS disorder treatments. Understanding healthy brain endothelial cell bioenergetics can give investigators a platform to begin studying disease-state alterations in brain endothelial cellular metabolism. A dysfunctional NVU has shown to be associated with various CNS disorders. This dysfunction can be associated with changes in brain endothelial cell metabolism. Different disease states can possibly exhibit a specific, altered, metabolic phenotype in brain endothelial cells. Targeting altered metabolic pathways in disease-state brain endothelial cells can provide a non-invasive method of treatment for diseases involved with NVU dysfunction. On the contrary, understanding healthy brain endothelial cell metabolism can also possibly prevent NVU dysfunction and age-associate pathologies of the NVU. Incorporating a diet, or developing supplements, that support healthy brain endothelial cell metabolism can, in turn, support healthy CNS

function. Adequate levels of glucose, glutamine, pyruvate, and other substances in blood serum can support healthy brain endothelial cell function, and thus healthy CNS function.

Though much was gathered from these studies, there is quite a lot of uncovered information regarding the bioenergetics of brain endothelial cells that can explored. Future studies can investigate, even further, the roles different metabolites play in hCMEC/D3 bioenergetics. Such metabolites can include fatty acids, lactate, various amino acids, TCA molecules, and other compositions. Other future studies may involve measuring cell bioenergetics in a hypoxic environment or by using a disease-state model to measure differences in energy production between healthy and disease-state. Effects of simulating blood flow, co-culture with other cells of the NVU, and *in vivo* studies can give insights to bioenergetics of brain endothelial cells in a more physiological environment. Metabolic enzyme expression and activity in brain endothelial cells can also reveal important information regarding brain endothelial cell bioenergetics. As with the effect of metabolites and metabolic pathways, changes in brain endothelial cell bioenergetics can very well involve changes in metabolic enzyme expression or activity. Given the highly glycolytic nature of these cells, it is possible that major changes would involve glycolytic enzymes. This could reveal other targets for diseases involving NVU dysfunction or, contrarily, insights to maintaining healthy NVU function. Measuring the bioenergetic properties, using extracellular flux analysis, of hCMEC/D3 cells revealed an abundance of information regarding brain endothelial cell metabolism. These studies provide a glance of brain endothelial cell bioenergetics *in vitro* and can be referred back to in future studies involving brain endothelial cell or NVU metabolism.

References

1 Abbott, N.J. (2013) Blood–brain barrier structure and function and the challenges for CNS drug delivery. *Journal of Inherited Metabolic Disease* 36, 437–449

2 Abbott, N.J. *et al.* (2010) Structure and function of the blood–brain barrier. *Neurobiology of Disease* 37, 13–25

3 Abbott, N.J. *et al.* (2006) Astrocyte–endothelial interactions at the blood–brain barrier. *Nature Reviews Neuroscience* 7, 41–53

4 Ballabh, P. *et al.* (2004) The blood–brain barrier: an overview: Structure, regulation, and clinical implications. *Neurobiology of Disease* 16, 1–13

5 Eigenmann, D.E. *et al.* (2013) Comparative study of four immortalized human brain capillary endothelial cell lines, hCMEC/D3, hBMEC, TY10, and BB19, and optimization of culture conditions, for an in vitro blood–brain barrier model for drug permeability studies. *Fluids Barriers CNS* 10, 33

6 Erdő, F. *et al.* (2017) Age-associated physiological and pathological changes at the blood–brain barrier: A review. *J Cereb Blood Flow Metab* 37, 4–24

7 Hawkins, B.T. and Davis, T.P. (2005) The Blood-Brain Barrier/Neurovascular Unit in Health and Disease. *Pharmacol Rev* 57, 173–185

8 Pérez-Escuredo, J. *et al.* (2016) Monocarboxylate transporters in the brain and in cancer. *Biochimica et Biophysica Acta (BBA) - Molecular Cell Research* 1863, 2481–2497

9 Sajja, R.K. *et al.* (2014) Impact of altered glycaemia on blood-brain barrier endothelium: an in vitro study using the hCMEC/D3 cell line. *Fluids Barriers CNS* 11, 8

10 Salmina, A.B. *et al.* (2015) Glycolysis-mediated control of blood-brain barrier development and function. *The International Journal of Biochemistry & Cell Biology* 64, 174–184

11 Urich, E. *et al.* (2012) Transcriptional Profiling of Human Brain Endothelial Cells Reveals Key Properties Crucial for Predictive In Vitro Blood-Brain Barrier Models. *PLOS ONE* 7, e38149

12 V, M. *et al.* The neurovascular unit – concept review. *Acta Physiologica* 210, 790–798

13 Wilhelm, I. *et al.* (2016) Heterogeneity of the blood-brain barrier. *Tissue Barriers* 4,

14 Keaney, J. and Campbell, M. The dynamic blood–brain barrier. *The FEBS Journal* 282, 4067–4079

15 Sandoval, K.E. and Witt, K.A. (2008) Blood-brain barrier tight junction permeability and ischemic stroke. *Neurobiology of Disease* 32, 200–219

16 Stanimirovic, D.B. and Friedman, A. (2012) Pathophysiology of the neurovascular unit: disease cause or consequence? *J Cereb Blood Flow Metab* 32, 1207–1221

17 Hansen, A.J. (1985) Effect of anoxia on ion distribution in the brain. *Physiological Reviews* 65, 101–148

18 Haseloff, R.F. *et al.* (2015) Transmembrane proteins of the tight junctions at the blood–brain barrier: Structural and functional aspects. *Seminars in Cell & Developmental Biology* 38, 16–25

19 Nitta, T. *et al.* (2003) Size-selective loosening of the blood-brain barrier in claudin-5–deficient mice. *The Journal of Cell Biology* 161, 653–660

20 Wolburg, H. and Lippoldt, A. (2002) Tight junctions of the blood–brain barrier: development, composition and regulation. *Vascular Pharmacology* 38, 323–337
21 Wolburg, H. *et al.* (2009) Brain endothelial cells and the glio-vascular complex. *Cell Tissue Res* 335, 75–96
22 Bhowmik, A. *et al.* (2015) Blood Brain Barrier: A Challenge for Effectual Therapy of Brain Tumors. *Biomed Res Int* 2015,
23 Pardridge, W.M. (2005) The Blood-Brain Barrier: Bottleneck in Brain Drug Development. *NeuroRx* 2, 3–14
24 Sanchez-Covarrubias, L. *et al.* (2014) Transporters at CNS Barrier Sites: Obstacles or Opportunities for Drug Delivery? *Curr Pharm Des* 20, 1422–1449
25 Günzel, D. and Yu, A.S.L. (2013) Claudins and the Modulation of Tight Junction Permeability. *Physiological Reviews* 93, 525–569
26 Ohtsuki, S. *et al.* (2008) mRNA expression levels of tight junction protein genes in mouse brain capillary endothelial cells highly purified by magnetic cell sorting. *Journal of Neurochemistry* 104, 147–154
27 Morita, K. *et al.* (1999) Endothelial Claudin. *J Cell Biol* 147, 185–194
28 Wang, G. *et al.* (2018) Disruption of Intracellular ATP Generation and Tight Junction Protein Expression during the Course of Brain Edema Induced by Subacute Poisoning of 1,2-Dichloroethane. *Front Neurosci* 12,
29 Denker, B.M. and Nigam, S.K. (1998) Molecular structure and assembly of the tight junction. *American Journal of Physiology-Renal Physiology* 274, F1–F9
30 Simpson, I.A. *et al.* (2007) SUPPLY AND DEMAND IN CEREBRAL ENERGY METABOLISM: THE ROLE OF NUTRIENT TRANSPORTERS. *J Cereb Blood Flow Metab* 27, 1766–1791
31 Ohtsuki, S. and Terasaki, T. (2007) Contribution of Carrier-Mediated Transport Systems to the Blood–Brain Barrier as a Supporting and Protecting Interface for the Brain; Importance for CNS Drug Discovery and Development. *Pharm Res* 24, 1745–1758
32 Ohtsuki, S. *et al.* (2013) Quantitative Targeted Absolute Proteomic Analysis of Transporters, Receptors and Junction Proteins for Validation of Human Cerebral Microvascular Endothelial Cell Line hCMEC/D3 as a Human Blood–Brain Barrier Model. *Molecular Pharmaceutics* 10, 289–296
33 Roberts, L.M. *et al.* (2008) Subcellular localization of transporters along the rat blood–brain barrier and blood–cerebral-spinal fluid barrier by in vivo biotinylation. *Neuroscience* 155, 423–438
34 Pierre, K. and Pellerin, L. (2005) Monocarboxylate transporters in the central nervous system: distribution, regulation and function. *Journal of Neurochemistry* 94, 1–14
35 Betz, A.L. *et al.* (1980) Polarity of the blood-brain barrier: Distribution of enzymes between the luminal and antiluminal membranes of brain capillary endothelial cells. *Brain Research* 192, 17–28
36 Joó, F. (1996) Endothelial cells of the brain and other organ systems: Some similarities and differences. *Progress in Neurobiology* 48, 255–273
37 Eelen, G. *et al.* (2017) Endothelial Cell Metabolism. *Physiological Reviews* 98, 3–58

38 Jin, L. and Zhou, Y. (2019) Crucial role of the pentose phosphate pathway in malignant tumors. *Oncol Lett* 17, 4213–4221
39 Moreno-Sánchez, R. *et al.* (2007) Energy metabolism in tumor cells. *The FEBS Journal* 274, 1393–1418
40 Beloueche-Babari, M. *et al.* (2017) MCT1 inhibitor AZD3965 increases mitochondrial metabolism, facilitating combination therapy and non-invasive magnetic resonance spectroscopy. *Cancer Res* 77, 5913–5924
41 Benjamin, D. *et al.* (2018) Dual Inhibition of the Lactate Transporters MCT1 and MCT4 Is Synthetic Lethal with Metformin due to NAD+ Depletion in Cancer Cells. *Cell Reports* 25, 3047-3058.e4
42 Halestrap, A.P. The monocarboxylate transporter family—Structure and functional characterization. *IUBMB Life* 64, 1–9
43 Brière, J.-J. *et al.* (2006) Tricarboxylic acid cycle dysfunction as a cause of human diseases and tumor formation. *American Journal of Physiology-Cell Physiology* 291, C1114–C1120
44 Kim, B. *et al.* (2017) Glutamine fuels proliferation but not migration of endothelial cells. *EMBO J.* 36, 2321–2333
45 Huang, H. *et al.* (2017) Role of glutamine and interlinked asparagine metabolism in vessel formation. *EMBO J* 36, 2334–2352
46 Jafri, M.S. *et al.* (2001) Cardiac Energy Metabolism: Models of Cellular Respiration. *Annu. Rev. Biomed. Eng.* 3, 57–81
47 Mookerjee, S.A. *et al.* (2017) Quantifying intracellular rates of glycolytic and oxidative ATP production and consumption using extracellular flux measurements. *J. Biol. Chem.* 292, 7189–7207
48 Corbet, C. and Feron, O. (2017) Cancer cell metabolism and mitochondria: Nutrient plasticity for TCA cycle fueling. *Biochimica et Biophysica Acta (BBA) - Reviews on Cancer* 1868, 7–15
49 Dang, C.V. (2009) MYC, microRNAs and glutamine addiction in cancers. *Cell Cycle* 8, 3243–3245
50 DeBerardinis, R.J. *et al.* (2008) The Biology of Cancer: Metabolic Reprogramming Fuels Cell Growth and Proliferation. *Cell Metabolism* 7, 11–20
51 Diers, A.R. *et al.* (2012) Pyruvate fuels mitochondrial respiration and proliferation of breast cancer cells: effect of monocarboxylate transporter inhibition. *Biochem J* 444, 561–571
52 Feron, O. (2009) Pyruvate into lactate and back: From the Warburg effect to symbiotic energy fuel exchange in cancer cells. *Radiotherapy and Oncology* 92, 329–333
53 Scalise, M. *et al.* (2018) The Human SLC1A5 (ASCT2) Amino Acid Transporter: From Function to Structure and Role in Cell Biology. *Front Cell Dev Biol* 6,
54 Wang, Y.-D. *et al.* (2013) Inhibition of Glucose Transporter 1 (GLUT1) Chemosensitized Head and Neck Cancer Cells to Cisplatin. *Technol Cancer Res Treat* 12, 525–535
55 Zhao, F. *et al.* (2016) Inhibition of Glut1 by WZB117 sensitizes radioresistant breast cancer cells to irradiation. *Cancer Chemother Pharmacol* 77, 963–972
56 Vander Heiden, M.G. *et al.* (2009) Understanding the Warburg Effect: The Metabolic Requirements of Cell Proliferation. *Science* 324, 1029–1033

57 Warburg, O. (1956) On the Origin of Cancer Cells. *Science* 123, 309–314
58 Corbet, C. *et al.* (2018) Interruption of lactate uptake by inhibiting mitochondrial pyruvate transport unravels direct antitumor and radiosensitizing effects. *Nature Communications* 9,
59 Curtis, N.J. *et al.* (2017) Pre-clinical pharmacology of AZD3965, a selective inhibitor of MCT1: DLBCL, NHL and Burkitt’s lymphoma anti-tumor activity. *Oncotarget* 8,
60 Takada, T. *et al.* (2016) Inhibition of monocarboxylate transporter 1 suppresses the proliferation of glioblastoma stem cells. *J Physiol Sci* 66, 387–396
61 Pearce, E.L. and Pearce, E.J. (2013) Metabolic Pathways in Immune Cell Activation and Quiescence. *Immunity* 38, 633–643
62 Ryall, J.G. *et al.* (2015) Metabolic Reprogramming of Stem Cell Epigenetics. *Cell Stem Cell* 17, 651–662
63 Shares, B.H. *et al.* (2018) Active mitochondria support osteogenic differentiation by stimulating β-catenin acetylation. *J. Biol. Chem.* 293, 16019–16027
64 Tan, Z. *et al.* (2015) The Monocarboxylate Transporter 4 Is Required for Glycolytic Reprogramming and Inflammatory Response in Macrophages. *J Biol Chem* 290, 46–55
65 Banks, W.A. (2012) Drug Delivery to the Brain in Alzheimer's Disease: Consideration of the Blood-brain Barrier. *Adv Drug Deliv Rev* 64, 629–639
66 Saraiva, C. *et al.* (2016) Nanoparticle-mediated brain drug delivery: Overcoming blood–brain barrier to treat neurodegenerative diseases. *Journal of Controlled Release* 235, 34–47
67 Rotstein, M. *et al.* (2010) Glut1 deficiency: Inheritance pattern determined by haploinsufficiency. *Annals of Neurology* 68, 955–958
68 Winkler, E.A. *et al.* (2015) GLUT1 reductions exacerbate Alzheimer's disease vasculo-neuronal dysfunction and degeneration. *Nature Neuroscience* 18, 521–530
69 Krützfeldt, A. *et al.* (1990) Metabolism of exogenous substrates by coronary endothelial cells in culture. *Journal of Molecular and Cellular Cardiology* 22, 1393–1404
70 Oldendorf, W.H. *et al.* (1977) The large apparent work capability of the blood-brain barrier: A study of the mitochondrial content of capillary endothelial cells in brain and other tissues of the rat. *Annals of Neurology* 1, 409–417
71 Romero, N. *et al.* (2018) , Quantifying Cellular ATP Production Rate Using Agilent Seahorse XF Technology.
72 Weksler, B. *et al.* (2013) The hCMEC/D3 cell line as a model of the human blood brain barrier. *Fluids Barriers CNS* 10, 16
73 Weksler, B.B. *et al.* (2005) Blood-brain barrier-specific properties of a human adult brain endothelial cell line. *The FASEB Journal* 19, 1872–1874
74 Psychogios, N. *et al.* (2011) The Human Serum Metabolome. *PLoS ONE* 6, e16957
75 Leighton, B. *et al.* (1987) Maximum activities of some key enzymes of glycolysis, glutaminolysis, Krebs cycle and fatty acid utilization in bovine pulmonary endothelial cells. *FEBS Letters* 225, 93–96
76 Pochini, L. *et al.* (2014) Membrane transporters for the special amino acid glutamine: structure/function relationships and relevance to human health. *Front Chem* 2, 61

77 Bender, T. and Martinou, J.-C. (2016) The mitochondrial pyruvate carrier in health and disease: To carry or not to carry? *Biochimica et Biophysica Acta (BBA) - Molecular Cell Research* 1863, 2436–2442
78 Divakaruni, A.S. *et al.* (2017) Inhibition of the mitochondrial pyruvate carrier protects from excitotoxic neuronal death. *J Cell Biol* 216, 1091–1105
79 Hunt, T.K. *et al.* (2007) Aerobically derived lactate stimulates revascularization and tissue repair via redox mechanisms. *Antioxid. Redox Signal.* 9, 1115–1124
80 Ruan, G.-X. and Kazlauskas, A. (2013) Lactate engages receptor tyrosine kinases Axl, Tie2, and vascular endothelial growth factor receptor 2 to activate phosphoinositide 3-kinase/Akt and promote angiogenesis. *J. Biol. Chem.* 288, 21161–21172
81 Sonveaux, P. *et al.* (2012) Targeting the lactate transporter MCT1 in endothelial cells inhibits lactate-induced HIF-1 activation and tumor angiogenesis. *PLoS ONE* 7, e33418
82 Gatenby, R.A. and Gillies, R.J. (2004) Why do cancers have high aerobic glycolysis? *Nature Reviews Cancer* 4, 891
83 Yoshida, G. (2015) Metabolic reprogramming: The emerging concept and associated therapeutic strategies. *Journal of Experimental & Clinical Cancer Research : CR* 34,
84 Chinnery, P.F. and Schon, E.A. (2003) Mitochondria. *Journal of Neurology, Neurosurgery & Psychiatry* 74, 1188–1199
85 Rinholm, J.E. *et al.* (2011) Regulation of Oligodendrocyte Development and Myelination by Glucose and Lactate. *J. Neurosci.* 31, 538–548
86 Adams, J.L. *et al.* (2015) Big opportunities for small molecules in immuno-oncology. *Nature Reviews Drug Discovery* 14, 603–622
87 Daneman, R. and Prat, A. (2015) The Blood–Brain Barrier. *Cold Spring Harb Perspect Biol* 7, a020412
88 Nancolas, B. *et al.* (2016) The anti-tumour agent lonidamine is a potent inhibitor of the mitochondrial pyruvate carrier and plasma membrane monocarboxylate transporters. *Biochem J* 473, 929–936
89 Li, H.-M. *et al.* (2017) Blockage of glycolysis by targeting PFKFB3 suppresses tumor growth and metastasis in head and neck squamous cell carcinoma. *J Exp Clin Cancer Res* 36,
90 Vijay, N. and Morris, M. (2014) Role of Monocarboxylate Transporters in Drug Delivery to the Brain. *Current Pharmaceutical Design* 20, 1487–1498
91 McCommis, K.S. and Finck, B.N. (2015) Mitochondrial pyruvate transport: a historical perspective and future research directions. *Biochem J* 466, 443–454
92 Mookerjee, S.A. *et al.* (2015) The contributions of respiration and glycolysis to extracellular acid production. *Biochimica et Biophysica Acta (BBA) - Bioenergetics* 1847, 171–181
93 Meireles, M. *et al.* (2013) Characterization and Modulation of Glucose Uptake in a Human Blood–Brain Barrier Model. *J Membrane Biol* 246, 669–677
94 Page, S. *et al.* (2016) Cerebral hypoxia/ischemia selectively disrupts tight junctions complexes in stem cell-derived human brain microvascular endothelial cells. *Fluids Barriers CNS* 13,

95 Al-Ahmad, A.J. (2017) Comparative study of expression and activity of glucose transporters between stem cell-derived brain microvascular endothelial cells and hCMEC/D3 cells. *American Journal of Physiology-Cell Physiology* 313, C421–C429
96 Pike Winer, L.S. and Wu, M. (2014) Rapid Analysis of Glycolytic and Oxidative Substrate Flux of Cancer Cells in a Microplate. *PLoS One* 9,
97 Oldendorf, W.H. and Brown, W.J. (1975) Greater Number of Capillary Endothelial Cell Mitochondria in Brain Than in Muscle , Greater Number of Capillary Endothelial Cell Mitochondria in Brain Than in Muscle. *Proceedings of the Society for Experimental Biology and Medicine* 149, 736–738
98 Poller, B. *et al.* The human brain endothelial cell line hCMEC/D3 as a human blood-brain barrier model for drug transport studies. *Journal of Neurochemistry* 107, 1358–1368
99 Jha, M.K. and Morrison, B.M. (2018) Glia-neuron energy metabolism in health and diseases: New insights into the role of nervous system metabolic transporters. *Experimental Neurology* 309, 23–31
100 Sewduth, R. and Santoro, M.M. (2016) "Decoding" Angiogenesis: New Facets Controlling Endothelial Cell Behavior. *Front Physiol* 7,
101 Harjes, U. *et al.* (2012) Endothelial cell metabolism and implications for cancer therapy. *Br J Cancer* 107, 1207–1212
102 Wolburg, H. *et al.* (2003) Localization of claudin-3 in tight junctions of the blood-brain barrier is selectively lost during experimental autoimmune encephalomyelitis and human glioblastoma multiforme. *Acta Neuropathol* 105, 586–592
103 Stapor, P. *et al.* (2014) Angiogenesis revisited – role and therapeutic potential of targeting endothelial metabolism. *J Cell Sci* 127, 4331–4341
104 Meireles, M. *et al.* (2013) Characterization and Modulation of Glucose Uptake in a Human Blood–Brain Barrier Model. *J Membrane Biol* 246, 669–677
105 Pinheiro, C. *et al.* (2012) Role of monocarboxylate transporters in human cancers: state of the art. *Journal of Bioenergetics and Biomembranes* 44, 127–139
106 Marchiq, I. and Pouysségur, J. (2016) Hypoxia, cancer metabolism and the therapeutic benefit of targeting lactate/H+ symporters. *J Mol Med (Berl)* 94, 155–171
107 Altman, B.J. *et al.* (2016) From Krebs to clinic: glutamine metabolism to cancer therapy. *Nature Reviews Cancer* 16, 619–634
108 Helms, H.C. *et al.* (2016) In vitro models of the blood–brain barrier: An overview of commonly used brain endothelial cell culture models and guidelines for their use. *J Cereb Blood Flow Metab* 36, 862–890
109 Krizbai, I.A. *et al.* (2015) Endothelial-Mesenchymal Transition of Brain Endothelial Cells: Possible Role during Metastatic Extravasation. *PLOS ONE* 10, e0119655
110 Wang, D. *et al.* (2018) Hypoxia induces lactate secretion and glycolytic efflux by downregulating mitochondrial pyruvate carrier levels in human umbilical vein endothelial cells. *Molecular Medicine Reports* 18, 1710–1717
111 Rohlenova, K. *et al.* (2018) Endothelial Cell Metabolism in Health and Disease. *Trends in Cell Biology* 28, 224–236

112 Daneman, R. and Prat, A. (2015) The Blood–Brain Barrier. *Cold Spring Harb Perspect Biol* 7,
113 Oldendorf, W.H. *et al.* (1977) The large apparent work capability of the blood-brain barrier: a study of the mitochondrial content of capillary endothelial cells in brain and other tissues of the rat. *Ann. Neurol.* 1, 409–417
114 Cucullo, L. *et al.* (2011) The role of shear stress in Blood-Brain Barrier endothelial physiology. *BMC Neurosci* 12, 40
115 Caja, S. and Enríquez, J.A. (2017) Mitochondria in endothelial cells: Sensors and integrators of environmental cues. *Redox Biol* 12, 821–827
116 Poller, B. *et al.* (2008) The human brain endothelial cell line hCMEC/D3 as a human blood-brain barrier model for drug transport studies. *Journal of Neurochemistry* 107, 1358–1368
117 Ohtsuki, S. *et al.* (2013) Quantitative Targeted Absolute Proteomic Analysis of Transporters, Receptors and Junction Proteins for Validation of Human Cerebral Microvascular Endothelial Cell Line hCMEC/D3 as a Human Blood–Brain Barrier Model. *Mol. Pharmaceutics* 10, 289–296
118 Linden, C.V. and Corbet, C. (2018) Killing two birds with one stone: Blocking the mitochondrial pyruvate carrier to inhibit lactate uptake by cancer cells and radiosensitize tumors. *Mol Cell Oncol* 5,
119 Corbet, C. *et al.* (2018) Interruption of lactate uptake by inhibiting mitochondrial pyruvate transport unravels direct antitumor and radiosensitizing effects. *Nat Commun* 9, 1208
120 Lee, Y.-M. *et al.* (2016) Inhibition of glutamine utilization sensitizes lung cancer cells to apigenin-induced apoptosis resulting from metabolic and oxidative stress. *International Journal of Oncology* 48, 399–408
121 Swerdlow, R.H. *et al.* (2013) Glycolysis–respiration relationships in a neuroblastoma cell line. *Biochimica et Biophysica Acta (BBA) - General Subjects* 1830, 2891–2898
122 Dott, W. *et al.* (2014) Modulation of mitochondrial bioenergetics in a skeletal muscle cell line model of mitochondrial toxicity. *Redox Biol* 2, 224–233
123 Sakamuri, S.S.V.P. *et al.* (2018) Measurement of respiratory function in isolated cardiac mitochondria using Seahorse XFe24 Analyzer: applications for aging research. *GeroScience* 40, 347–356
124 Calton, M.A. *et al.* (2018) Method for measuring extracellular flux from intact polarized epithelial monolayers. *Mol Vis* 24, 425–433
125 Dranka, B.P. *et al.* (2010) Mitochondrial reserve capacity in endothelial cells: The impact of nitric oxide and reactive oxygen species. *Free Radical Biology and Medicine* 48, 905–914
126 Readnower, R.D. *et al.* (2012) Standardized bioenergetic profiling of adult mouse cardiomyocytes. *Physiological Genomics* 44, 1208–1213
127 Dier, U. *et al.* (2014) Bioenergetic Analysis of Ovarian Cancer Cell Lines: Profiling of Histological Subtypes and Identification of a Mitochondria-Defective Cell Line. *PLoS One* 9,
128 Diers, A.R. *et al.* (2013) Mitochondrial Bioenergetics of Metastatic Breast Cancer Cells in Response to Dynamic Changes in Oxygen Tension: Effects of HIF-1α. *PLoS One* 8,

129 Cerutti, C. and Ridley, A.J. (2017) Endothelial cell-cell adhesion and signaling. *Exp Cell Res* 358, 31–38
130 Hervé, F. *et al.* (2008) CNS Delivery Via Adsorptive Transcytosis. *AAPS J* 10, 455–472
131 Jose, C. *et al.* (2011) Choosing between glycolysis and oxidative phosphorylation: A tumor's dilemma? *Biochimica et Biophysica Acta (BBA) - Bioenergetics* 1807, 552–561
132 Yellen, G. (2018) Fueling thought: Management of glycolysis and oxidative phosphorylation in neuronal metabolism. *J Cell Biol* 217, 2235–2246
133 Wu, H. *et al.* (2016) Lactic acidosis switches cancer cells from aerobic glycolysis back to dominant oxidative phosphorylation. *Oncotarget* 7, 40621–40629
134 Handel, M.E. *et al.* (2019) The Whys and Hows of Calculating Total Cellular ATP Production Rate. *Trends in Endocrinology & Metabolism* 30, 412–416
135 Végran, F. *et al.* (2011) Lactate Influx through the Endothelial Cell Monocarboxylate Transporter MCT1 Supports an NF-κB/IL-8 Pathway that Drives Tumor Angiogenesis. *Cancer Res* 71, 2550–2560
136 Buchwald, P. (2011) A local glucose-and oxygen concentration-based insulin secretion model for pancreatic islets. *Theor Biol Med Model* 8, 20
137 Nitta, T. *et al.* (2003) Size-selective loosening of the blood-brain barrier in claudin-5–deficient mice. *J Cell Biol* 161, 653–660
138 Mokgokong, R. *et al.* (2014) Ion transporters in brain endothelial cells that contribute to formation of brain interstitial fluid. *Pflugers Arch - Eur J Physiol* 466, 887–901
139 Kamiie, J. *et al.* (2008) Quantitative Atlas of Membrane Transporter Proteins: Development and Application of a Highly Sensitive Simultaneous LC/MS/MS Method Combined with Novel In-silico Peptide Selection Criteria. *Pharm Res* 25, 1469–1483
140 Psychogios, N. *et al.* (2011) The Human Serum Metabolome. *PLoS One* 6,
141 Peters, K. *et al.* (2009) Changes in Human Endothelial Cell Energy Metabolic Capacities during in vitro Cultivation. The Role of "Aerobic Glycolysis" and Proliferation. *CPB* 24, 483–492
142 Siebeneicher, H. *et al.* (2016) Identification and Optimization of the First Highly Selective GLUT1 Inhibitor BAY-876. *ChemMedChem* 11, 2261–2271
143 Krebs, H.A. (1937) THE INTERMEDIATE METABOLISM OF CARBOHYDRATES. *The Lancet* 230, 736–738
144 Hunt, T.K. *et al.* (2007) Aerobically Derived Lactate Stimulates Revascularization and Tissue Repair via Redox Mechanisms. *Antioxidants & Redox Signaling* 9, 1115–1124
145 Ruan, G.-X. and Kazlauskas, A. (2013) Lactate Engages Receptor Tyrosine Kinases Axl, Tie2, and Vascular Endothelial Growth Factor Receptor 2 to Activate Phosphoinositide 3-Kinase/Akt and Promote Angiogenesis. *J. Biol. Chem.* 288, 21161–21172
146 Wang, G. *et al.* (2018) Disruption of Intracellular ATP Generation and Tight Junction Protein Expression during the Course of Brain Edema Induced by Subacute Poisoning of 1,2-Dichloroethane. *Front Neurosci* 12,